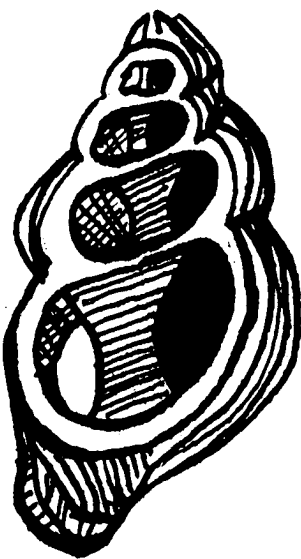


# **NONLINEAR AND ACTIVE COCHLEAR MODELS: ANALYSIS AND SOLUTION METHODS**



**ROB DIEPENDAAL**

**TR diss  
1644**

436638

317.8757

TA diss, 644

# NONLINEAR AND ACTIVE COCHLEAR MODELS: ANALYSIS AND SOLUTION METHODS

# NONLINEAR AND ACTIVE COCHLEAR MODELS: ANALYSIS AND SOLUTION METHODS

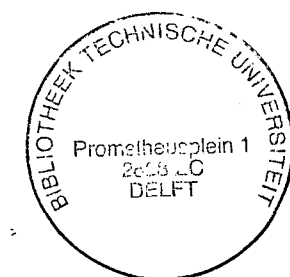
## PROEFSCHRIFT

ter verkrijging van de graad van doctor  
aan de Technische Universiteit Delft,  
op gezag van de Rector Magnificus,  
prof.dr. J.M. Dirken,  
in het openbaar te verdedigen  
ten overstaan van een commissie  
door het College van Dekanen daartoe aangewezen,  
op donderdag 16 juni 1988 te 14.00 uur

door

ROBBERT JACOBUS DIEPENDAAL

geboren te 's-Gravenhage,  
wiskundig ingenieur



TR diss  
1644

Dit proefschrift is goedgekeurd door de promotoren:

prof.dr.ir. M.A. Viergever

prof.dr. E. de Boer

This work has been supported by the Netherlands Organization for the Advancement  
of Pure Research (ZWO)

The following journals gave their permission to reproduce copyrighted material  
The Journal of the Acoustical Society of America (American Institute of Physics)  
Hearing Research (Elsevier Science Publishers)

**Stellingen behorende bij het proefschrift**

**"Nonlinear and active cochlear models:  
analysis and solution methods"**

van

**Rob Diependaal**

- [1] Uit de recent gemeten, scherp afgestemde snelheidskrommen van het basilaire membraan kan worden afgeleid dat de cochlea een actief mechanisch filter bevat dat zich manifesteert op het niveau van de basilair membraan beweging.
- [2] Drukverschillen in de breedterichting van het basilaire membraan hebben slechts geringe invloed op de membraanbeweging.
- [3] De Liouville-Green methode is niet geschikt voor het rekenen aan cochleamodellen met een longitudinale koppeling in het basilaire membraan.
- [4] In een wiskundig model van de cochleaire micromechanica mag de substantie in de subtectoriale spleet niet als vloeistof worden beschouwd. De viscositeit van deze vloeistof zou de energie die getransporteerd wordt van de buitenste naar de binnenste haarcellen te sterk dissiperen.
- [5] Zelfs bij informatiesystemen die op maat ontwikkeld heten te zijn, zijn vaak de gewenste organisatorische procedures aangepast aan het geautomatiseerde systeem in plaats van andersom.
- [6] Gezien de verschillen tussen de vroegere vijfjarige en de huidige vierjarige opleiding tot ingenieur aan de Technische Universiteiten, is het het overwegen waard in plaats van de titel ingenieur de titel doctorandus te verlenen na het met goed gevolg afsluiten van de vierjarige opleiding. Het ingenieursexamen zou dan de afsluiting kunnen zijn van een tweede fase beroepsopleiding.
- [7] De huidige politieke situatie in Nederland kan als volgt gekenschetst worden: eerst komt het voortbestaan van de coalitie, dan de (politieke) moraal.
- [8] De naam *latin-american* voor een groep stijldanssoorten waartoe onder andere de jive, de rock 'n roll en de paso doble behoren, is misleidend. De jive en rock 'n roll zijn afkomstig uit de Verenigde Staten van Amerika, de paso doble komt uit Frankrijk. Daarentegen wordt de tango, wel afkomstig uit Latijns-Amerika (Argentinië), niet ingedeeld bij de *latin-american* dansen maar bij de *ballroom* dansen.
- [9] De uitgang "e" in de geografische naam Duitse bocht is essentieel daar anders ten onrechte de suggestie gewekt zou kunnen worden dat de verontreinigingen die zich op dat deel van de Noordzee ophopen alleen uit Duitsland afkomstig zijn.
- [10] Het is vanuit muziekhistorisch oogpunt juister Beethoven en Schubert als eerste generatie romantici te beschouwen dan ze samen met Haydn en Mozart tot de Weense Klassieken te rekenen.
- [11] De indeling van de goeddeels koperen saxofoon bij de houten blaasinstrumenten doet geen recht aan het unieke karakter ervan.

## PREFACE

This thesis consists of an introduction, six chapters, a summary, and a summary in Dutch.

Chapter 1 has been published: Viergever, M.A. and Diependaal, R.J. (1986). Quantitative validation of cochlear models using the Liouville-Green approximation. Hearing Res. 21, 1-15.

Chapter 2 has been published: Diependaal, R.J., Viergever, M.A., and Boer, E. de (1986). Are active elements necessary in the basilar membrane impedance? J. Acoust. Soc. Am. 80, 124-132.

Chapter 3 has been published: Diependaal, R.J., Boer, E. de, and Viergever, M.A. (1987). Cochlear power flux as an indicator of mechanical activity. J. Acoust. Soc. Am. 82, 917-926.

Chapter 4 has been published: Diependaal, R.J., Duifhuis, H., Hoogstraten, H.W., and Viergever, M.A. (1987). Numerical methods for solving one-dimensional cochlear models in the time domain. J. Acoust. Soc. Am. 82, 1655-1666.

Chapter 5 is submitted for publication: Diependaal, R.J. and Viergever, M.A. (1988). Nonlinear and active two-dimensional cochlear models: time-domain solution. J. Acoust. Soc. Am. -, -.

Chapter 6 is submitted for publication: Diependaal, R.J. and Viergever, M.A. (1988). Nonlinear and active three-dimensional cochlear models: time-domain solution. J. Acoust. Soc. Am. -, -.

**CONTENTS**

|  |     |
|--|-----|
| PREFACE  | 5   |
| INTRODUCTION   | 9   |
| CHAPTER 1. QUANTITATIVE VALIDATION OF COCHLEAR MODELS<br>USING THE LIOUVILLE-GREEN APPROXIMATION | 13  |
| CHAPTER 2. ARE ACTIVE ELEMENTS NECESSARY IN THE BASILAR<br>MEMBRANE IMPEDANCE?                   | 37  |
| CHAPTER 3. COCHLEAR POWER FLUX AS AN INDICATOR OF<br>MECHANICAL ACTIVITY                         | 55  |
| CHAPTER 4. NUMERICAL METHODS FOR SOLVING ONE-DIMENSIONAL<br>COCHLEAR MODELS IN THE TIME DOMAIN   | 77  |
| CHAPTER 5. NONLINEAR AND ACTIVE TWO-DIMENSIONAL<br>COCHLEAR MODELS: TIME-DOMAIN SOLUTION         | 103 |
| CHAPTER 6. NONLINEAR AND ACTIVE THREE-DIMENSIONAL<br>COCHLEAR MODELS: TIME-DOMAIN SOLUTION       | 125 |
| SUMMARY  | 153 |
| SAMENVATTING   | 157 |
| CURRICULUM VITAE   | 163 |

## INTRODUCTION

The peripheral auditory system converts acoustic stimuli to patterns of action potentials along the auditory-nerve fibres. The middle ear responds to a pressure at the eardrum by a motion of the middle-ear ossicles. The third of these, the stapes, is situated in the oval window of the cochlea (inner ear). The fluid in the cochlea is set into motion by the stapes movements, which causes the basilar membrane (BM) to vibrate. These mechanical vibrations are converted into electrochemical signals. It has become known during the last few years that the sharpness of tuning of BM motion is comparable to that of hair cell receptor potentials and nerve fiber firings (Khanna and Leonard, 1982; Sellick *et al.*, 1982, 1983; Robles *et al.*, 1986).

The first topic discussed in this thesis is the question of whether or not macromechanical cochlear models can mimic the recently observed sharply tuned data of BM vibration (chapter 1). In cochlear macromechanics the organ of Corti/tectorial membrane complex is considered to move in unison with the BM. Furthermore, macromechanical models are defined as being passive (*i.e.*, there are no internal sources of mechanical energy) and linear (Viergever, 1986). In the first chapter of the thesis it is shown that the older, mildly tuned BM responses (*e.g.*, Johnstone and Yates, 1974; Wilson and Johnstone, 1975; Rhode, 1971, 1978) can be simulated very well by linear, passive models. However, the newer, sharply tuned data (Khanna and Leonard, 1982; Sellick *et al.*, 1982, 1983; Robles *et al.*, 1986) cannot be matched satisfactorily by a linear, passive model. It has been hypothesized that the difference in tuning between the older and newer measurements is due to a sharpening mechanism in the outer hair cells, the output of which is fed back to the mechanics of the BM (*e.g.*, Viergever, 1980). In this concept the mildly tuned BM vibration data have been recorded in pathological

cochleas in which the feedback process is, at least largely, destroyed. The model results presented in chapter 1 strongly suggest that the sharpening mechanism is governed by a mechanically active process; that is, mechanical energy is created at the level of the hair cells.

The presence of mechanical activity at the BM is further examined in chapters 2 and 3. Two methods are developed in order to answer the question of whether or not the tuning observed in the BM vibration data reflects an active cochlear process that manifests itself at the level of BM motion. The mechanical characteristics of the BM are usually described by a point-impedance function, the real part of which represents the damping. The cochlea dissipates energy when the real part of the BM impedance function is positive, whereas energy is created in regions of the BM where the real part is negative. Consequently, it is useful to develop a method that can calculate the BM point-impedance function from measured BM velocity patterns. It is found, however, that this computational problem is ill-posed in the sense that small changes in the velocity curve may induce large changes in the real part of the impedance (chapter 2). To overcome this difficulty a method is developed to calculate, from a given BM vibration pattern, the power flux through a cross-section of the cochlear channel (chapter 3). The power flux, as a function of place along the BM, is an important indicator of mechanical activity. This is because the slope of the power flux function corresponds to the amount of energy absorbed or created at that point of the BM; a rise in the power flux function indicates creation of mechanical energy. In contrast with the real part of the BM impedance function, the power flux is less sensitive to small changes in the BM velocity. In chapter 3 the power flux method is applied to both mildly tuned and sharply tuned BM vibration data. In the framework of the assumptions made in the formulation of the model equations, it is concluded that in the experiments of Johnstone and Yates (1974) the cochlea behaved as a passive filter. On the other hand, for the sharply tuned responses measured by Robles *et al.* (1986) and Sellick *et al.* (1983) it is concluded that the cochlea behaved as an active filter.

The nonlinearity of the cochlear response to sound stimuli has been firmly established for a long time. Nonlinear behavior has been found in many neurophysiological and psychophysical experiments. Reviews on this topic are given by De Boer (1984) and Kim (1986). The presence of cochlear nonlinearity at the mechanical level has been observed by Rhode (1971, 1978),

LePage and Johnstone (1980), Sellick *et al.* (1982), and Robles *et al.* (1986). While the mechanisms underlying the nonlinear behavior are far from understood, it has been shown that cochlear models equipped with (largely phenomenological) nonlinear features can reproduce at least some of the effects found experimentally (Hubbard and Geisler, 1972; Hall, 1974, 1977; see also Kim, 1986). On the other hand, Johnstone and Yates (1974) and Wilson and Johnstone (1975) did not find any evidence for nonlinear behavior in their measured BM vibration data. The discrepancy between the two sets of data gives arguments for the following concept. The BM is intrinsically linear, whereas the hair cells behave nonlinearly. The nonlinearity manifests itself at the level of BM vibration via a feedback loop, which might be the same as the one by which the active process influences the response of the BM. This concept is further supported by the fact that nonlinearity and sharp tuning are either both present or both absent in the measurements.

Since the mechanisms underlying the nonlinear and active cochlear behavior are hardly known, it is useful to study models with different types of nonlinear and active features. In order to analyse the responses of such models to various input signals, a robust and efficient method for solving cochlear models in the time domain is needed. Furthermore, from macromechanical models it is known that two-dimensional (2D) and three-dimensional (3D) cochlear models show a quite different, and more realistic, behavior than one-dimensional (1D) models. Therefore, in chapters 4, 5, and 6, numerical solution methods for respectively 1D, 2D, and 3D nonlinear and active cochlear models are developed. For 3D models a general non-asymptotic solution method has not been published before, not even in the frequency domain for linear passive cochlear models. The solution procedure is as follows: In the 1D case, the partial differential equation describing the model is discretized in the spatial variable. In the 2D and 3D cases the model equations are first rewritten as a 1D integral equation, without losing the multi-dimensional character of the fluid dynamics. This integral equation is then spatially discretized. In all cases, the place discretization yields a system of ordinary differential equations in the time variable, which is solved by a variable step size fourth-order Runge-Kutta scheme. The selected solution method is both robust and efficient and hence is well suited for evaluating future nonlinear and active cochlear models of arbitrary dimension.

**REFERENCES**

- Boer, E. de (1984). Auditory Physics. Physical principles in hearing theory II. *Phys. Rep.* **105**, 141-226.
- Hall, J.L. (1974). Two-tone distortion products in a nonlinear model of the basilar membrane. *J. Acoust. Soc. Am.* **56**, 1818-1828.
- Hall, J.L. (1977). Two-tone suppression in a nonlinear model of the basilar membrane. *J. Acoust. Soc. Am.* **61**, 802-810.
- Hubbard, A.E., and Geisler, C.D. (1972). A hybrid-computer model of the cochlear partition. *J. Acoust. Soc. Am.* **51**, 1895-1903.
- Johnstone, B.M., and Yates, G.K. (1974). Basilar membrane tuning curves in the guinea pig. *J. Acoust. Soc. Am.* **55**, 584-587.
- Khanna, S.M., and Leonard, D.G.B. (1982). Basilar membrane tuning in the cat cochlea. *Science* **215**, 305-306.
- Kim, D.O. (1986). An overview of nonlinear and active cochlear models. In: *Peripheral Auditory Mechanisms*, pp. 239-249. Editors: J.B. Allen, J.L. Hall, A. Hubbard, S.T. Neely, and A. Tubis. Springer Verlag, Berlin, Heidelberg, New York.
- LePage, E.L., and Johnstone, B.M. (1980). Nonlinear mechanical behaviour of the basilar membrane in the basal turn of the guinea pig cochlea. *Hearing Res.* **2**, 183-189.
- Rhode, W.S. (1971). Observations of the vibration of the basilar membrane in squirrel monkeys using the Mössbauer technique. *J. Acoust. Soc. Am.* **49**, 1218-1231.
- Rhode, W.S. (1978). Some observations on cochlear mechanics. *J. Acoust. Soc. Am.* **64**, 158-176.
- Robles, L., Ruggero, M.A., and Rich, N.C. (1986). Basilar membrane mechanics at the base of the chinchilla cochlea. I. Input-output functions, tuning curves, and response phases. *J. Acoust. Soc. Am.* **80**, 1364-1374.
- Sellick, P.M., Patuzzi, R., and Johnstone, B.M. (1982). Measurement of basilar membrane motion in the guinea pig using the Mössbauer technique. *J. Acoust. Soc. Am.* **72**, 131-141.
- Sellick, P.M., Yates, G.K., and Patuzzi, R. (1983). The influence of Mössbauer source size and position on phase and amplitude measurements of the guinea pig basilar membrane. *Hear. Res.* **10**, 101-108.
- Viergever, M.A. (1980). Mechanics of the Inner Ear - A mathematical approach. Doctoral dissertation, Delft University Press, Delft, The Netherlands.
- Viergever, M.A. (1986). Cochlear macromechanics - A review. In: *Peripheral Auditory Mechanisms*, pp. 63-72. Editors: J.B. Allen, J.L. Hall, A. Hubbard, S.T. Neely, and A. Tubis. Springer Verlag, Berlin, Heidelberg, New York.
- Wilson, J.P., and Johnstone, J.R. (1975). Basilar membrane and middle-ear vibration in guinea pig measured by capacitive probe. *J. Acoust. Soc. Am.* **75**, 705-723.

## CHAPTER ONE

# Quantitative validation of cochlear models using the Liouville-Green approximation.

**Abstract** This article is devoted to the question of whether linear and passive models of the cochlea can mimic the recently observed sharply tuned data of basilar membrane vibration. The model equations are solved by means of an asymptotic approach, the Liouville-Green approximation, which is adequate for quantitative comparisons with experimental data. The conclusions are: (i) the older, mildly tuned basilar membrane responses can be matched very well by means of linear, passive models; (ii) the newer, sharply tuned data cannot be matched satisfactorily by linear, passive modelling. Hence, this study supports the view that the cochlea must contain an active mechanical filter which manifests itself at the level of BM vibration.

## INTRODUCTION

Observation of acoustic emissions (pioneered by Kemp, 1978) and measurements of basilar membrane (BM) motion (Khanna and Leonard, 1982; Sellick *et al.*, 1982) have firmly established that the nonlinearity and the sharp tuning of the cochlea are present at the level of BM vibration. While evidence is accumulating that these features originate from hair cell processes, theories about the mechanisms creating them are not yet beyond the conjectural stage.

In this article we shall refrain from contributing to the discussion concerning the origin of nonlinear and tuned behaviour, and restrict ourselves to the question where we stand with conventional (that is, linear and passive) modelling of the cochlea in view of the recent findings. This may seem strange, inasmuch as linear models cannot adequately describe nonlinear phenomena. We can avoid this problem, however, by considering only one stimulus level, preferably near threshold, where the cochlea is supposedly still quite linear. The question then becomes: *Can passive models of the cochlea produce the sharp tuning as seen in the BM response?*

In order to answer this question we formulate the equations of the conventional one-, two- and three-dimensional (1D, 2D, 3D) models. Our starting

point is the 3D model provided with a viscoelastic, orthotropic plate. If the plate has no longitudinal stiffness, it effectively becomes a series of parallel beams. The model then has well-defined 1D and 2D analogues, and the BM properties can be characterized in terms of a point-impedance. The equations are solved by means of an asymptotic method, the Liouville-Green (LG) approximation, often referred to as WKB or WKBJ approximation. The model parameters are fixed insofar as they can be reliably estimated from anatomical data, the remaining parameters are curve-fitted to the experimental results.

We consider two types of measurement results of BM motion, *viz.* midly tuned responses in which the middle ear and the cochlea behave essentially as a low-pass filter, and sharply tuned responses having much more band-pass like characteristics. It appears that the former results can be matched excellently by means of a conventional method (2D or 3D), the latter not. We have extended the model by including a second degree of freedom, which may, for example, represent the vibration of the tectorial membrane. This reduces the difference with the sharply tuned data slightly, but a structural discrepancy remains. Consequently, the present article supports the view that *the recent observations of BM motion cannot be explained by a passive cochlear model.*

## I. THREE-DIMENSIONAL MODEL EQUATIONS

The 1D, 2D and 3D descriptions of cochlear mechanics all derive from the same model geometry, shown in Fig. 1.

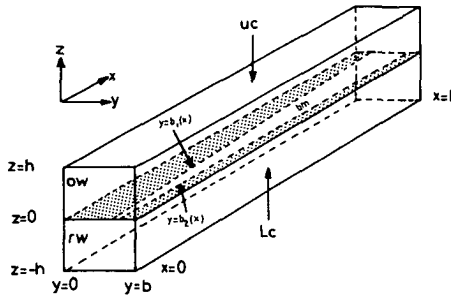


Figure 1. Geometry of the three-dimensional model.

The model consists of two identical rectangular channels, filled with an incompressible, inviscid fluid that behaves linearly. The channels are

separated by the cochlear partition, the plane  $z=0$ . The BM has a width  $\beta(x)$ ; it occupies a fraction  $\epsilon = \beta/b$  of the width  $b$  of the partition. We consider the system to be driven in push-pull; the component  $P$  of the fluid pressure<sup>1</sup> that induces a travelling wave along the BM is, consequently, antisymmetric with respect to the plane  $z=0$ . Hence we can confine ourselves to events occurring in the upper channel.

Like the fluid surrounding it, the BM is assumed to operate linearly, which enables us to eliminate the time variable  $t$  from the problem. The input of the system, the vibration of the stapes, is supposed to be a harmonic oscillation in time of radian frequency  $\omega$ . All time-dependent quantities  $q(x,y,z,t)$  may hence be written as (the real part of)  $Q(x,y,z;j\omega)\exp(j\omega t)$ , and thus be represented by the complex-valued quantities  $Q$  in our equations<sup>2</sup>.

Owing to the assumptions made about the fluid filling the model, the fluid pressure must satisfy Laplace's equation for potential flow. We write the equation not in terms of fluid pressure itself, but in terms of a difference pressure  $P$  which is defined as

$$P(x,y,z) = P_{lc}(x,y,-z) - P_{uc}(x,y,z); z > 0 \quad (1)$$

where  $P_{lc}$  and  $P_{uc}$  are the (antisymmetric parts of) the fluid pressures in the lower channel and the upper channel, respectively. Laplace's equation now reads

$$\frac{\partial^2 P}{\partial x^2} + \frac{\partial^2 P}{\partial y^2} + \frac{\partial^2 P}{\partial z^2} = 0 \quad (2)$$

This elliptic partial differential equation is subject to boundary conditions at the six walls. At each wall, the normal derivative of  $P$  is proportional to the normal component of the fluid velocity. The condition at the base of the cochlea is a prescribed oval window velocity driving the system. The error involved in assuming that this velocity is constant with respect to  $y$  and  $z$  is insignificant (Viergever, 1980). Hence, taking the velocity of the stapes equal

1. The fluid pressure consists of two parts. The antisymmetric part which we consider is uninfluenced by fluid compressibility. In addition, there is a symmetric part that does depend on compressibility but, because of the symmetry with respect to the plane  $z=0$ , not on the characteristics of the cochlear partition. The latter pressure component is irrelevant for the motion of the BM.
2. For brevity, the dependence of quantities  $Q$  on the radian frequency  $\omega$  will henceforth not be shown explicitly.

to one unit of velocity, we get

$$\frac{\partial P}{\partial x} \Big|_{x=0} = 2j \omega \rho A_{st} / bh, \quad (3)$$

where  $A_{st}$  is the area of the stapes footplate.

At the rigid walls the normal component of the fluid velocity vanishes, which is expressed by

$$\frac{\partial P}{\partial x} \Big|_{x=l} = 0, \quad (4)$$

$$\frac{\partial P}{\partial y} \Big|_{y=0} = 0, \quad (5)$$

$$\frac{\partial P}{\partial y} \Big|_{y=b} = 0, \quad (6)$$

$$\frac{\partial P}{\partial z} \Big|_{z=h} = 0. \quad (7)$$

Finally, at the cochlear partition we have

$$\frac{\partial P}{\partial z} \Big|_{z=0} = \begin{cases} 2j \omega \rho V(x, y) & b_1(x) < y < b_2(x) \\ 0 & 0 \leq y \leq b_1(x), b_2(x) \leq y \leq b \end{cases} \quad (8)$$

where  $\rho$  is the fluid density and  $V(x, y)$  is the velocity of the BM, defined positive when directed upwards.

In order to complete the boundary value problem we must specify the relation between  $P$  and  $V$  at the level of the BM. Since the BM is not under tension in its resting state, it is a plate rather than a membrane in the terminology of mechanics. The plate is highly *anisotropic* in intact cochleae, as was demonstrated by Voldrich (1978). This is in conformity with anatomic data (Iurato, 1962) which show that the BM consists of a cottony ground substance reinforced with transverse fibers (*i.e.* in the  $y$ -direction). The plate equation for such a structure is (Timoshenko and Woinowsky-Krieger, 1959)

$$\frac{\partial^2}{\partial x^2} \left( D \frac{\partial^2 V}{\partial x^2} + \nu D \frac{\partial^2 V}{\partial y^2} \right) + \frac{\partial^2}{\partial y^2} \left( (D + D_f) \frac{\partial^2 V}{\partial y^2} + \nu D \frac{\partial^2 V}{\partial x^2} \right) + 2(1-\nu) \frac{\partial^2}{\partial x \partial y} \left( \frac{\partial^2 V}{\partial x \partial y} \right) - \rho_p \omega^2 H V = j \omega P(x, y, 0), \quad b_1(x) < y < b_2(x) \quad (9)$$

where  $\rho_p$  is the constant density of the structure,  $H$  is the thickness of the

plate,  $D$  is the bending stiffness of the ground substance (which is assumed to be isotropic),  $D_f$  is the bending stiffness of the fibers, and  $\nu$  is Poisson's elastic constant of the ground substance. The quantities  $H$ ,  $D$  and  $D_f$  are *complex-valued* quantities as a consequence of the visco-elastic properties of the BM. We suppose that the BM consists of Kelvin material, the simplest visco-elastic material for a solid (Flügge, 1975). This implies that  $D$  and  $D_f$  each have the form  $D_l + j\omega D_2$ , with  $D_l$  and  $D_2$  real-valued quantities. The damping thus introduced ensures the stability of the model response<sup>3</sup>.

The boundary conditions for Eq. (9) remain to be specified. For our purpose it will be sufficient to consider the long edges of the BM. These edges are to a good approximation simply supported (Steele, 1976), which means that the deflection and the bending moments along them must be zero:

$$V=0, \frac{\partial^2 V}{\partial n^2}=0, \text{ at } y=b_1(x), y=b_2(x) \quad (10)$$

where  $\partial/\partial n$  denotes the normal derivative.

Equations (2)-(10) describe the 3D fluid flow and the motion of the BM in the model of Fig. 1. The corresponding 2D and 1D descriptions can be obtained by averaging the pressure over the channel width and the channel cross-section respectively:

$$P^{2D}(x, z) = b^{-1} \int_0^b P(x, y, z) dy \quad (11)$$

$$P^{1D}(x) = h^{-1} \int_0^h P^{2D}(x, z) dz \quad (12)$$

## II. ONE- AND TWO-DIMENSIONAL MODEL EQUATIONS

The 1D and 2D models to be studied in this article are all analogues of a simplified form of the 3D model, *viz.* when the BM has no *longitudinal coupling*. This occurs when the stiffness  $D$  of the ground substance of the BM is negligibly small in comparison with the stiffness  $D_f$  of the fibers. Equation (9) then becomes

---

3. Alternatively, damping can be introduced into the model by taking into account fluid viscosity. A calculation of fluid viscosity effects has shown, however, that these are negligible as compared with the internal damping of the BM complex (Viergever, 1980).

$$D_f(x) \frac{\partial^4 V(x,y)}{\partial y^4} - \rho_p \omega^2 H(x)V(x,y) = j\omega P(x,y,0), b_1 < y < b_2 \quad (13)$$

This is the equation for a beam in the transverse direction of the BM. Obviously, the assumption  $|D| \ll |D_f|$  has converted the visco-elastic plate into a system of *parallel visco-elastic beams*. The solution of Eq. (13) subject to the boundary conditions (10) is derived in the Appendix. The resulting 1D and 2D analogues are also formulated there.

In order to work with the LG approximation it is advantageous to introduce the concept of a *point-impedance function* to present the mechanical properties of the BM. In this concept the velocity  $V$  at a certain point of the BM depends on the transmembrane pressure  $P$  at that point only, not on the pressure difference at neighbouring points. Specifying the relation between  $P$  and  $V$  is not a trivial matter because of the  $y$ -dependence of these quantities. In the Appendix it is shown how the point-impedance function is best defined. The result is

$$Z(x) = \frac{2}{\beta V_1} \int_{b_1}^{b_2} P(x,y,0) \sin\{\pi(y-b_1)/\beta\} dy \quad (14)$$

where  $P(x,y,0)$  is the trans-BM pressure and  $V_1(x)$  is the velocity of the centreline of the BM. The relation between  $Z(x)$  and the beam parameters is

$$Z = \left( \frac{\pi}{\beta} \right)^4 \frac{D_f}{j\omega} + j\omega \rho_p H \quad (15)$$

Figure 2 presents, in condensed form, the 2D and 1D analogues of the parallel beams model in terms of the BM impedance.

### III. THE LIOUVILLE-GREEN APPROXIMATION

In order to examine whether the models considered in this paper adequately describe the mechanical phenomena in the cochlea, we have to compare model calculations with experimental results. Such a validation is complicated by the difference in output mode of models and measurements. The data are recorded at a fixed point on the BM as a function of stimulus frequency; the output of the models is BM velocity as a function of the longitudinal coordinate  $x$  for a fixed input frequency. Consequently, a direct comparison between the two requires solution of the model equations for a large number of frequencies. In addition, the principal model parameters are known only

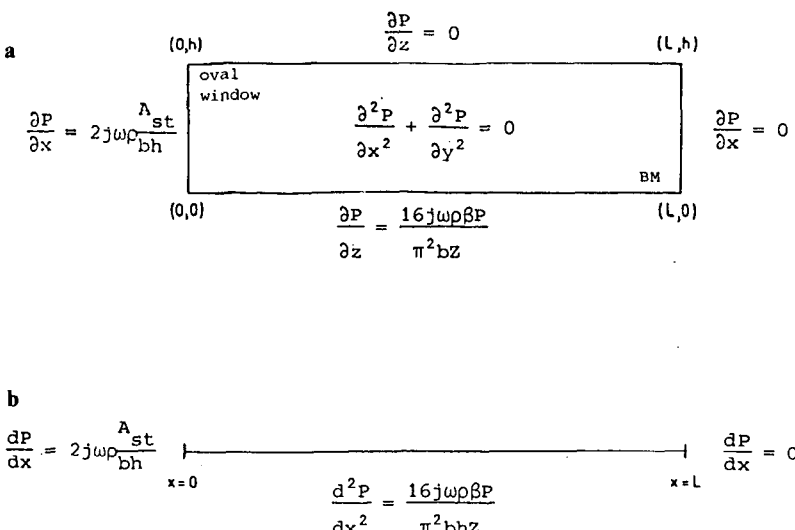


Figure 2. (a) Two-dimensional analogue of the three-dimensional model without longitudinal BM coupling;  $P$  is shorthand for  $P^{2D}(x,z;j\omega)$ . (b) Corresponding one-dimensional analogue;  $P$  is shorthand for  $P^{1D}(x;j\omega)$ .

by order-of-magnitude estimates, which necessitates extensive parameter variation in fitting the observations. These two reasons call for a solution method which is not only *accurate*, but also *computationally fast*.

The model equations are so complicated, particularly owing to the intricate structure of the cochlear partition, that they do not admit an analytic solution. Approximating the solution by a straightforward numerical technique has neither been accomplished yet in the 3D model because of computer storage problems. For the 2D case numerical solutions have been obtained (Allen, 1977; Allen and Sondhi, 1979; Viergever, 1980; Neely, 1981a), but the long computation times preclude numerical experimentation with the parameters. We must, accordingly, settle for an asymptotic approach. The most suitable asymptotic method for solving cochlear mechanics problems is the *Liouville-Green (LG) approximation*, which is based on the assumption that the BM wave travels in a medium of which the propagation properties do not vary much within one wavelength. For a discussion on the merits and shortcomings of the LG method we refer to De Boer and Viergever (1982).

The efficient way to derive the LG solution of cochlear models is by means of the *energy approach*, proposed by Whitham (1974) and introduced into the

field of cochlear mechanics by Steele (1974). It has been worked out in detail for various 3D models, including models that allow for motions of the bony shelf and the arches of Corti in addition to motions of the basilar membrane (Taber, 1979; Taber and Steele, 1981). The method, based on a variational principle applied to the time-average Lagrangian density of the system, formally is valid only for real waves in conservative systems, but it gives correct results also for dissipative systems (Steele, 1980).

Upon applying the energy approach to the parallel beams model derived in Section II, we find that the LG solution for the velocity  $V_c(x)$  of the centre-line of the BM can be written as (cf. Steele and Taber, 1979)

$$V_c(x) = -jA_{st} \frac{\pi\kappa(0)}{2\beta(0)} \left| \frac{\beta(0)dG(0)/d\kappa}{\beta(x)dG(x)/d\kappa} \right|^{\frac{1}{2}} \exp \left[ -j \int_0^x \kappa(\xi) d\xi \right] \quad (16)$$

with the complex-valued wave number  $\kappa(x)$  satisfying

$$G(x;\kappa) = Q(\kappa) + \frac{Z(x)}{2j\omega\rho} = 0 \quad (17)$$

The function  $Q(\kappa)$  depends on several features of the cochlear model, *viz.* the dimensionality of the fluid flow and geometrical parameters as channel height and ratio BM width/channel width. It represents the height of the fluid column that resists the motion of the BM. Using the impedance definition of the preceding section, we find for the 3D model

$$Q^{3D}(\kappa) = \frac{8\beta}{\pi^2 b} \left| \frac{1}{\kappa \tanh(\kappa h)} + \frac{1}{2} \sum_{k=1}^{\infty} \frac{(\cos(k\pi b_1/b) + \cos(k\pi b_2/b))^2}{\{1 - (k\beta/b)^2\}^2 m_k \tanh(m_k h)} \right| \quad (18)$$

where

$$m_k = \{(k\pi/b)^2 + \kappa^2\}^{\frac{1}{2}} \quad (19)$$

The  $Q$ -functions for the 2D and 1D analogues of the parallel beams model are

$$Q^{2D}(\kappa) = \frac{8\beta}{\pi^2 b} \cdot \frac{1}{\kappa \tanh(\kappa h)} \quad (20)$$

$$Q^{1D}(\kappa) = \frac{8\beta}{\pi^2 b} \cdot \frac{1}{\kappa^2 h} \quad (21)$$

Notice that (20) is just the leading term of (18), while (21) is the long-wave

(i.e.,  $|kh| \ll 1$ ) asymptote of (20).

Equation (17) can be conceived as the *dispersion relation* for the cochlea wave, since it expresses the way in which the radian frequency  $\omega$  - implicit in  $Z(x)$  - relates to the wave number  $\kappa$ . In fact, the LG formulation can be derived using dispersive wave theory (De Boer and Viergever, 1984).

The solution for the full plate representation of Section I is similar to that of the parallel beams model. The basic formula (16) still applies, and the  $Q$ -function is given by Eqs. (18) and (19). The dispersion relation no longer has the simple appearance of Eq. (17), however, but it takes the form

$$G(x; \kappa) = Q(\kappa) + \frac{1}{2j\omega\rho} \left[ Z(x) + \frac{D}{D+D_f} \left\{ 2 \left( \frac{\pi}{\beta} \right)^2 \kappa^2 + \kappa^4 \right\} \frac{D_f}{j\omega} \right] = 0 \quad (22)$$

The extra term can be conceived as an additional part of the impedance (dependent on the wave number) which represents longitudinal BM coupling. The point-impedance function of the plate thus becomes

$$Z(x; \kappa) = \left[ \left( \frac{\pi}{\beta} \right)^4 + \frac{D}{D+D_f} \left\{ 2 \left( \frac{\pi}{\beta} \right)^2 \kappa^2 + \kappa^4 \right\} \right] \frac{D_f}{j\omega} + j\omega\rho_p H \quad (23)$$

This characterization of the plate is valid *only within the framework of the LG approximation* as can most simply be gathered from the fact that  $\kappa$  is the LG wave number. The impedance of the parallel beams system, given by Eq. (15) (and by Eq. (23) upon inserting  $D=0$ ) is *not* subject to this limitation.

#### IV. COMPARISON WITH EXPERIMENTAL DATA

Measurements of BM motion have evolved a great deal in the last two decades. Von Békésy's (1960) observations on cadaver cochleae were the only standard for a long time. The responses seen by him had much too broad an amplitude maximum to explain the frequency discrimination capabilities of the cochlea. Around 1970 sharper BM characteristics were obtained *in vivo* (Johnstone and Yates, *et al.*, 1970; Kohlöffel, 1972; Johnstone and Yates, 1974; Wilson and Johnstone, 1975), but the overall impression was still that of a linear low-pass filtering of the middle-ear and the cochlea which could be reconciled with the highly peaked neural frequency threshold curves only by assuming a second (post-BM) filter (Evans and Wilson,

1975).

Rhode (1971, 1978) found a further increase in tuning which already gave the impression of band-pass like behaviour. Moreover, he discovered a saturating-type nonlinearity in the peak region. It was hypothesized that these features differed from those mentioned above owing to less damage done to the cochlea by the invasiveness of the experimental surgery. This idea has recently been given firm ground by Khanna and Leonard (1982) and Sellick *et al.* (1982), who measured a sharpness of tuning on the BM comparable to that of neural responses. The nonlinear properties detected by Rhode were also confirmed. The new data are believed to reflect the behaviour of physiologically almost intact cochleae, although damage can still be demonstrated (Leonard and Khanna, 1984).

In this section result of *curve-fitting* model calculations with four sets of experimental data are presented. The paradigm is as follows. In conformity with Eq. (15) we write, since  $D_f$  is a complex-valued quantity,

$$Z(x) = j\omega M(x) + R(x) + S(x)/j\omega \quad (24)$$

and prescribe that  $M$ ,  $R$  and  $S$  have the form

$$\begin{aligned} M(x) &= M_0 \exp(M_1 x) \\ R(x) &= R_0 \exp(R_1 x) \\ S(x) &= S_0 \exp(S_1 x) \end{aligned} \quad (25)$$

with  $M_0$ ,  $R_0$ ,  $S_0$ ,  $M_1$ ,  $R_1$ ,  $S_1$  constants.

The quantities  $A_{st}$ ,  $\beta(x)$ ,  $b$ ,  $h$ ,  $M_1$ ,  $R_1$ , and  $S_1$  are estimated from anatomical data. The fluid desity  $\rho$  is also a fixed parameter. The remaining parameters  $M_0$ ,  $R_0$  and  $S_0$  cannot be estimated to a sufficient degree for quantitative comparisons and hence are kept free in the curve-fitting procedure.

The experimental data are frequency responses observed at one point of the BM. This observation point  $x_{obs}$  is usually not specified by the experimenters, so its value is estimated. The LG solutions are calculated up to this point for a large number of frequencies, and the values at  $x_{obs}$  are stored. The frequency response of the model is then displayed and compared visually with the measurement results. The parametrs  $M_0$ ,  $R_0$ , and  $S_0$  are adjusted until a best fit has been obtained. Details of the calculation procedure can be found in Viergever (1980).

We did many of our calculations using the *2D model*, for three reasons. Firstly, the higher accuracy of 3D versus 2D modelling is partly undone by the slightly inferior performance of the 3D LG approximation (the decay after the peak has been reached is too steep; see De Boer and Viergever, 1982). Secondly, the 3D computations can be quite lengthy because the series in the *Q*-function (18) converges slowly in the resonance frequency region for many parameter sets. In the 1D case, the computing time is shorter still and the LG approximation again more accurate than in two dimensions, but the difference in response between the 3D model and the 1D model, even if the latter is endowed with added fluid mass, is prohibitively large for most parameter sets. The third reason for using a 2D model is that the parameters are often in a range where the 3D response is well approximated by that of a 2D model with added mass. If this did not apply, we switched to the *3D model*.

Figure 3 shows a comparison of our calculations with BM/stapes transfer ratios measured by Johnstone and Yates (1974).

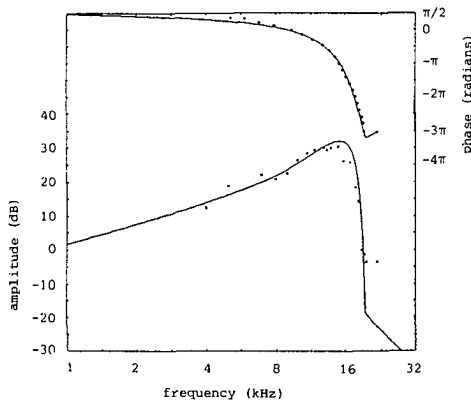


**Figure 3.** Comparison of 2D model results with data ( $\times$ , amplitude;  $\cdot$ , phase), observed in the guinea pig by Johnstone and Yates (1974, Fig. 3). The quantity displayed is the BM/stapes transfer ratio. Parameter values:  $x_{obs} = 3 \text{ mm}$ ,  $b = 0.5 \text{ mm}$ ,  $h = 1.4 \text{ mm}$ ,  $A_{st} = 0.7 \text{ mm}^2$ ,  $\rho = 1.0 \text{ mg/mm}^3$ ,  $\beta = 0.08 \exp(0.04x) \text{ mm}$ ,  $M = 0.098 \text{ mg/mm}^2$ ,  $R = 3.8 \exp(-0.275x) \mu\text{Ns/mm}^3$ ,  $S = 7.7 \exp(-0.55x) \text{ N/mm}^3$ .

These data were obtained using the Mössbauer technique. The Mössbauer source covers a large part of the BM width, so the measured response will be an average in the lateral direction rather than the velocity of the centreline. We estimated that the data represent an average over 2/3 of the width of the BM. In our model the BM velocity has a half-sine-shaped distribution over

the width. Hence we multiplied  $V(x)$  by a factor  $3\sqrt{3}/2\pi$ , which amounts to a reduction of 1.65 dB.

The agreement between model calculations and experimental data is excellent. The value assigned to the parameter  $M_0$  seems realistic; it is approximately equal to the mass of the organ of Corti. The value of  $S_0$  agrees well with the stiffness measurement data of Gummer *et al.* (1981) and Miller (1983). Similar results were obtained for other mildly tuned BM responses. A 2D approach is quite adequate for this type of data, as follows from a comparison between 2D and 3D model results for frequencies in the peak region. Previously published 2D results failed to achieve a simultaneous amplitude and phase match mainly because of an incorrect interpretation of the output of the model (Viergever and Diependaal, 1983).

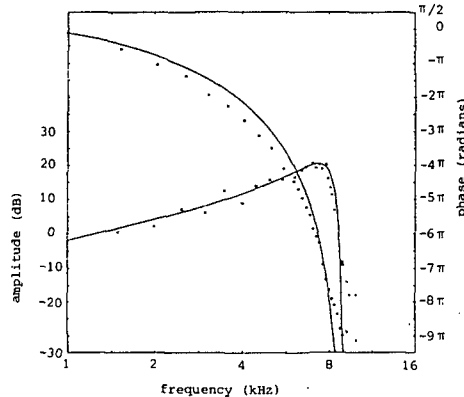


**Figure 4.** Comparison of 2D model results with Rhode's 69-473 squirrel monkey data (x, amplitude; ·, phase). The data were transformed to BM/stapes ratios using Rhode's (1978, Fig. 5) stapes/malleus transform function. Parameter values:  $x_{obs} = 15 \text{ mm}$ ,  $b = 0.5 \text{ mm}$ ,  $h = 0.5 \text{ mm}$ ,  $A_{st} = 0.25 \text{ mm}$ ,  $\rho = 1.0 \text{ mg/mm}^3$ ,  $\beta = 0.08 \exp(0.05x) \text{ mm}$ ,  $M = 0.16 \text{ mg/mm}^2$ ,  $R = 1.9 \exp(-0.10x) \mu\text{Ns/mm}^3$ ,  $S = 10.7 \exp(-0.20x) \text{ N/mm}^3$ .

Figure 4 presents a match of model calculations to a measurement of Rhode (1971). The data were recorded as BM/malleus transfer functions, while the cochlea model yields a BM/stapes ratio. We therefore adapted the data in conformity with Rhode's (1978, Fig. 5) stapes/malleus transfer ratios. The resulting reduction of the peak of the amplitude curve is consistent with Rhode's own findings. In addition, the mentioned Mössbauer correction was applied. The agreement of model and measurement results is clearly less satisfactory than in Fig. 3. The 2D approach was still adequate here, although not as good as in the previous figure.

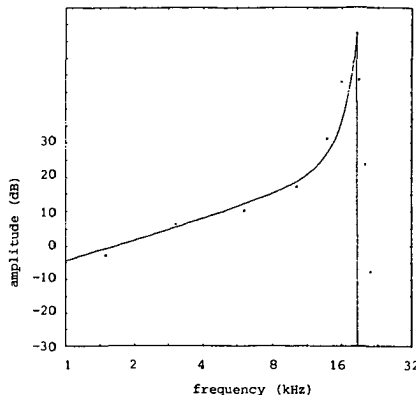


**Figure 5.** Comparison of 3D model results with measurement data of Sellick *et al.* (1982, Fig. 10) in the guinea pig. The data were transformed to BM/stapes ratios using a middle-ear transfer filter as described in the text. Parameter values:  $x_{obs} = 3 \text{ mm}$ ,  $b = 0.5 \text{ mm}$ ,  $h = 1.4 \text{ mm}$ ,  $A_{st} = 0.7 \text{ mm}^2$ ,  $\rho = 1.0 \text{ mg/mm}^3$ ,  $\beta = 0.08 \exp(0.04x) \text{ mm}$ ,  $M = 0.6 \text{ mg/mm}^2$ ,  $R = 0.024 \exp(-0.275x) \mu\text{Ns/mm}^3$ ,  $S = 42.8 \exp(-0.55x) \text{ N/mm}^3$ .

In Fig. 5 we present a comparison with a sharp BM response measured by Sellick *et al.* (1982), again using the Mössbauer approach. The data are ratios of BM displacement and sound pressure at the eardrum. Therefore, they are modified, apart from the Mössbauer correction, by a middle-ear transfer filter. The filter represents stapes displacement over pressure at the eardrum, with a value of  $5 \times 10^{-8} \text{ m/Pa}$  at frequencies  $< 1 \text{ kHz}$ , and decaying at  $6 \text{ dB/octave}$  above  $1 \text{ kHz}$ . The figure of  $6 \text{ dB}$  is a conservative estimate. The results of Wilson and Johnstone (1975) justify a higher decay rate of  $8 \text{ dB/octave}$  which would make the BM/stapes transfer ratio even more difficult to match.

The comparison shows a large difference between 3D model and measurement results, in spite of the conservative estimate of the middle-ear filter, and in spite of the fact that only the amplitude of the response was matched; the corresponding phase were not reported on by the experimenters<sup>4</sup>. The peak values of the calculated response and the measured response can be made equal, but the bandwidth of the model response is clearly too small. The discrepancy was even more pronounced with 2D model calculations. A similar picture can be seen in Fig. 6 for a BM frequency threshold curve measured by Khanna and Leonard (1982) using laser interferometry. The same

<sup>4</sup>. In a later paper, the same group did publish phase data (Sellick *et al.*, 1983).

middle-ear transfer function as described above was used to arrive at BM/stapes transfer ratios. Here also, only amplitude data are available.

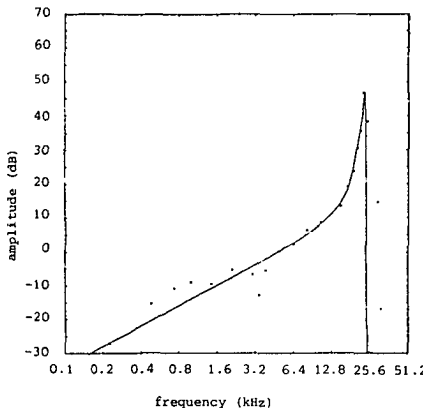


**Figure 6.** Comparison of 3D model results with BM tuning curves measured in the cat by Khanna and Leonard (1982, Fig. 2). The data were transformed to BM/stapes transfer ratios as described in the text. Parameter values:  $x_{obs} = 3 \text{ mm}$ ,  $b = 1 \text{ mm}$ ,  $h = 1.26 \text{ mm}$ ,  $a_{st} = 0.6 \text{ mm}^2$ ,  $\rho = 1.0 \text{ mg/mm}^3$ ,  $\beta = 0.12 \exp(0.04x) \text{ mm}$ ,  $M = 0.45 \exp(0.08x) \text{ mg/mm}^2$ ,  $R = 0.2 \exp(0.05x) \mu\text{Ns/mm}^3$ ,  $S = 33.8 \exp(-0.32x) \text{ N/mm}^3$ .

Apparently, the model is not equipped to simulate the both sharp and relatively broad tuning of the recent BM data. There are several possibilities to extend the model with features which were omitted in formulating it. We shall pursue two of them in the present article. A first attempt is to include *longitudinal coupling* of the BM, since this feature is known to broaden the response (Allen and Sondhi, 1979; Taber, 1979; Taber and Steele, 1981). Inclusion into the model of longitudinal coupling is accomplished by replacing the dispersion relation (17) for the parallel beams system with that of the full plate representation (22). Figure 7 shows computations of the plate model, compared with the data used in Fig. 5. The response is indeed broadened, but not in a way which closer resembles the data. Even a minute amount of longitudinal stiffness makes the amplitude plateau start right after the peak; in the corresponding figure for the parallel beams model (Fig. 5), the plateau is not visible because it appears at a very low level.

A second, more rigorous modification of the model is to allow for a *second degree of freedom* in addition to BM motion. This increases the number of parameters greatly and thus the possibility of obtaining good agreement with the observations. The next section is devoted to this extension.

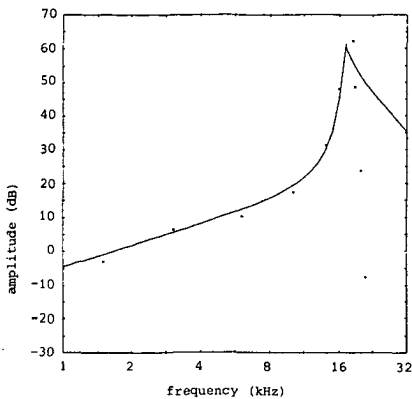


Figure 7. Comparison of calculations on the 3D cochlear model including longitudinal BM coupling with the data of Fig. 5. Parameter values: as in Fig. 5, except  $M = 0.7 \text{ mg/mm}^2$ ,  $D/(D+D_f) = 10^{-5}$ . The value of the mass was increased somewhat to counterbalance the stiffness added to the system.

## V. FOURTH-ORDER MODEL

A model of the cochlear partition with *independent resonances of the basilar and tectorial membranes* has been proposed by Zwischki (1980a, 1980b) and Allen (1980). The model has two degrees of freedom: the vertical motion of the BM and the radial motion of the tectorial membrane (TM); the vertical motion of TM is assumed to follow BM motion. The two resonant systems are coupled elastically by the stereocilia of the outer hair cells and viscously by the fluid between the two membranes (Fig. 8).

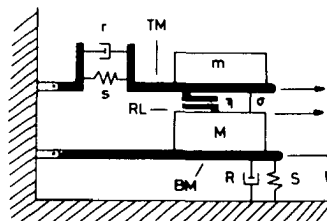


Figure 8. Schematic representation of the fourth-order (two degrees of freedom) model with resonant tectorial membrane. RL: reticular lamina. Other symbols are described in the text. Adapted from Allen (1980) and Neely (1981b).

The resulting fourth-order model has been used both to achieve a transduction from BM motion to hair cell shearing which closely matches measurements of neural response (Neely, 1981b) and to reduce the discrepancies between cochlear model calculations and experimental data on BM vibration (Zwischki, 1983).

The LG solution of the fourth-order model is readily obtained. Equations (16) and (17) remain valid, and the  $Q$ -functions (18)-(21) are also unchanged. The impedance  $Z(x)$  in the dispersion relation has to be redefined, however. Instead of Eq. (24) we now have

$$Z(x) = Z_1(x) + \frac{Z_2(x)Z_3(x)}{Z_2(x)+Z_3(x)} \quad (26)$$

with

$$\begin{aligned} Z_1(x) &= j\omega M(x) + R(x) + S(x)/j\omega \\ Z_2(x) &= j\omega m(x) + r(x) + s(x)/j\omega \\ Z_3(x) &= \eta(x) + \sigma(x)/j\omega \end{aligned} \quad (27)$$

Here,  $Z_1(x)$  represents the BM impedance,  $Z_2(x)$  the TM impedance and  $Z_3(x)$  the coupling of BM and TM by the outer hair cell stereocilia and the subtectorial fluid. We refer to the cited papers for details of the derivations. The newly defined impedance components are written as

$$\begin{aligned} m(x) &= m_0 e^{m_1 x} \\ r(x) &= r_0 e^{r_1 x} \\ s(x) &= s_0 e^{s_1 x} \\ \eta(x) &= \eta_0 e^{\eta_1 x} \\ \sigma(x) &= \sigma_0 e^{\sigma_1 x} \end{aligned} \quad (28)$$

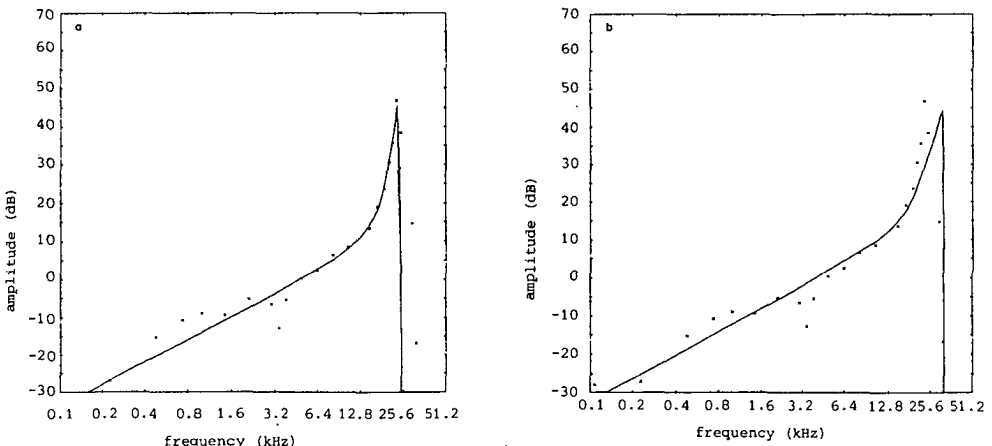


**Figure 9.** Comparison of the fourth-order (two degrees of freedom) 3D model with the data of Fig. 6. Parameter values: (a) as in Fig. 6, except  $R=0.1 \exp(-0.3x) \mu\text{Ns}/\text{mm}^3$ ,  $m=0.003 \exp(0.03x) \text{mg}/\text{mm}^2$ ,  $r=0.5 \exp(-0.3x) \mu\text{Ns}/\text{mm}^3$ ,  $s=1.33 \exp(-0.56x) \text{N}/\text{mm}^3$ ,  $\eta=0.25 \exp(-0.2x) \mu\text{Ns}/\text{mm}^3$ ,  $\sigma=1.5 \exp(-0.47x) \text{N}/\text{mm}^3$ ; (b) as in Fig. 6, except  $M=0.15 \exp(0.08x) \text{mg}/\text{mm}^2$ ,  $S=22.5 \exp(-0.32x) \text{N}/\text{mm}^3$ ,  $m=0.012 \exp(0.03x) \text{mg}/\text{mm}^2$ ,  $r=0.005 \exp(-0.3x) \mu\text{Ns}/\text{mm}^3$ ,  $s$ ,  $\eta$ ,  $\sigma$  as in (a).

The exponents (index 1) are again estimated from anatomical and physiological data. The coefficients (index 0) are added to the set of free parameters.

Figure 9 presents a comparison of fourth-order model calculations and a measured BM response showing sharp tuning. We selected the experiment of Khanna and Leonard discussed in the previous section because of the availability of a good set of TM and coupling parameters for the cat (Neely, 1981b). Figure 9a closely resembles Fig. 6.

The second resonant system hardly influences BM motion here. By another choice of parameters the BM response can be greatly modified, as in Fig. 9b, but not in a direction so as to reduce the discrepancy with the experimental results. A comparison with the data of Sellick *et al.* (1982) gives a qualitatively similar picture, with more uncertainties about the values of the parameters.

## VI. DISCUSSION

In this article we have examined whether it is possible to simulate measurements of BM motion quantitatively using a passive, linear model of the cochlea. We have foregone the problems associated with the nonlinear phenomena observed in most of the recent experiments by assuming that the cochlea behaves approximately as a linear system at low stimulus levels, and considering the lowest stimulus level used in the experiments.

Our findings are:

- *BM responses with a low tuning can be matched very well by calculations on a passive linear model.* This is consistent with the observation of linear behaviour of these responses over a considerable range of stimulus levels. Midly tuned BM responses are nowadays believed to reflect pathological cochleas, the pathology being due to the invasiveness of the measuring technique.
- *BM responses with a sharp tuning, which are thought to represent the behaviour of physiologically intact or almost intact cochleae, cannot be matched sufficiently using a passive linear model.* This is true even when the model has fourth order (two degrees of freedom) partition dynamics.
- Rhode's (1971, 1978) data, which are in between the two extremes as regards sharpness of tuning, can be matched to a limited extent, but not

really satisfactorily.

Consequently, linear passive models do their job quite well in situations where they may be expected to do so. For intact cochleae, the models are apparently inadequate. This conclusion is in contrast with that of Zwislocki (1983) who claims that a model with two degrees of freedom (the model considered in Fig. 8) can account qualitatively as well as quantitatively for the BM transfer characteristics. We disagree with his conclusions for three reasons:

- In Zwislocki's comparison with Sellick *et al.*'s (1982) data, one quite important measurement point has been omitted. This makes the bandwidth of the measured response seem smaller than it really is.
- The discrepancy between the model calculations and the data is, in our opinion, large. It is very similar to the discrepancy found in Fig. 5. In particular, the bandwidth of the model response is much smaller than that of the measured response.
- The experimental curves are ratios of BM displacement and sound pressure at the eardrum. The model output is BM/stapes transfer ratio. The required transfer function for sound pressure at the eardrum to stapes displacement was not taken into account by Zwislocki.

It is necessary to examine the possible reasons for the failure of passive cochlea models, lest we jump to the conclusion that the models should have active (that is, energy producing) features. Since the conclusions are valid within the framework set by the models, any simplification made could have caused the shortcoming. We have argued already that the restriction to linear phenomena is presumably admissible. Many other simplifications have been justified by Viergever (1980). The most dubious feature of the model is the representation of the organ of Corti. More detailed models, as for instance that of Taber and Steele (1981) which has four degrees of freedom, might give a better agreement with the data. We consider this unlikely though, in view of the results of the model containing two degrees of freedom (Section V). Of course, a distributed parameter model would provide for a perfect match, but it is unclear to us in which way the mechanical structure of the cochlea could induce such a model. Hence we arrive at the conclusion that *cochlear mechanics most likely requires a description in terms of an active model*.

The view that the cochlea is an active system, first suggested by Gold (1948), has gained appreciably in the last few years. Kemp (1978) discovered that sound energy is emitted by the auditory system into the external ear canal, following impulsive acoustic excitation. The emissions are inhibited by damage to the system, which makes it likely that their origin is a physiologically active mechanism. Also, spontaneous acoustic emissions from the cochlea have been observed (Kemp, 1979; Wilson, 1980). Bialek and Wit (1984) showed that such emissions are the result of an (unstable) active filtering process rather than being filtered noise. Bialek (1983a, 1983b) furthermore demonstrated that the threshold auditory signal is comparable to the expected level of quantum noise, and that the thermal noise of the stereocilia is at least 40 dB above the threshold signal. The only possible mechanism of noise reduction appears to be active mechanical feedback by means of quantum-limited amplifier at the level of stereocilium mechanics.

The conclusion of the present article signifies that the activity probably manifests itself already at the level of BM vibration. This supports De Boer's (1983a, 1983b) conclusion that active features are needed to account for the steep rise of the amplitude of the BM response on the low frequency side of the peak. Yet the active versus passive modelling controversy does not seem closed. Recently, an inverse method has been developed which allows determination of the BM impedance  $Z$  directly from BM velocity data. The real part of  $Z$  appears to be so sensitive to changes in the velocity response that any conclusion concerning active versus passive behaviour is unwarranted (Diependaal *et al.*, 1986). Consequently, more research is needed before a definitive conclusion can be drawn about the (im)possibility to reconcile the sharply tuned data of BM motion with a passive, linear model of the cochlea.

#### ACKNOWLEDGEMENT

This research has been supported in part by the Netherlands Organization for the Advancement of Pure Research (ZWO).

#### APPENDIX: 1D AND 2D ANALOGUES OF THE PARALLEL-BEAMS MODEL

Equation (13) of the main text describes the representation of the BM by a series of parallel viscoelastic beams. The boundary value problem consisting

of Eq. (13) and the boundary conditions (10) is readily solved by expanding  $V(x,y)$  in a Fourier sine series in  $y$ :

$$V(x,y) = \sum_{k=1}^{\infty} V_k(x) \sin\{k \pi(y - b_1)/\beta\}, \quad b_1 < y < b_2 \quad (\text{A1})$$

Notice that this expansion obeys the boundary conditions at  $y = b_1$  and  $y = b_2$ . On physical grounds we suppose that  $V(x,y)$  is a continuous function of bounded variation in  $b_1 < y < b_2$ . The series in Eq. (A1) then converges uniformly to  $V$  in this interval, and the coefficients  $V_k$  follow from

$$V_k(x) = \frac{2}{\beta} \int_{b_1}^{b_2} V(x,y) \sin\{k \pi(y - b_1)/\beta\} dy \quad (\text{A2})$$

The trans-BM pressure  $P(x,y,0)$  is expanded likewise over the width of the BM:

$$P(x,y,0) = \sum_{k=1}^{\infty} P_k(x) \sin\{k \pi(y - b_1)/\beta\}, \quad b_1 < y < b_2, \quad (\text{A3})$$

$$P_k(x) = \frac{2}{\beta} \int_{b_1}^{b_2} P(x,y,0) \sin\{k \pi(y - b_1)/\beta\} dy. \quad (\text{A4})$$

Upon inserting the expansions (A1) and (A3) into the beam equation (13), we obtain

$$V_k = \frac{j \omega P_k}{(k \pi/\beta)^4 D_f - \rho_p \omega^2 H} \quad (\text{A5})$$

Equations (A1) and (A5) give the solution  $V(x,y)$  to the boundary value problem (13)+(10) in terms of the Fourier sine coefficients  $P_k$ . Upon combining this with Eq. (8) we arrive at

$$\left. \frac{\partial P}{\partial z} \right|_{z=0} = \begin{cases} -2\rho\omega^2 \sum_{k=1}^{\infty} \frac{P_k \sin\{k \pi(y - b_1)/\beta\}}{(k \pi/\beta)^4 D_f - \rho_p \omega^2 H}, & b_1 < y < b_2 \\ 0, & 0 \leq y \leq b_1, b_2 \leq y \leq b. \end{cases} \quad (\text{A6})$$

The 3D model in which the BM is represented by a system of parallel simply supported visco-elastic beams, is now described by Eqs. (2)-(7) of the main text and (A6). The 2D analogue is found in a straightforward manner by application of Eq. (11). The result is (Viergever, 1980)

$$\frac{\partial^2 P^{2D}}{\partial x^2} + \frac{\partial^2 P^{2D}}{\partial z^2} = 0 \quad (\text{A7})$$

$$\frac{\partial P^{2D}}{\partial x} \Big|_{x=0} = 2j\omega\rho A_{st}/bh \quad (\text{A8})$$

$$\frac{\partial P^{2D}}{\partial x} \Big|_{x=l} = 0 \quad (\text{A9})$$

$$\frac{\partial P^{2D}}{\partial z} \Big|_{z=h} = 0 \quad (\text{A10})$$

$$\frac{\partial P^{2D}}{\partial z} \Big|_{z=0} = -\frac{16\rho\omega^2\beta P^{2D}}{\pi^2 b} \times \sum_{k=1,3,5,\dots}^{\infty} \frac{1}{k^2 \{(k\pi/\beta)^4 D_f - \rho_p \omega^2 H\}} \quad (\text{A11})$$

Subsequent application of Eq. (12) gives the 1D analogue:

$$\frac{d^2 P^{1D}}{dx^2} = -\frac{16\rho\omega^2\beta P^{1D}}{\pi^2 bh} \times \sum_{k=1,3,5,\dots}^{\infty} \frac{1}{k^2 \{(k\pi/\beta)^4 D_f - \rho_p \omega^2 H\}} \quad (\text{A12})$$

$$\frac{dP^{1D}}{dx} \Big|_{x=0} = 2j\omega\rho A_{st}/bh \quad (\text{A13})$$

$$\frac{dP^{1D}}{dx} \Big|_{x=l} = 0 \quad (\text{A14})$$

An impedance representation is easily derived for the parallel beams model. The convergence of the series (A1) towards the BM velocity  $V(x,y)$  is very fast; the  $V_k$  are  $O(k^{-5})$  as  $k \rightarrow \infty$ , which follows from repeated partial integration of the right-hand side of Eq. (A2) and application of the boundary conditions (10). We therefore make a negligibly small error if we replace the series with its leading term. In fact, Taber (1979) showed that the error is only 0.14% for a uniform (that is, independent of  $y$ ) trans-BM pressure. So we have

$$V(x,y) = V_1(x) \sin\{\pi(y-b_1)/\beta\} \quad (\text{A15})$$

if we exclude unrealistic pressure distributions like a point load somewhere on the BM. This result means that *any distribution of pressure over the width causes the BM to have a half-sine-shaped velocity distribution* (see also Diependaal and Viergever, 1983).

All we have to do now to characterize the behaviour of the BM by a point-impedance function is to replace the actual trans-BM pressure  $P(x,y,0)$  by a half sine shaped distribution that produces the same velocity pattern. This

is, of course, the first term of the Fourier sine expansion in Eq. (A3). Hence we arrive at the following definition of the specific acoustic impedance of the BM (*i.e.*, the quotient of trans-BM pressure and BM particle velocity):

$$Z(x) = \frac{P_1(x)}{V_1(x)} = \frac{2}{\beta V_1} \int_{b_1}^{b_2} P(x, y, 0) \sin\{\pi(y - b_1)/\beta\} dy \quad (A16)$$

The relation between  $Z(x)$  and the beam parameters is found from Eq. (A5) for  $k=1$ . It reads

$$Z = \left( \frac{\pi}{\beta} \right)^4 \frac{D_f}{j\omega} + j\omega\rho_p H \quad (A17)$$

The consequences of the impedance representation for the 2D and 1D analogues of the parallel beams model are easily found. For the 2D model, the boundary condition (A11) becomes

$$\frac{\partial P^{2D}}{\partial z} \Big|_{z=0} = \frac{16j\omega\rho\beta P^{2D}}{\pi^2 b Z} \quad (A18)$$

and for the 1D model the differential equation (A14) changes into

$$\frac{d^2 P^{1D}}{dx^2} = \frac{16j\omega\rho\beta P^{1D}}{\pi^2 b h Z} \quad (A19)$$

## REFERENCES

- Allen, J.B. (1977). Two-dimensional cochlear fluid flow model: New results. *J. Acoust. Soc. Am.* 61, 110-119.
- Allen, J.B. (1980). A cochlear micromechanical model of transduction. In: *Psychophysical, Physiological and Behavioural Studies in Hearing*, pp. 85-95. Editors: G. van den Brink and F.A. Bilsen. Delft University Press, Delft.
- Allen, J.B. and Sondhi, M.M. (1979). Cochlear macromechanics: Time-domain solutions. *J. Acoust. Soc. Am.* 66, 123-132.
- Békésy, G. von (1960). *Experiments in Hearing*. McGraw-Hill, New York.
- Bialek, W.S. (1983a). Quantum effects in the dynamics of biological systems. Doctoral dissertation, Lawrence Berkeley Laboratory and University of California, Berkeley.
- Bialek, W.S. (1983b). Thermal and quantum noise in the inner ear, in *Mechanics of Hearing*, pp. 185-192. Editors: E. de Boer and M.A. Viergever. Martinus Nijhoff Publishers/Delft U.P., Delft.
- Bialek, W.S. and Wit, H.P. (1984). Quantum limits to oscillatory stability theory and experiments on acoustic emissions from the human ear, *Phys. Lett.* 104A, 173-178.
- Boer, E. de (1983a). No sharpening? A challenge for cochlear mechanics. *J. Acoust. Soc. Am.* 73, 567-573.
- Boer, E. de (1983b). On active and passive cochlear models - Towards a generalized analysis. *J. Acoust. Soc. Am.* 73, 574-576.
- Boer, E. de and Viergever, M.A. (1982). Validity of the Liouville-Green (or WKB) method

- for cochlear mechanics. *Hear. Res.* 8, 131-155.
- Boer, E. de and Viergever, M.A. (1984). Wave propagation and dispersion in the cochlea. *Hearing Res.* 13, 101-112.
- Diependaal, R.J. and Viergever, M.A. (1983). Point-impedance characterization of the basilar membrane in a three-dimensional cochlea model. *Hear. Res.* 11, 33-40.
- Diependaal, R.J., Viergever, M.A., and Boer, E. de (1986). Are active elements necessary in the basilar membrane impedance? *J. Acoust. Soc. Am.* 80, 124-132.
- Evans, E.F. and Wilson, J.P. (1975). Cochlear tuning properties: Concurrent basilar membrane and single nerve fiber measurements. *Science* 190, 1218-1221.
- Flügge, W. (1975). Viscoelasticity. Springer, Berlin.
- Gold, T. (1948). Hearing II. The physical basis of the action of the cochlea. *Proc. R. Soc. Edinb.* B135, 492-498.
- Gummer, A.W., Johnstone, B.M. and Armstrong, N.J. (1981). Direct measurement of basilar membrane stiffness in the guinea pig. *J. Acoust. Soc. Am.* 70, 1298-1309.
- Iurato, S. (1962). Functional implications of the nature and submicroscopic structure of the tectorial and basilar membranes. *J. Acoust. Soc. Am.* 34, 1386-1395.
- Johnstone, B.M. and Yates, G.K. (1974). Basilar membrane tuning curves in the guinea pig. *J. Acoust. Soc. Am.* 55, 584-587.
- Johnstone, B.M., Taylor, K.J. and Boyle, A.J. (1970). Mechanics of the guinea pig cochlea. *J. Acoust. Soc. Am.* 47, 504-509.
- Kemp, D.T. (1978). Stimulated acoustic emissions from within the human auditory system. *J. Acoust. Soc. Am.* 64, 1386-1391.
- Kemp, D.T. (1979). Evidence of nonlinearity and frequency selective wave amplification in the cochlea. *Arch. Oto-Rhino-Laryngol.* 224, 37-45.
- Khanna, S.M. and Leonard, D.G.B. (1982). Basilar membrane tuning in the cat cochlea. *Science* 215, 305-306.
- Kohlöffel, L.U.E. (1972). A study of basilar membrane vibrations. *Acustica* 27, 49-89.
- Leonard, D.G.B. and Khanna, S.M. (1984). Histological evaluation of damage in cat cochleas used for measurement of basilar membrane mechanics. *J. Acoust. Soc. Am.* 75, 515-527.
- Miller, C.E. (1983). Static point-load measurements of basilar membrane compliance. In: *Mechanics of Hearing*, pp. 203-210. Editors: E. de Boer and M.A. Viergever. Martinus Nijhoff Publ., The Hague/Delft University Press, Delft.
- Neely, S.T. (1981a). Finite difference solution of a two-dimensional mathematical model of the cochlea. *J. Acoust. Soc. Am.* 69, 1386-1393.
- Neely, S.T. (1981b). Fourth-order partition dynamics for a two-dimensional model of the cochlea. Doctoral dissertation, Washington University, St. Louis, MO.
- Rhode, W.S. (1971). Observations of the vibration of the basilar membrane in squirrel monkeys using the Mössbauer technique. *J. Acoust. Soc. Am.* 49, 1218-1231.
- Rhode, W.S. (1987). Some observations on cochlear mechanics. *J. Acoust. Soc. Am.* 64, 158-176.
- Sellick, P.M., Patuzzi, R., and Johnstone, B.M. (1982). Measurements of basilar membrane motion in guinea pig using the Mössbauer technique. *J. Acoust. Soc. Am.* 72, 131-141.
- Sellick, P.M., Yates, G.K., and Patuzzi, R. (1983). The influence of Mössbauer source size and position on phase and amplitude measurements of the guinea pig basilar membrane. *Hear. Res.* 10, 101-108.
- Steele, C.R. (1974). Behavior of the basilar membrane with pure-tone excitation. *J. Acoust. Soc. Am.* 55, 148-162.
- Steele, C.R. (1976). Cochlear mechanics. In: *Handbook of Sensory Physiology*, Vol. V/3: *Auditory System: Clinical and Special Topics*, pp. 443-478. Editors: W.D. Keidel and W.D. Neff. Springer-Verlag, Berlin.
- Steele, C.R. (1980). Lecture notes on cochlear mechanics. Conference on Mathematical Modeling of the Hearing Process, Troy, NY.
- Steele, C.R. and Taber, L.A. (1979). Comparison of WKB calculations and experimental results for a three-dimensional cochlear models. *J. Acoust. Soc. Am.* 65, 1007-1018.

- Taber, L.A. (1979). An analytic study of realistic cochlear models including three-dimensional fluid motion. Doctoral dissertation, Stanford University, Stanford, CA.
- Taber, L.A. and Steele, C.R. (1981). Cochlear model including three-dimensional fluid and four modes of partition flexibility. *J. Acoust. Soc. Am.* 70, 426-436.
- Timoshenko, S.P. and Woinowsky-Krieger, S. (1959). Theory of plates and shells. McGraw-Hill Kogakusha, Tokyo.
- Viergever, M.A. (1980). Mechanics of the inner ear - A mathematical approach. Doctoral dissertation, Delft University of Technology, Delft University Press, Delft.
- Viergever, M.A. and Diependaal, R.J. (1983). Simultaneous amplitude and phase match of cochlear model calculations and basilar membrane vibration data. In: *Mechanics of Hearing*, pp. 53-61. Editors: E. de Boer and M.A. Viergever. Martinus Nijhoff Publ., The Hague/Delft University Press, Delft.
- Voldrich, L. (1978). Mechanical properties of the basilar membrane. *Acta Otolaryngol.* 86, 331-335.
- Whitham, G.B. (1974). *Linear and Nonlinear Waves*. Wiley, New York.
- Wilson, J.P. (1980). Evidence for a cochlear origin for acoustic re-emission, threshold fine structure and tinnitus. *Hearing Res.* 2, 233-252.
- Wilson, J.P. and Johnstone, J.R. (1975). Basilar membrane and middle-ear vibration in guinea pig measured by capacitive probe. *J. Acoust. Soc. Am.* 57, 705-723.
- Zwislocki, J.J. (1980a). Two possible mechanisms for the second cochlear filter. In: *Psychophysical, Physiological and Behavioural Studies in Hearing*, pp. 16-23. Editors: G. van den Brink and F.A. Bilsen. Delft University Press, Delft.
- Zwislocki, J.J. (1980b). Five decades of research on cochlear mechanics. *J. Acoust. Soc. Am.* 67, 1679-1685.
- Zwislocki, J.J. (1983). Sharp vibration maximum in the cochlea without wave reflection. *Hearing Res.* 9, 103-111.

## CHAPTER TWO

# Are active elements necessary in the basilar membrane impedance?

**Abstract** This article is motivated by the current hypothesis [Kim *et al.*, Psychological, Physiological and Behavioral Studies in Hearing (Delft U.P., The Netherlands, 1980); Neely, Doctoral dissertation, Washington University, St. Louis, MO (1981); De Boer, J. Acoust. Soc. Am. 73, 567-573 (1983a) and 73, 574-576 (1983b)] that it is necessary to include active elements in the basilar membrane (BM) impedance in order to explain recent data on the vibration of the BM [Khanna and Leonard, Science 215, 305-306 (1982); Sellick *et al.*, J. Acoust. Soc. Am. 72, 131-141 (1982); Robles *et al.*, Peripheral Auditory Mechanisms (Springer, New York, 1986)]. In order to test this hypothesis, first, a method which is an inversion of the customary description of cochlear mechanics is described. Instead of computing the BM velocity for a given point impedance of the membrane, we show how to compute the impedance function from a given BM velocity pattern in response to a sinusoidal input at the stapes. This method is then used to study the sensitivity of the recovered impedance to perturbations in the velocity pattern. The simulations used show that the real part of the impedance is extremely sensitive to such perturbations. Therefore, measured velocity patterns are unlikely to resolve the issue of whether active elements should be included. Frequency responses measured at a few points on the membrane are even less likely so.

## INTRODUCTION

Recent measurements of Khanna and Leonard (1982), Sellick *et al.* (1982), and Robles *et al.* (1986) show very sharp tuning of the basilar membrane (BM) as compared to the earlier data observed by, e.g., Rhode (1971), and Johnstone and Yates (1974). This poses a great problem for cochlear modeling. The mildly tuned responses can all be matched quite well by calculations on a passive model but the sharply tuned responses do not seem to admit of such a match (Viergever and Diependaal, 1983, 1986).

In recent years many investigators (Kim *et al.*, 1980; Neely, 1981; Neely and Kim, 1983) have made use of a negative resistance to match model results with experimental data. In fact, De Boer (1983a, 1983b) concludes that active properties are needed to account for the steep rise of the amplitude of the BM response on the low-frequency side of the peak. This conclusion is reached by first approximating the BM velocity by a revcor-

spectrum-like response and next showing that such a response can only be simulated by a cochlear model when the real part of the impedance is made negative in the region to the left of the response peak.

This shift towards cochlea models with active elements makes it necessary to enlarge our knowledge about the mechanical properties of the BM. These properties are often described by a complex-valued point impedance function. The profile of the real part of this impedance is our main concern: We would like to know whether, and if so, in which region, this quantity should be negative in order that the sharply tuned BM data are adequately modeled.

There are several approaches for estimating the mechanical properties of the BM.

- Direct measurement of the impedance components. This has only been achieved for the compliance and mass parts, not for the resistance. Compliance measurements have been performed by Von Békésy (1960), Gummer *et al.* (1981), and Miller (1983, 1985). However, the picture that can be formed from these data is far from complete.
- Measurement of both BM velocity and trans-BM pressure. After such experiments the impedance is found by simply dividing pressure and velocity. Although intracochlear sound pressure measurements have been reported by Burgeat *et al.* (1963), Nedzelnitsky (1974), and Dancer and Franke (1980), experiments in which pressure and velocity are measured simultaneously are not known to us. So the impedance has to be derived from pressure and velocity data obtained in different experiments. Another objection is that it is quite difficult to measure the trans-BM pressure. On either side of the BM the probe must be situated very close to the membrane, because of the short-wave character of the fluid motion near the place of maximum BM velocity. The reported pressure measurements do not seem to satisfy this condition.
- Curve fitting of model results to experimental data. The starting point of this approach is the construction of a model that describes the dynamics of the cochlea (Fig. 1). By means of this model the BM velocity is computed based on a rough estimate of the impedance parameters. A comparison of the results with BM vibration data shows in which way the parameters should be modified. The procedure is repeated until the best possible agreement (in some sense) of model results with experimental

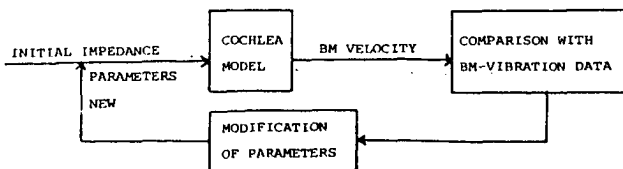


Figure 1. Flow diagram of the curve fitting procedure.

data has been obtained. Curve fitting has been used more or less successfully by many investigators (for a survey, see Viergever and Diependaal, 1983). The advantage of this approach is that *a priori* knowledge about the impedance, such as the global behavior of the parameters as a function of the coordinate along the membrane, can be used. The drawback is that the procedure needs many computer runs before satisfactory results are obtained.

- Measurement of impulse response at the stapes. Sondhi (1981) formulated an integral equation from which the stiffness of the BM can be computed. His method requires measurement of the pressure just inside the cochlea at the stapes end in response to an impulse of stapes velocity. For our present purpose, however, this method is not useful because it does not provide the resistive component of the impedance.
- Measurement of spatial velocity pattern for sinusoidal inputs. Neely (1980) sketched a method of determining the BM impedance from spatial pattern of the motion of the partition in response to a sinusoidal input. He assumed a two-dimensional cochlea.

The approach we present here is in the spirit of Neely's. However, in order to clearly expose the possibilities and limitations of the method we will restrict ourselves to a one-dimensional formulation. From the standard cochlea model equations we derive an expression for the impedance in terms of the BM velocity. The impedance parameters can then be computed from any set of BM vibration data in the spatial domain.

It is important to note that our method requires the spatial distribution of velocity. To our knowledge no one has ever been able to measure this function in living animals. Our purpose, however, is not to derive the BM impedance from measurements, but to decide whether or not measurements of velocity can ever give us the impedance with any degree of reliability. In the succeeding sections we will give some answers to this question by

simulation studies.

The plan of the paper is as follows: In Sec. I we give the formulation of the forward problem for the 1D cochlear model, and in Sec. II the corresponding inverse problem is solved. The method is validated in Sec. III by using simulated BM data as input. In the same section we investigate, again by simulation, the consequences of slight perturbations in the velocity data which are used as input to the inverse problem. If the BM impedance is to be estimated this way, the reconstruction should be insensitive to unavoidable experimental errors. However, our simulations show that slight perturbations may cause very large deviations in the results, especially in the real part of the computed impedance function. Why this is so is analyzed in Sec. IV. The conclusion, that the inverse method presented here is at best adequate for estimating the imaginary part of the BM impedance, is discussed in Sec. V. Suggestions as to how the method may be improved are given.

## I. THE FORWARD PROBLEM

In the 1D (long-wave) formulation, the dynamics of the BM is represented by a second-order ordinary differential equation (see e.g. Viergever, 1980):

$$\frac{d^2(ZV)}{dx^2} - \frac{2j\omega\rho\beta}{A}V = 0. \quad (1)$$

To complete the model two boundary conditions are needed:

$$\frac{d(ZV)}{dx} = 2j\omega\rho, \quad x=0 \quad (2a)$$

$$ZV=0, \quad x=L. \quad (2b)$$

Since the longitudinal fluid velocity (*i.e.*, the velocity in the  $x$  direction) is proportional to  $d(ZV)/dx$ , condition (2a) is equivalent to prescribing the stapes velocity. The second condition expresses that the transmembrane pressure, which equals  $ZV$ , vanishes at the helicotrema ( $x=L$ ).

The symbols are defined as follows:

|                 |   |
|-----------------|---|
| $x \in [0, L]$  | coordinate along the BM   |
| $L$             | length of the BM  |
| $j$             | imaginary unit  |
| $\omega$        | radian frequency of stapes motion   |
| $\rho$          | fluid density   |
| $\beta(x)$      | BM width  |
| $A(x)$          | area of cross section of one channel<br>(the model consists of two channels<br>having equal cross sections) |
| $Z(x; j\omega)$ | specific acoustic impedance of the BM   |
| $V(x; j\omega)$ | velocity of BM normalized to<br>the stapes velocity   |

The dependence of  $Z(x; j\omega)$  and  $V(x; j\omega)$  on the radian frequency  $\omega$  will not be shown explicitly further on in this article.

## II. THE INVERSE PROBLEM

In order to derive the formulation of the inverse problem we start with Eq. (1), but instead of Eqs. (2a) and (2b) we consider the following conditions:

$$ZV=0, \quad x=L \quad (3a)$$

$$\frac{d(ZV)}{dx}=P_L, \quad x=L. \quad (3b)$$

Conditions (3a) and (3b) lead to a numerical more stable inverse problem than do conditions (2a) and (2b). The conditions express, effectively, that at the helicotrema the transmembrane pressure is equal to zero and that the longitudinal fluid velocity is some constant.

Now we can solve the inverse problem by integrating Eq. (1) twice, using (3a) and (3b). The result is:

$$Z(x)V(x)=P_L(x-L)+2j\omega\rho\int_x^L\int_\eta^L\frac{\beta(\xi)V(\xi)}{A(\xi)}d\xi d\eta. \quad (4)$$

The right-hand side of Eq. (4) can be reduced to a single integral using integration by parts so that we obtain the following explicit expression for the impedance of the BM:

$$Z(x) = \frac{P_L(x-L)}{V(x)} + \frac{2j\omega\rho}{V(x)} \int_x^L (\xi-x) \frac{\beta(\xi)V(\xi)}{A(\xi)} d\xi. \quad (5a)$$

If we exclude the lowest frequencies in the range of hearing, the first term of the right-hand side of Eq. (5a) is much smaller than the second term along the relevant part of the BM (*i.e.*, everywhere except for the apical part, where the response is negligibly small). We therefore approximate Eq. (5a) by

$$Z(x) = \frac{2j\omega\rho}{V(x)} \int_x^L (\xi-x) \frac{\beta(\xi)V(\xi)}{A(\xi)} d\xi. \quad (5b)$$

From Eq. (5b) it is clear that in order to determine the impedance at the place  $x$ , we only need to know, apart from geometry parameters, the BM velocity between  $x$  and  $L$ .

### III. NUMERICAL RESULTS

#### A. Validation of the method

In order to validate the inverse method we select a reference impedance and solve the forward problem [Eqs. (1), (2a), (2b)]. This is done numerically by substituting central difference quotients for the differential quotients in Eq. (1). The BM velocity function generated this way is substituted in Eq. (5b) to yield the impedance. The integral is evaluated by the trapezoidal rule.

In Fig. 2 the results of the validation are shown for a 1 kHz tone (for other parameters see the legend to the figure). In Fig. 2(a) the impedance has an overall passive behavior whereas in Fig. 2(b) the real part of the impedance is negative over a limited region on the basal side of the velocity amplitude peak.

At this point a remark has to be made. The velocity amplitude peak in the active case is only about 5 dB higher than that in the passive case. A higher amplitude peak can be realized by making the real part of the impedance more negative. It is difficult, however, to realize a higher amplitude peak in a long-wave model without generating reflections in the response. For the purpose of this paper we have avoided such complications, and restricted ourselves to active impedance functions that give only a moderate elevation of the velocity amplitude peak.

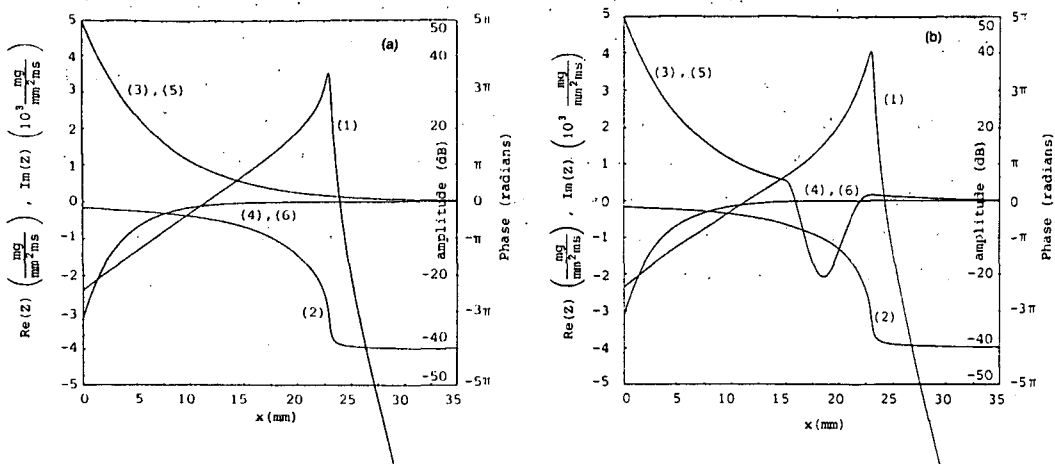


**Figure 2.** Comparison of reconstructed impedance function to reference impedance function. Parameters:  $L = 35 \text{ mm}$ ,  $\omega = 2\pi \text{ kHz}$ ,  $\rho = 1 \text{ mg/mm}^3$ ,  $\beta = 0.08 \exp(0.05x) \text{ mm}$ ,  $A = 1 \text{ mm}^2$ . Selected reference impedance  $Z = j\omega M + R + S/(j\omega)$  with  $M = 0.5 \text{ mg/mm}^2$ ,  $R = R_0 \exp(-0.15x) \text{ mg}/(\text{mm}^2 \text{ ms})$ . (a)  $R_0 = 5 \text{ mg}/(\text{mm}^2 \text{ ms})$ , (b)  $R_0 = 20 \cos[2\pi(x-15)/8] - 15 \text{ mg}/(\text{mm}^2 \text{ ms})$ ,  $15 < x \leq 23 \text{ mm}$ ,  $R_0 = 5 \text{ mg}/(\text{mm}^2 \text{ ms})$ , elsewhere.  $S = 20000 \exp(-0.3x) \text{ mg}/(\text{mm}^2 \text{ ms}^2)$ . Curves: (1) amplitude of BM velocity, (2) phase of BM velocity, (3) real part of reference impedance, (4) imaginary part of reference impedance, (5) real part of reconstructed impedance, (6) imaginary part of reconstructed impedance.

Difference between the selected impedance function and the reconstructed one are not noticeable in either figure. This leads us to the conclusion that the inversion method is sufficient accurate in the numerical sense.

## B. Simulation

Given a set of BM vibration data, we can obtain the impedance from Eq. (5b). But at this point there appears a problem; in order to use Eq. (5b) the BM velocity must be known as a function of place for a given frequency. The experiments, however, yield frequency response curves; that is, the BM velocity as a function of frequency at a fixed position on the membrane. Hence, in order to find the impedance from experimental data, we would have to transform the data from the frequency domain into the spatial domain using a cochlear map. This cochlear map is, however, not independent of the BM impedance, which complicates matters considerably. In this article we avoid the problems associated with defining a proper cochlear map by generating a BM velocity pattern in the desired form (fixed frequency, variable space coordinate).

Simulation of inversion from measured data is carried out in the following way. We first select a reference impedance (parameters in a physiologically realistic range) and compute the BM velocity function solving the forward problem. Then the amplitude or the phase of the response function is slightly perturbed, thus simulating measurement inaccuracies and errors resulting from a cochlear map. The impedance functions reconstructed from these perturbed data may show a deviant, rather unpredictable, behavior as is illustrated Figs. 3 and 4.

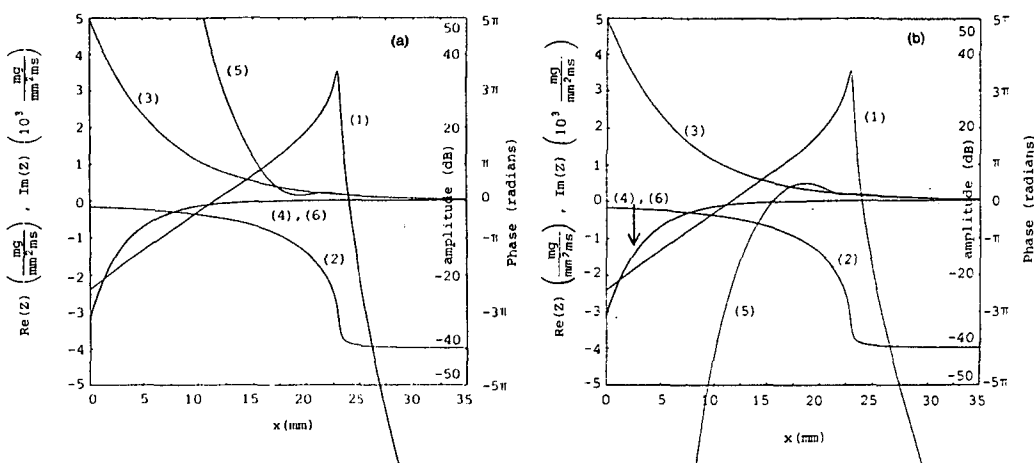


**Figure 3.** Impedance reconstruction for apically disturbed amplitude of BM velocity function (passive case). Amplitude disturbance: (a)  $\Delta a(x) = -10(x-23.5)/11.5 \text{ dB}$ ,  $23.5 \leq x \leq 35 \text{ mm}$ . (b)  $\Delta a(x) = +10(x-23.5)/11.5 \text{ dB}$ ,  $23.5 \leq x \leq 35 \text{ mm}$ , (a) and (b)  $\Delta a(x) = 0$ , elsewhere. Curves: (1) disturbed amplitude of BM velocity, (2) phase of BM velocity, (3) real part of reference impedance, (4) imaginary part of reference impedance, (5) real part of reconstructed impedance, (6) imaginary part of reconstructed impedance. Parameters as in Fig. 2(a).

Figure 3 relates to a cochlea exhibiting an overall passive behavior and Fig. 4 to a cochlea in which locally active properties are incorporated. The perturbations [ $\Delta a(x)$ ] added to the amplitude of the velocity data consist of making the slope of the amplitude curve at the apical side of the peak steeper [Figs. 3(a) and 4(a)] or less steep [Figs. 3(b) and 4(b), see legends to the figures]. In both pictures the imaginary part of the impedance is seen to be reconstructed quite well. [Compare curves (4) and (6) of the figures.] For the real part, on the other hand, things are worse. When we go along the BM from the helicotrema to the stapes we see that the real part is reconstructed well up to the place of maximum velocity amplitude and a few mm beyond.

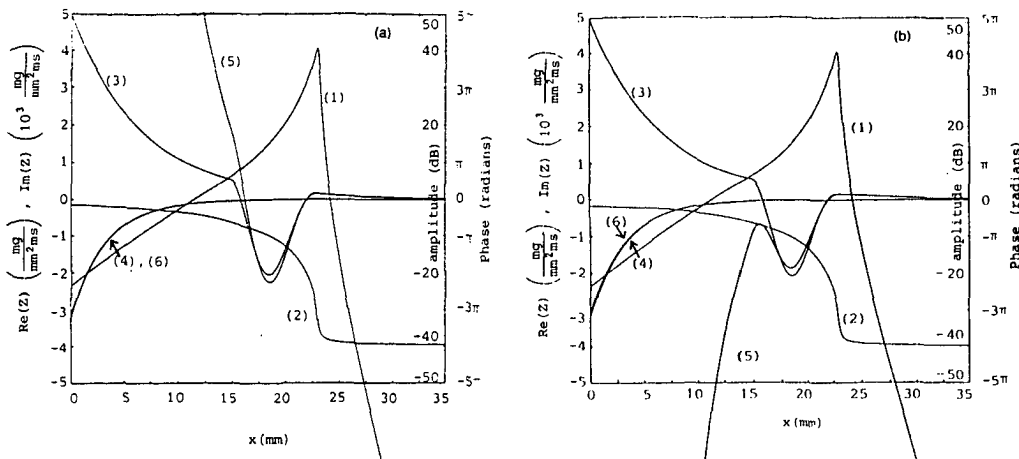


**Figure 4.** Impedance reconstruction for apically disturbed amplitude of BM velocity function (active case). Curves: (1) disturbed amplitude of BM velocity, (2) phase of BM velocity, (3) real part of reference impedance, (4) imaginary part of reference impedance, (5) real part of reconstructed impedance, (6) imaginary part of reconstructed impedance. Parameters as in Fig. 2(b),  $\Delta a(x)$  as in Fig. 3.

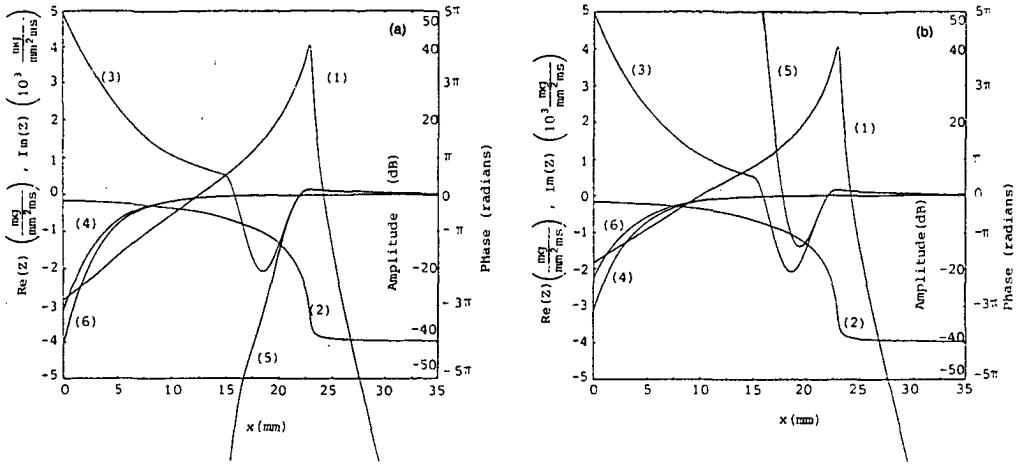
Further towards the base the departure from the reference curve is considerable. [Compare curves (3) and (5) in the figures.] Even the sign of the real part of the reconstructed impedance can be opposite here to that of the reference impedance [Figs. 3(b) and 4(b)].

Figure 5 shows two results of the reconstruction where the initial slope of the BM velocity amplitude has been perturbed (for details, see legend to the figure). Now the influence of the perturbations on the reconstruction of the imaginary part is larger than in Figs. 3 and 4, but the result is still acceptable. [Compare the difference between curves (4) and (6).] The reconstructed real part again deviates much from its reference value up to several mm to the left of the amplitude peak.

We also reconstructed the impedance from a BM velocity function of which the phase function has been perturbed by an amount  $\Delta\phi(x)$ . The results are plotted in Fig. 6. Once again the imaginary part of the impedance is reconstructed quite well but the real part of the reconstructed impedance deviates to an unacceptable extend from the reference curve.

### C. Re-validation

The results in Sec. IIIB casts doubt on the reconstructed impedance. Could



**Figure 5.** Impedance reconstruction for basally disturbed amplitude of BM velocity function (active case). Amplitude disturbance: (a)  $\Delta\alpha(x) = -5(22-x)/22 \text{ dB}$ ,  $0 \leq x \leq 22 \text{ mm}$ , (b)  $\Delta\alpha(x) = +5(22-x)/22 \text{ dB}$ ,  $0 \leq x \leq 22 \text{ mm}$ , (a) and (b)  $\Delta\alpha(x) = 0$ , elsewhere. Curves: (1) disturbed amplitude of BM velocity, (2) phase of BM velocity, (3) real part of reference impedance, (4) imaginary part of reference impedance, (5) real part of reconstructed impedance, (6) imaginary part of reconstructed impedance. Parameters as in Fig. 2(b).

its peculiar behavior be due to errors introduced by the numerical scheme, in spite of the validation made in Sec. IIIA? We therefore rechecked the validity of the inversion method with respect to numerical inaccuracies in the following way. Three BM velocity functions are computed and plotted in Fig. 7. The velocity response with label (1) is computed directly [by solving Eqs. (1), (2a), and (2b) using the reference impedance]. The curves labeled (2) represent the perturbed BM velocity. [For Fig. 7(a) and (b) the same perturbations have been used as for Fig. 5(a) and (b), respectively; for details, see the legends to these figures.] The response labeled (3) is the result of the forward problem using the impedance reconstructed from the perturbed data [curves (5) and (6) of Fig. 5].

No difference can be observed between the curves (2) and (3) of Fig. 7. This confirms the numerical accuracy of the reconstruction procedure.

Apparently, small changes in the velocity function may cause large variations (in the real part of) the impedance. Or, putting it in another way, impedances that differ much in their real parts may lead to velocity patterns with only small differences. Because of this property it is useful to analyze the sensitivity of the real and imaginary parts of the reconstructed

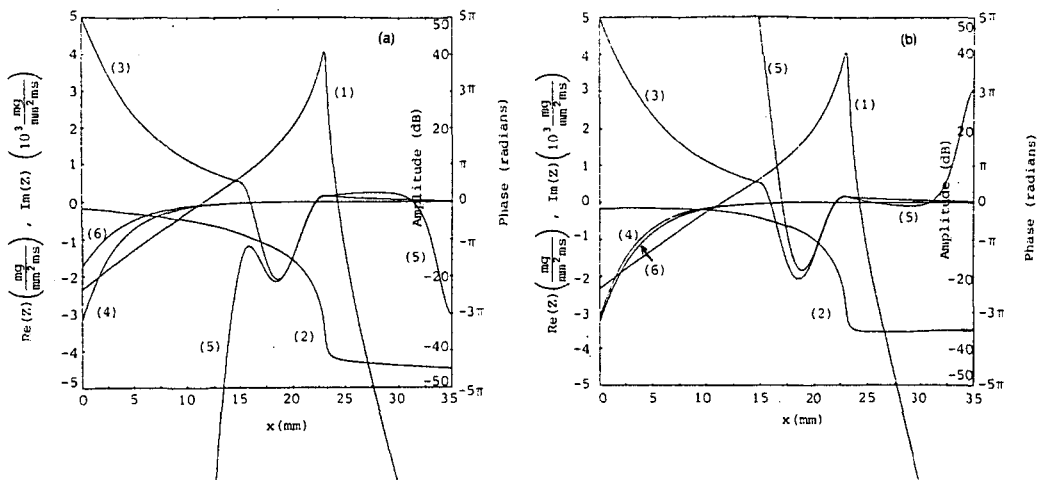


**Figure 6.** Impedance reconstruction for disturbed phase of BM velocity function (active case). Phase disturbance: (a)  $\Delta\phi(x) = -\pi x/70$ , (b)  $\Delta\phi(x) = +\pi x/70$ . Curves: (1) amplitude of BM velocity, (2) disturbed phase of BM velocity, (3) real part of reference impedance, (4) imaginary part of reference impedance, (5) real part of reconstructed impedance, (6) imaginary part of reconstructed impedance. Parameters as in Fig. 2(b).

impedances to perturbations in the BM velocity data. This is subject of the next section.

#### IV. SENSITIVITY ANALYSIS

In this section we shall attempt to explain the behavior described in the preceding section: Almost equal BM velocities may correspond to greatly different impedances, especially when the impedance differences concerns the real parts.

The starting point of our analysis is Eq. (5b). We first split this equation into its real and imaginary parts by introducing new variables  $Z_R$ ,  $Z_I$ ,  $a$ , and  $\phi$  as follows:

$$Z(x) = Z_R(x) + jZ_I(x), \quad Z_R \text{ and } Z_I \text{ real}, \quad (6)$$

$$V(x) = a(x) \exp[j\phi(x)], \quad a \text{ and } \phi \text{ real}, \quad a \geq 0. \quad (7)$$

These substitutions change Eq. (5b) into

$$Z_R(x) = \frac{2\omega\rho}{a(x)} \int_x^L (\xi - x) \frac{\beta(\xi)a(\xi)}{A(\xi)} \sin[\phi(x) - \phi(\xi)] d\xi \quad (8)$$

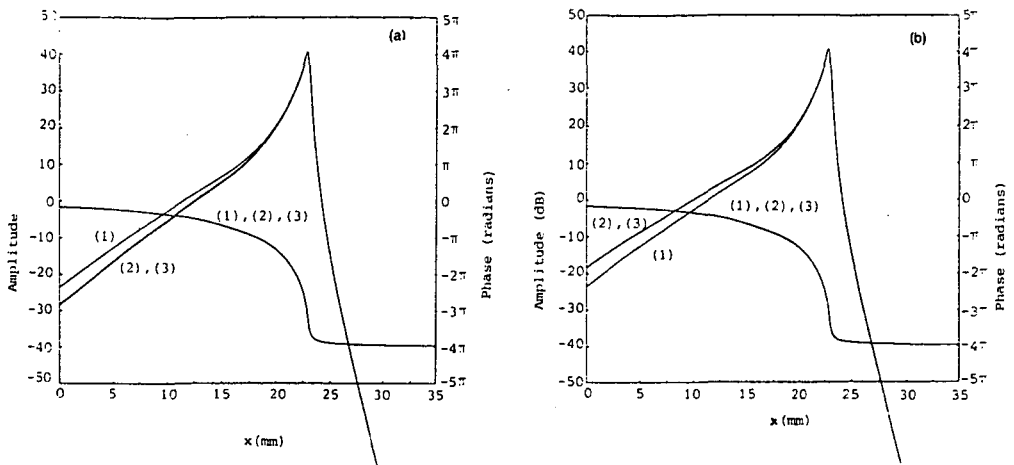


Figure 7. Revalidation of the method. Curves: (1) BM velocity computed using the reference impedance plotted in Fig. 5 [curves (3) and (4)], (2) disturbed version of (1), (3) BM velocity computed using the reconstructed impedance plotted in Fig. 5 [curves (5) and (6)].

and

$$Z_I(x) = \frac{2\omega\rho}{a(x)} \int_x^L (\xi-x) \frac{\beta(\xi)a(\xi)}{A(\xi)} \cos[\phi(x)-\phi(\xi)] d\xi. \quad (9)$$

With this formulation we can independently study the influence of perturbations in the amplitude ( $a$ ) and phase ( $\phi$ ) of the BM velocity on the real and the imaginary parts of the impedance. A change in the amplitude at one point  $x=x_0$  of the BM is represented by

$$a^{pert}(x) = a(x) + \epsilon_1 \delta(x-x_0), \quad (10)$$

where  $a^{pert}(x)$  is the perturbed amplitude and  $\delta(x)$  is the Dirac delta function. For perturbation in the phase we have

$$\phi^{pert}(x) = \phi(x) + \epsilon_2 \delta(x-x_0), \quad (11)$$

where  $\phi^{pert}(x)$  is the perturbed phase of the BM velocity. The form of the disturbance (a Dirac delta function) allows us to observe the propagation of the impedance deviations along the BM. Let us call the real and imaginary part of the deviant impedance  $Z_R^{pert}(x)$  and  $Z_I^{pert}(x)$ . We consider the relative deviations in the real and imaginary parts of the impedance given by

$$\Delta_R(x) = [Z_R^{pert}(x) - Z_R(x)]/Z_R(x), \quad (12)$$

and

$$\Delta_I(x) = [Z_I^{pert}(x) - Z_I(x)]/Z_I(x). \quad (13)$$

Omitting terms of order 2 and higher in  $\epsilon_1$  and  $\epsilon_2$  we find that for an amplitude perturbation

$$\Delta_R(x) = \begin{cases} \frac{2\omega\rho\epsilon_1\beta(x_0)}{Z_R(x)a(x)A(x_0)}(x_0-x)\sin[\phi(x)-\phi(x_0)], & x < x_0 \\ -\frac{\epsilon_1}{a(x_0)}, & x = x_0 \\ 0, & x > x_0, \end{cases} \quad (14a)$$

$$\Delta_R(x) = \begin{cases} -\frac{\epsilon_1}{a(x_0)}, & x = x_0 \\ 0, & x > x_0, \end{cases} \quad (14b)$$

$$\Delta_R(x) = \begin{cases} 0, & x > x_0, \end{cases} \quad (14c)$$

and

$$\Delta_I(x) = \begin{cases} \frac{2\omega\rho\epsilon_1\beta(x_0)}{Z_I(x)a(x)A(x_0)}(x_0-x)\cos[\phi(x)-\phi(x_0)], & x < x_0 \\ -\frac{\epsilon_1}{a(x_0)}, & x = x_0 \\ 0, & x > x_0, \end{cases} \quad (15a)$$

$$\Delta_I(x) = \begin{cases} -\frac{\epsilon_1}{a(x_0)}, & x = x_0 \\ 0, & x > x_0, \end{cases} \quad (15b)$$

$$\Delta_I(x) = \begin{cases} 0, & x > x_0, \end{cases} \quad (15c)$$

For a phase perturbation we have

$$\Delta_R(x) = \begin{cases} -\frac{2\omega\rho\epsilon_2\beta(x_0)a(x_0)}{Z_R(x)a(x)A(x_0)}(x_0-x)\cos[\phi(x)-\phi(x_0)], & x < x_0 \\ \epsilon_2 \frac{Z_I(x_0)}{Z_R(x_0)}, & x = x_0 \\ 0, & x > x_0, \end{cases} \quad (16a)$$

$$\Delta_R(x) = \begin{cases} \epsilon_2 \frac{Z_I(x_0)}{Z_R(x_0)}, & x = x_0 \\ 0, & x > x_0, \end{cases} \quad (16b)$$

$$\Delta_R(x) = \begin{cases} 0, & x > x_0, \end{cases} \quad (16c)$$

and

$$\Delta_I(x) = \begin{cases} \frac{2\omega\rho\epsilon_2\beta(x_0)a(x_0)}{Z_I(x)a(x)A(x_0)}(x_0-x)\sin[\phi(x)-\phi(x_0)], & x < x_0 \\ -\epsilon_2 \frac{Z_R(x_0)}{Z_I(x_0)}, & x = x_0 \\ 0, & x > x_0, \end{cases} \quad (17a)$$

$$\Delta_I(x) = \begin{cases} -\epsilon_2 \frac{Z_R(x_0)}{Z_I(x_0)}, & x = x_0 \\ 0, & x > x_0, \end{cases} \quad (17b)$$

$$\Delta_I(x) = \begin{cases} 0, & x > x_0, \end{cases} \quad (17c)$$

A conspicuous feature is that the deviations only propagate backwards (that

is, to the base of the cochlea). This is, of course, due to the chosen boundary conditions of our inversion procedure. Furthermore, it can be seen that an amplitude perturbation leads to the same *local* relative deviations in real and imaginary parts of the impedance [Eqs. (14b) and (15b)], while for a phase perturbation the local relative deviations in real and imaginary parts are reciprocal in magnitude [Eqs. (16b) and (17b)]. When we introduce a perturbation at a place apical to the resonance point, we find results as shown in Fig. 8. Figure 9 presents the results for a perturbation at a place basal to the resonance point.

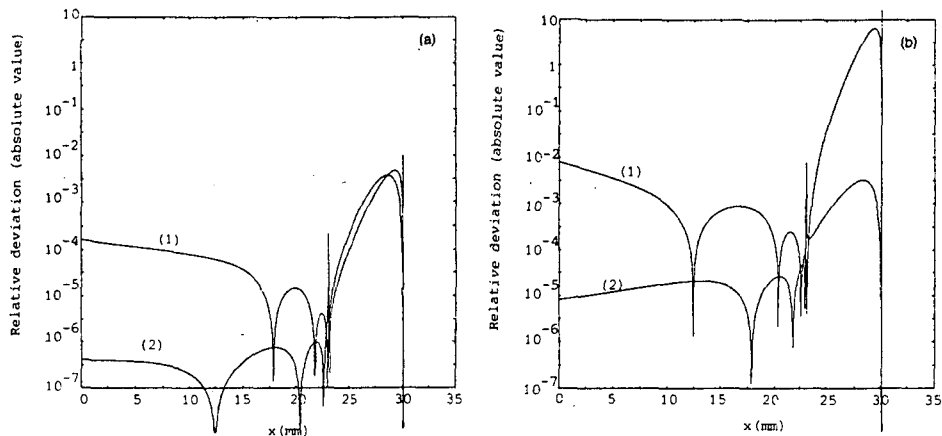


**Figure 8.** Relative deviations in impedance caused by a disturbance in the BM velocity apical to the resonance point. (a) Disturbance in the amplitude of BM velocity function, (b) disturbance in the phase of BM velocity function. Curves: (1)  $|\Delta_R(x)|$ , (2)  $|\Delta_I(x)|$ . Parameters:  $x_0 = 30 \text{ mm}$ ,  $\epsilon_1 = a(x_0)/100$ ,  $\epsilon_2 = \pi/10$ . Other parameters as in Fig. 2(a).

We can observe from Figs. 8 and 9 that the relative deviation in the imaginary part of the impedance,  $\Delta_I(x)$ , is smaller than the relative deviation in the real part of the impedance,  $\Delta_R(x)$ , for almost every  $x$ . This property can be explained as follows.

Comparison of Eqs. (14a) and (15a) [respectively, Eqs. (16a) and (17a)], shows that the absolute deviations [ $Z_R^{pert}(x) - Z_R(x)$  and  $Z_I^{pert}(x) - Z_I(x)$ ] are of the same order of magnitude. However, at nearly every point of the BM  $Z_I(x)$  is much greater than  $Z_R(x)$ , which accounts for the relative deviation in the imaginary part [ $\Delta_I(x)$ ] being smaller than the relative deviation in the real part [ $\Delta_R(x)$ ] of the impedance.

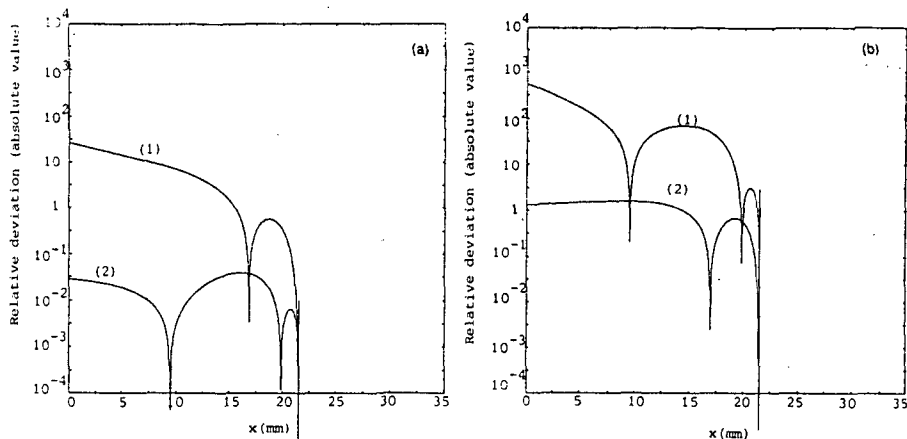


**Figure 9.** Relative deviations in impedance caused by a disturbance in the BM velocity basal to the resonance point. (a) Disturbance in the amplitude of BM velocity function, (b) disturbance in the phase of BM velocity function. Curves: (1)  $|\Delta_R(x)|$ , (2)  $|\Delta_I(x)|$ . Parameters:  $x_0 = 21.5 \text{ mm}$ ,  $\epsilon_1 = a(x_0)/100$ ,  $\epsilon_2 = \pi/10$ . Other parameters as in Fig. 2(a).

Furthermore, the figures show that the relative deviation in the real part of the impedance increases from its origin towards the stapes. On the other hand, the relative deviation in the imaginary part does not increase in this direction. The just presented argument explains why the real part of the reconstructed impedance is so sensitive to perturbations in the BM velocity.

## V. CONCLUSIONS

We have developed a simple method for reconstructing the BM impedance from spatial BM velocity data. Our main goal was to investigate whether such a reconstruction could be helpful in interpreting experimental data of BM motion. In particular, we would like to infer from the data whether they show evidence of (local) mechanical activity. For this purpose we have opted for a 1D cochlea configuration. This makes the formulation of the inverse problem simple and it is sufficient to illustrate qualitatively the results to be expected.

The conclusion of our study is that the imaginary part of the impedance is rather well determined in most cases. The real part, however, is very sensitive to disturbances in the BM velocity. That is, small changes in the velocity function cause large deviations in the real part of the impedance

function. The main reason for this result is the fact that there is an order of magnitude difference between the real and imaginary parts of the impedance over most of the BM.

Under the conditions and assumptions used in this paper, our results have far-reaching consequences: Any direct deduction concerning features related to the real part of the impedance from measurements of BM motion is unreliable, or, at least, questionable. Hence, using the method outlined in this paper, it is impossible to decide just from experimental BM velocity data whether the cochlea acts as a locally active filter or not, let alone to determine the regions where active behavior could be localized.

The absence of negative resistance in the BM does not necessarily mean that the cochlea is passive. On the contrary, there are experiments which strongly suggest the presence of an active mechanical process in the cochlea. Kemp (1978) discovered that sound energy is emitted by the human ear into the external ear canal, following impulsive acoustic excitation. The emissions are inhibited by the damage to the system, which makes it likely that their origin is a physiologically active mechanism. Also, spontaneous acoustic emissions from within the auditory system have been observed (Kemp, 1979, Wilson, 1980). Bialek and Wit (1984) have shown, by analysis of the amplitude distribution of the emissions, that these are due to oscillations rather than being filtered noise. Bialek (1983a, 1983b), furthermore, showed that the threshold auditory signal is comparable to the expected level of quantum noise. The thermal noise of the stereocilia is at least 40 dB above the threshold signal. Bialek argues that the only possible mechanism of noise reduction would be an active mechanical filter subsequent to BM mechanics.

In this article we did not reconstruct impedances directly from experimental data. In the light of the foregoing it is clear that accurate reconstructions will not be feasible, because the measurements are contaminated with errors. Moreover, transforming the velocity data from the frequency domain into the place domain will introduce additional errors.

Within the realm of the method described here little improvement seems possible. We might, for instance, impose physical realizability constraints on allowed forms of the reconstructed impedance functions. Or else, we can try to extend the present elaborations to two- and three-dimensional models. Such refinements will supposedly only produce marginal effects, however. A

more radically different approach, *viz.*, one based on energy flow principles, is presently being studied. This method has already been found promising (*cf.* Diependaal, De Boer, and Viergever, 1986), a detailed account will be published later.

## ACKNOWLEDGEMENTS

This work has been supported by the Netherlands Organization for the Advancement of Pure Research (ZWO). We thank Dr. M.M. Sondhi (AT&T Bell Labs.) for his suggestions which helped improve the manuscript.

## REFERENCES

- Békésy, G. von (1960). *Experiments in Hearing*. McGraw-Hill, New York.
- Bialek, W.S. (1983a). Quantum effects in the dynamics of biological systems. Doctoral dissertation, Lawrence Berkeley Laboratory and University of California, Berkeley, CA.
- Bialek, W.S. (1983b). Thermal and quantum noise in the inner ear. In: *Mechanics of Hearing*, pp. 185-192. Editors: E. de Boer and M.A. Viergever. Martinus Nijhoff Publishers/Delft U.P., Delft.
- Bialek, W.S. and Wit, H.P. (1984). Quantum limits to oscillatory stability theory and experiments on acoustic emissions from the human ear. *Phys. Lett.* 104A, 173-178.
- Boer, E. de (1983a). No sharpening? A challenge for cochlear mechanics. *J. Acoust. Soc. Am.* 73, 567-573.
- Boer, E. de (1983b). On active and passive cochlear models - Towards a generalized analysis. *J. Acoust. Soc. Am.* 73, 574-576.
- Burgeat, M., Burgeat-Menguy, C., and Lehmann, R. (1963). Etude de la transmission des pressions acoustiques du milieu aérien aux liquides cochlaires au moyen de sondes microphoniques. *Acustica* 13, 377-382.
- Dancer, M. and Franke, R. (1980). Intracochlear sound pressure measurements in guinea pigs. *Hearing Res.* 2, 191-205.
- Diependaal, R.J., Boer, E. de, and Viergever, M.A. (1986). Determination of the cochlear power flux from basilar membrane vibration data. In: *Peripheral Auditory Mechanisms*, pp. 189-196. Editors: J.B. Allen, J.L. Hall, A. Hubbard, S.T. Neely, and A. Tubis. Springer, New York.
- Gummer, A.W., Johnstone, B.M. and Armstrong, N.J. (1981). Direct measurement of basilar membrane stiffness in the guinea pig. *J. Acoust. Soc. Am.* 70, 1298-1309.
- Johnstone, B.M. and Yates, G.K. (1974). Basilar membrane tuning curves in the guinea pig. *J. Acoust. Soc. Am.* 55, 584-587.
- Kemp, D.T. (1978). Stimulated acoustic emissions from within the human auditory system. *J. Acoust. Soc. Am.* 64, 1386-1391.
- Kemp, D.T. (1979). Evidence of nonlinearity and frequency selective wave amplification in the cochlea. *Arch. Oto-Rhino-Laryngol.* 224, 37-45.
- Khanna, S.M. and Leonard, D.G.B. (1982). Basilar membrane tuning in the cat cochlea. *Science* 215, 305-306.
- Kim, D.O., Neely, S.T., Molnar, C.E., and Matthews, J.W. (1980). An active cochlear model with negative damping in the partition: Comparison with Rhode's ante- and post-mortem observations. In: *Psychological, Physiological and Behavioural Studies in Hearing*, pp. 7-15. Editors: G. van den Brink and F.A. Bilsen. Delft University Press, Delft.

- Miller, C.E. (1983). Static point-load measurements of basilar membrane compliance. In: Mechanics of Hearing, pp. 203-210. Editors: E. de Boer and M.A. Viergever. Martinus Nijhoff Publ., The Hague/Delft University Press, Delft.
- Miller, C.E. (1985). Structural implications of basilar membrane compliance measurements. *J. Acoust. Soc. Am.* 77, 1465-1474.
- Nedzelnitsky, V. (1974). Measurements of sound pressure in the cochleae of anesthetized cats. In: Facts and Models in Hearing, pp. 45-55. Editors: E. Zwicker and E. Terhardt. Springer, Berlin.
- Neely, S.T. (1980). Backward solution of a two-dimensional cochlear model. *J. Acoust. Soc. Am. Suppl. 1* 67, S75-S76.
- Neely, S.T. (1981). Fourth order partition mechanics for two-dimensional cochlear model. Doctoral dissertation, Washington University, St. Louis, MO.
- Neely, S.T. and Kim, D.O. (1983). An active cochlear model showing sharp tuning and high sensitivity. *Hearing Res.* 9, 123-130.
- Rhode, W.S. (1971). Observations of the vibration of the basilar membrane in squirrel monkeys using the Mössbauer technique. *J. Acoust. Soc. Am.* 49, 1218-1231.
- Robles, L., Ruggero, M.A., and Rich, N.C. (1986). Mössbauer measurements of the mechanical response to single-tone and two-tone stimuli at the base of the chinchilla cochlea. In: Peripheral Auditory Mechanisms, pp. 121-128. Editors: J.B. Allen, J.L. Hall, A. Hubbard, S.T. Neely, and A. Tubis. Springer, New York.
- Sellick, P.M., Patuzzi, R., and Johnstone, B.M. (1982). Measurement of basilar membrane motion in guinea pig using the Mössbauer technique. *J. Acoust. Soc. Am.* 72, 131-141.
- Sondhi, M.M. (1981). Acoustical inverse problem for the cochlea. *J. Acoust. Soc. Am.* 69, 500-504.
- Viergever, M.A. (1980). Mechanics of the inner ear - A mathematical approach. Doctoral dissertation, Delft University of Technology, Delft University Press, Delft.
- Viergever, M.A. and Diependaal, R.J. (1983). Simultaneous amplitude and phase match of cochlear model calculations and basilar membrane vibration data. In: Mechanics of Hearing, pp. 53-61. Editors: E. de Boer and M.A. Viergever. Martinus Nijhoff Publishers/Delft U.P., Delft.
- Viergever, M.A. and Diependaal, R.J. (1986). Quantitative validation of cochlear models using Liouville-Greene approximation. *Hearing Res.* 21, 1-15.
- Wilson, J.P. (1980). Evidence for a cochlear origin for acoustic reemission, threshold fine-structure and tinnitus. *Hearing Res.* 2, 233-252.

**CHAPTER THREE****Cochlear power flux as an indicator of mechanical activity**

**Abstract** The question of whether one can conclude just from basilar membrane (BM) vibration data that the cochlea is an active mechanical system is addressed. To this end a method is developed which computes the power flux through a channel cross section of a short-wave cochlear model from a given BM vibration pattern. The power flux is an important indicator of mechanical activity because a rise in this function corresponds to creation of mechanical energy. The power flux method is applied to BM velocity patterns as measured by Johnstone and Yates [J. Acoust. Soc. Am. 55, 584-587 (1974)] and Sellick *et al.* [Hear. Res. 10, 101-108 (1983)] in the guinea pig and by Robles *et al.* [Peripheral Auditory Mechanisms, edited by J.B. Allen, J.L. Hall, A.E. Hubbard, S.T. Neely, and A. Tubis (Springer, New York, 1986a), pp. 121-128, and J. Acoust. Soc. Am. 80, 1364-1374 (1986b)] in the chinchilla. Before the calculations are performed, the BM data are interpolated and smoothed in order to avoid numerical errors as a result of too few and noisy data points. The choice of the smoothing method influences the computed power flux function considerably. Nevertheless, the calculations appear to make a clear distinction between the "old" data showing broad BM tuning (Johnstone and Yates, 1974) and the "new" data in which the response is much more peaked (Sellick *et al.*, 1983; Robles *et al.*, 1986a,b). The former do not give rise to a significant increase of the power flux, the latter do, although less convincingly for the Sellick *et al.* (1983) data than for the Robles *et al.* (1986a,b) data. It is thus concluded that the recently obtained sharply tuned BM responses reflect the presence of mechanical activity in the cochlea.

**LIST OF MAIN SYMBOLS**

|            |   |
|------------|---|
| $x$        | coordinate along the basilar membrane (BM)          |
| $z$        | coordinate normal to the BM                         |
| $j$        | imaginary unity                                     |
| $b, h$     | width and height of a channel of the cochlear model |
| $x_{res}$  | resonance location                                  |
| $\beta(x)$ | $=\beta_0 \exp(\beta_1 x)$ , BM width               |

|                      |   |
|----------------------|---|
| $\epsilon(x)$        | $=\beta(x)/b=\epsilon_0 \exp(\epsilon_1 x)$           |
| $\omega$             | radian frequency in experiments (variable)            |
| $\omega_0$           | radian stimulus frequency in model (fixed)            |
| $x_0$                | point of observation                                  |
| $\rho$               | fluid density   |
| $p_{BM}(x, j\omega)$ | trans membrane pressure at the center line of the BM  |
| $v_{BM}(x, j\omega)$ | BM center line velocity normalized to stapes velocity |
| $A(x, j\omega)$      | amplitude of BM velocity                              |
| $\phi(x, j\omega)$   | phase of BM velocity                                  |
| $p(x, z, j\omega)$   | fluid pressure in a channel of the cochlear model     |
| $v_x(x, z, j\omega)$ | fluid (point) velocity in the x direction             |
| $E_x(x, z, j\omega)$ | average acoustic intensity in the x direction         |
| $F_x(x, j\omega)$    | power flux through a channel cross section            |
| $W(x, j\omega)$      | amplitude of the BM displacement                      |
| $\kappa(x, j\omega)$ | wave number of the BM velocity wave                   |
| $\alpha$             | cochlear map parameter                                |
| $p_{res}$            | trans membrane pressure at $x_{res}$                  |

## INTRODUCTION

In recent years many investigators have been modelling the cochlea as an active system (Zwicker (1979), Kim *et al.* (1980), De Boer (1983a, b); see, furthermore, the proceedings of the 1983 Mechanics of Hearing Symposium, edited by De Boer and Viergever; and the proceedings of the 1985 Mechanics of Hearing Workshop, edited by Allen *et al.*). Evidence to include active features in descriptions of cochlear functioning has been supplied by experimental results concerning acoustic emissions (pioneered by Kemp, 1978). Bialek and Wit (1984) have shown that such emissions are the result of an (unstable) oscillatory process rather than merely being sharply filtered noise. Also, a comparison of the threshold auditory signal to the expected levels of quantum noise and thermal noise of the stereocilia provides arguments that the cochlea is an active system (Bialek, 1983a,b).

Measurements of Khanna and Leonard (1982), Sellick *et al.* (1982, 1983) and Robles *et al.* (1986a,b) show very sharp tuning of the basilar membrane

(BM), much sharper than is evident from earlier data. This strongly suggests that the active behavior manifests itself at the level of BM vibration. In the present article we examine this suggestion or, otherwise stated, we address the question of whether we can conclude just from BM vibration data whether or not the cochlea is an active mechanical system. To this end a method is developed in which the power flux through a channel cross section of a short-wave cochlear model is computed from a given BM vibration pattern. The power flux function is an important indicator of active behavior of the cochlea, since an increase (decrease) in this function corresponds to creation (dissipation) of mechanical energy. We have opted for a short-wave model description of cochlear mechanics because (i) in the region of the steep rise of the amplitude of the BM response, the wavelength of the travelling wave is at most of the order of  $2\pi$  times the channel height; (ii) the short-wave approximation provides for a simple relationship between the power flux and the BM velocity.

A direct indicator of active behavior of the cochlea is the BM impedance. A negative real part of the impedance function corresponds to creation of mechanical energy. However, simulation studies in which the (variations of the) impedance have been computed from BM velocity data have shown that the impedance function is very sensitive to small disturbances in BM velocity (Diependaal *et al.*, 1986b). Since experimental data are liable to be corrupted by measurement errors, this is a most unfortunate situation indeed. The power flux function is much less sensitive to such disturbances in the velocity as follows from simulation studies.

The organization of the article is as follows: The method of calculating the power flux is outlined in Sec. I. The method expects a BM velocity pattern as a function of place for a given frequency. However, in all recent experiments the velocity is measured as a frequency response curve, *i.e.* BM velocity as a function of frequency at a fixed place. Hence, we need a transformation from the frequency domain into the spatial domain so as to be able to apply the method. Such a transformation is discussed in the Sec. II. Furthermore, the BM data are interpolated and smoothed in order to avoid numerical errors as a result of too few and noisy data points. Several interpolation and smoothing methods are discussed in the same section. In Sec. III we actually compute the power flux function from BM vibration data sets using the method developed. The effects of interpolating and smoothing the data

points on the numerical results are shown as well. In the final section (IV) the results are summarized and discussed in the light of the assumptions made in developing the method.

## I. MODEL AND METHOD

For a fluid wave in a two-dimensional (2D) linear cochlear model the average acoustic intensity (energy per unit time per unit cross-sectional area) in the longitudinal ( $x$ ) direction is given by

$$E_x(x, z, j\omega_0) = \frac{1}{2} \operatorname{Re}[p(x, z, j\omega_0)v_x^*(x, z, j\omega_0)], \quad (1)$$

where \* means complex conjugate. We assume that the mechanical properties of the cochlea do not vary much within a wavelength of the wave propagated along the BM. This provides the basis for applying the Liouville-Green (LG) approximation which gives the following expressions for pressure and longitudinal fluid velocity in the customary 2D model (Steele and Taber, 1979)

$$p(x, z, j\omega_0) = -\frac{2\omega_0^2 \rho \epsilon W}{\pi \kappa \sinh[\kappa h]} \cosh[\kappa(z-h)] e^{-j\kappa x}, \quad (2)$$

$$v_x(x, z, j\omega_0) = -\frac{2\omega_0 \epsilon W}{\pi \sinh[\kappa h]} \cosh[\kappa(z-h)] e^{-j\kappa x}. \quad (3)$$

The real part of the wave number  $\kappa$  is positive, since the LG approximation implies that waves are only travelling in the positive  $x$  direction, *i.e.*, from the base towards the apex of the cochlea.

To arrive at the total power flux through a channel cross section, we substitute Eqs. (2) and (3) into Eq. (1) and integrate the result over the width  $b$  and the height  $h$  of the channel:

$$\begin{aligned} F_x(x, j\omega_0) &= b \int_0^h E_x(x, z, j\omega_0) dz = \\ &= \frac{b \omega_0^3 \rho \epsilon^2 W^2 \{\sinh[2\operatorname{Re}(\kappa)h] + \frac{\operatorname{Re}(\kappa)}{\operatorname{Im}(\kappa)} \sin[2\operatorname{Im}(\kappa)h]\}}{\pi^2 |\kappa|^2 \{\cosh[2\operatorname{Re}(\kappa)h] - \cos[2\operatorname{Im}(\kappa)h]\}} e^{2\operatorname{Im}(\kappa)x}. \end{aligned} \quad (4)$$

Defining movements in the direction of scala vestibuli as positive (as opposed to the convention used in most of the experiments), we have

$$p_{BM}(x, j\omega_0) = -2p(x, 0, j\omega_0). \quad (5)$$

Equations (2), (4) and (5) jointly yield

$$F_x(x, j\omega_0) = \frac{b}{16\omega_0\rho} \frac{\tanh[2\operatorname{Re}(\kappa)h] + \frac{\operatorname{Re}(\kappa)\sin[2\operatorname{Im}(\kappa)h]}{\operatorname{Im}(\kappa)\cosh[2\operatorname{Re}(\kappa)h]} \times \\ \times |p_{BM}(x, j\omega_0)|^2. \quad (6)$$

We now assume that the wavelengths of the propagating waves are short with respect to  $2\pi$  times the channel height  $h$ . Under this assumption we may take the limit  $\operatorname{Re}[\kappa h] \rightarrow \infty$  with the result that the wave number is eliminated from expression (6). If we suppose that the mechanical properties of the BM can be characterized by a point-impedance function, the short-wave model is described by the differential equation (see, e.g., De Boer, 1983d)

$$\frac{dp_{BM}}{dx} + \frac{16\omega_0\rho\epsilon}{\pi^2} v_{BM} = 0. \quad (7)$$

The difference in coefficients with respect to De Boer's formulation arises from the fact that we have defined the pressure and velocity as center line quantities rather than as averages over the BM width (Diependaal and Viergever, 1983; Viergever and Diependaal, 1986).

A suitable boundary condition for Eq. (7) is

$$p_{BM} = p_{res} \quad \text{at } x = x_{res}. \quad (8)$$

The resonance location,  $x_{res}$ , is the point where the imaginary part of the impedance function vanishes. Apical to this point the short-wave assumption can no longer hold true (Viergever, 1980). Using Eq. (8), we integrate Eq. (7) to arrive at

$$p_{BM}(x, j\omega_0) = p_{res} + \frac{16\omega_0\rho}{\pi^2} \int_x^{x_{res}} \epsilon(\xi) v_{BM}(\xi, j\omega_0) d\xi. \quad (9)$$

Since the travelling wave along the BM is almost extinct when it reaches the resonance location, we can neglect  $p_{res}$  with respect to the integral in Eq. (9) on the whole BM except for a fraction of the last millimeter before  $x_{res}$ . Substituting expression (9) into Eq. (6) and taking the limit for  $\operatorname{Re}[\kappa h] \rightarrow \infty$ , we arrive at the following form for the power flux:

$$F_x(x, j\omega_0) = \frac{16\omega_0\rho}{\pi^4} \left| \int_x^{x_{res}} \epsilon(\xi) v_{BM}(\xi, j\omega_0) d\xi \right|^2. \quad (10)$$

Note that in this model  $v_{BM}$  is the ratio of BM velocity and stapes velocity. From Eq. (10) we can determine the power flux at any point on the BM once we know the BM velocity pattern for all positions apical to it up to the resonance location.

## II. SELECTION AND PREPROCESSING OF THE DATA

In order to apply our method to experimental BM vibration data, we selected sets of BM responses collected in three different series of experiments in which both amplitude and phase data were reported. The results of Johnstone and Yates (1974) were chosen to represent the "older" *in vivo* data, which are nowadays interpreted as typifying the behavior of a pathological cochlea. As a representation of the more recent, sharply tuned data, we chose the results of Sellick *et al.* (1983) and Robles *et al.* (1986a,b). Sellick *et al.* (1983) also studied the effects of the size and the location of the Mössbauer source on the measured BM response curves. One common feature of the results selected is that they were all obtained by Mössbauer experiments. There are, however, differences, namely, the species in which the experiments were performed, *viz.*, guinea pig (Johnstone and Yates, 1974; Sellick *et al.*, 1983), and chinchilla (Robles *et al.*, 1986a,b).

The power flux method requires an input of BM vibration data in a form which differs from the form in which the measurement results are presented. Hence, we consider several operations on the data, *viz.*, a middle-ear transfer function, interpolation and smoothing, and a transformation from the frequency into the place domain. The middle-ear transfer function is needed for the data of Robles *et al.* (1986a,b), because they published their data with respect to the sound pressure at the eardrum. Interpolation of the BM velocity data is mandatory in order to have enough points for numerical integration; the measurements provide us with only few (approximately 20) points per response curve. The data must also be smoothed, because they are afflicted with measurement errors. Finally, the velocity data must be transformed from the frequency into the place domain, since the power flux is to be calculated in the place domain [see Eq. (10)], whereas BM velocities are obtained as frequency response curves. All these data manipulations will

be treated in the next subsections.

#### A. Middle-ear transfer function

Robles *et al.* (1986a,b) published their amplitude data as sound pressure at the eardrum necessary to produce a certain BM velocity as a function of frequency. Their phase data are given as BM displacement with respect to rarefaction at the eardrum. Our power flux method expects as input the ratio of BM velocity and stapes velocity. Therefore, the data of Robles *et al.* (1986a,b) have to be modified by a middle-ear transfer function. [We do not need a middle-ear transfer function for the measurements of Johnstone and Yates (1974) and Sellick *et al.* (1983), because their data are already transfer ratios of BM velocity and stapes velocity].

The middle-ear transfer function represents stapes displacement over pressure at the eardrum. The amplitude of the function we use, has a value of  $C_A \text{ mm/mPa}$  at frequencies  $< f_A \text{ kHz}$ , and decays with a slope of  $S_A \text{ dB/octave}$  above  $f_A \text{ kHz}$ . The phase of the filter has a value 0 at frequencies  $< f_P \text{ kHz}$ , and decays at a rate of  $S_P \text{ radians/octave}$  above  $f_P \text{ kHz}$ . The filter parameters  $C_A$ ,  $f_A$ ,  $f_P$ ,  $S_A$ , and  $S_P$  can be estimated from Guinan and Peake (1967) for the cat, but corresponding middle-ear characteristics for the chinchilla are not known to us. Therefore, we used several middle-ear parameter sets in the calculations. Variations of these parameters alter the power flux function, but we found that these changes in the power flux function were small so that they did not influence the decision whether the underlying behavior of the cochlea was active or passive.

#### B. Interpolation and smoothing

Only few measurement points per response curve (of the order of 20) are available. In order to limit the errors in the numerical integration, some sort of interpolation of the BM velocity data is mandatory. Furthermore, we have to smooth the data in order to reduce spurious irregularities caused by measurement errors. Interpolating and smoothing the measured velocity data can be done in various ways. In Diependaal *et al.* (1986a), a cubic spline interpolation method and a least-squares smoothing method have been discussed. In this article we introduce another smoothing method (cubic spline smoothing) and compare it with the previously used techniques.

In the least-squares smoothing procedure amplitude and phase data are

characterized by polynomials of chosen fixed degrees. The number of parameters which uniquely determine such a polynomial equals the degree of the polynomial plus one. The values of the parameters are computed by means of the least-squares method.

In cubic splines smoothing amplitude and phase data are smoothed by functions with continuous first and second derivatives with respect to frequency. From this set of functions the function  $f$  which minimizes

$$\frac{1}{n} \sum_{j=1}^n [f(\omega_j) - y_j]^2 + \lambda \int_{\omega_1}^{\omega_n} \left[ \frac{d^2 f(\omega)}{d \omega^2} \right]^2 d\omega \quad (11)$$

is chosen as smoothing function. The function  $f$  is a cubic spline function, *i.e.*, a polynomial of the third degree on each interval between two adjacent data points. In Eq.(11),  $n$  is the number of data points, and the  $\omega_j$  are the frequencies at which the amplitude (or phase)  $y_j$  of the BM velocity has been measured. The parameter  $\lambda$  controls the tradeoff between the "roughness" of the smoothing function, as measured by  $\int_{\omega_1}^{\omega_n} [d^2 f(\omega)/d \omega^2]^2 d\omega$ , and

the infidelity to the data as measured by  $\frac{1}{n} \sum_{j=1}^n [f(\omega_j) - y_j]^2$ . If  $\lambda=0$ , we are

just interpolating the data with cubic splines without any smoothing. Results of this procedure (with  $\lambda=0$ ) are presented in Diependaal *et al.* (1986a). The optimal value of  $\lambda$  is derived by means of the method of generalized cross-validation (GCV). For the details of this method we refer to the article by Craven and Wahba (1979).

The difference between the two smoothing procedures can be outlined as follows. Suppose we know nothing about the form of the BM velocity function *a priori*, but may assume that the data points are corrupted by independent random errors. In such a case smoothing the data with spline functions by the method of GCV is an appropriate procedure. If one knows, for theoretical reasons, the form of the BM velocity function *a priori*, a good smoothing procedure is to approximate this function by an appropriate trial function which is fitted to the data points by application of the least-squares method. If, as we do in this article, polynomials are used, the degree of these polynomials must be low because in that case only few parameters have to be determined. This corresponds to simple cochlear models with limited variations

of the parameters.

The amplitude curves are smoothed on a logarithmic scale, the phase curves on a linear scale. Figure 1 shows the results of smoothing with the two methods. We have taken one data set of Sellick *et al.* (1983) as an example and have smoothed the curves by means of polynomials of the sixth degree (amplitude) and of the third degree (phase) using the least-squares method. The results are plotted in Fig. 1(a) and 1(b). Figure 1(c) and 1(d) shows the results when both the amplitude and the phase curves are smoothed by a polynomial of the eleventh degree, using the least-squares method. Results of smoothing the data by cubic splines using the method of GCV are plotted in Fig. 1(e) and 1(f). It may be expected that the choice of how to smooth the data influences the computed power flux function. Despite the rather small variations in the smoothed curves, the influence on the results can be very large, as will be shown below.

### C. Cochlear map

From Eq. (10), we see that the power flux is calculated in the place domain. Since in all recent experiments the velocity is measured as a frequency response curve, we need a transformation from the frequency domain into the place domain in order to be able to apply the present method. For several species, a frequency-position map is described in the literature. Such a map is a relation between characteristic frequency and characteristic place along the BM. Often that relation is formulated as place being a logarithmic [or nearly logarithmic] function of characteristic frequency (Robertson and Johnstone, 1979 (guinea pig); Eldredge *et al.*, 1981 (chinchilla); Liberman, 1982 (cat)]. Viergever (1980) shows that, under certain restrictions on the mechanical parameters of the BM, the LG-solution of a two-dimensional cochlear model is frequency-shift invariant for a place to log frequency transformation only when the BM velocity is normalized to its value at the resonance place. Hence, we try and improve the transformation by including the mentioned normalization factor. The customary place to log frequency transformation reads

$$T : x = x_0 + \frac{2}{\alpha} \ln \frac{\omega}{\omega_0}. \quad (12)$$

Its inverse, given by

$$T^{-1} \cdot \omega = [\omega_0^2 e^{\alpha(x-x_0)}]^{1/2}, \quad (13)$$

transforms the BM vibration data from the frequency domain into the place domain. The error we make when applying Eqs. (12) and (13) can be corrected approximately in the following way. In the region where the stiffness part (assumed to decay exponentially) dominates the BM impedance, the short-wave LG solution of the BM velocity is given by

$$v_{BM}(x, j\omega) = C_1 \omega^2 \exp\{\alpha x - j[\frac{\pi}{2} + C_2 \omega^2 (e^{(\alpha+\epsilon_1)x} - 1)]\} \quad (14)$$

Thus, in this region, the following quantities are to be invariant under transformation T:

$$\begin{array}{ccc} \left| \begin{array}{l} A(x, j\omega_0) \\ \phi(x, j\omega_0) + \frac{\pi}{2} \\ \hline \omega_0^2 (e^{(\alpha+\epsilon_1)x} - 1) \end{array} \right. & \xrightarrow{T} & \left| \begin{array}{l} A(x_0, j\omega) \\ \phi(x_0, j\omega) + \frac{\pi}{2} \\ \hline \omega^2 (e^{(\alpha+\epsilon_1)x_0} - 1) \end{array} \right. \end{array} \quad (15)$$

Expression (15) defines the corrected cochlear map to transform  $A$  and  $\phi$  from the frequency into the place domain. Simulation studies have shown that this map gives (slightly) improved results as compared with the simple place to log frequency transformation. The transformation defined by Eq. (15) contains four parameters, *viz.*,  $\omega_0$ ,  $x_0$ ,  $\alpha$ , and  $\epsilon_1$ . Variation of these parameters does not produce significant changes in the global shape of the power flux function.

### III. CALCULATED POWER FLUX FUNCTIONS

Before calculating the power flux from actual measurement results, we tested the cubic spline smoothing method on computer-generated BM velocity patterns. This has been done in a similar way as described in Diependaal *et al.* (1986b) (for the long-wave model). Measurement errors were simulated by introducing several disturbances to these patterns and studying their effects on the power flux. The values of these disturbances were chosen such that they are realistic with respect to the magnitude of the measurement errors. For all disturbances considered, the resulting deviations in the power flux function were small, in sharp contrast with the corresponding deviations in

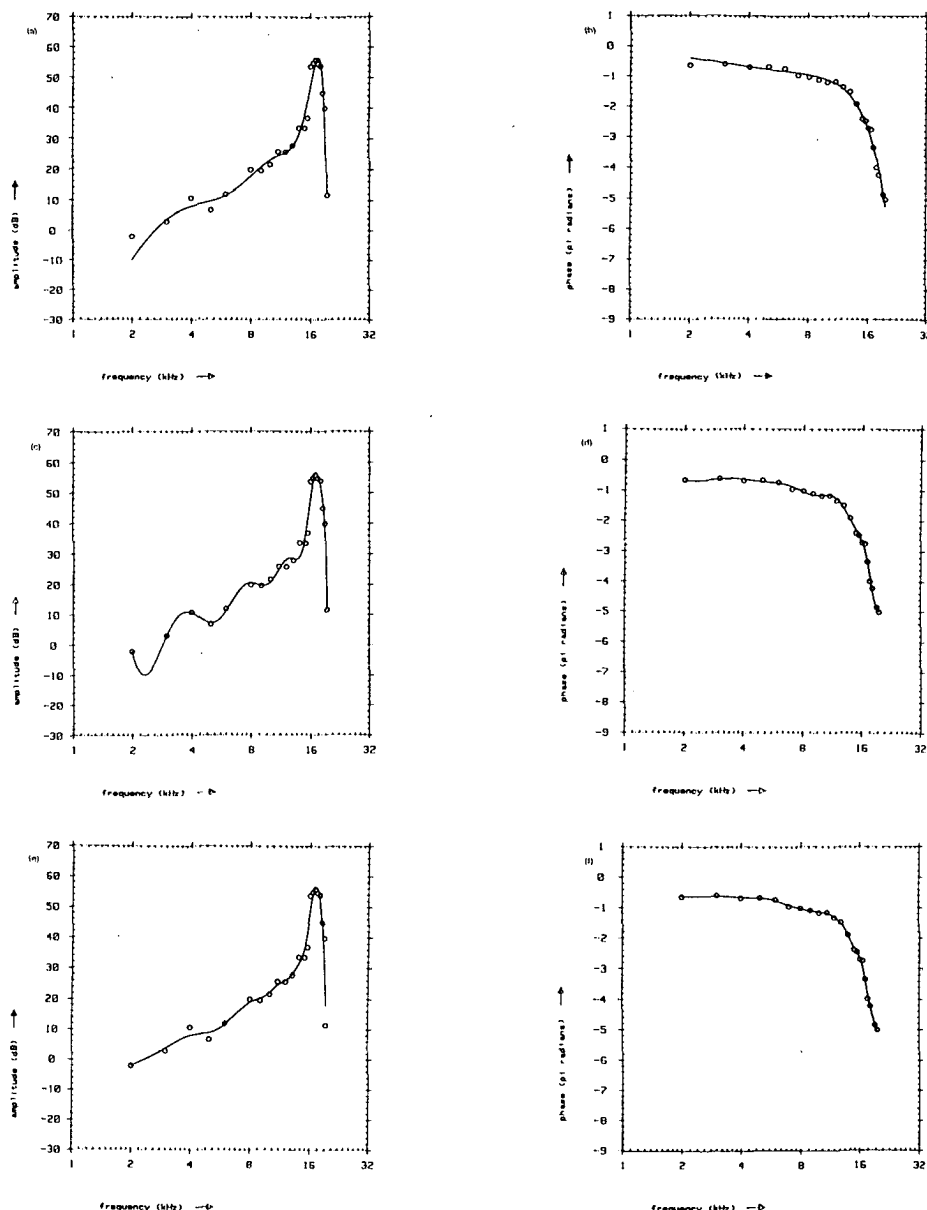


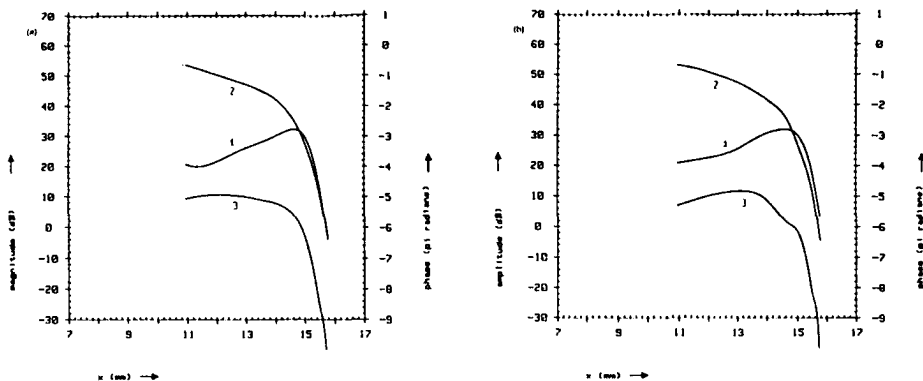
**Figure 1.** BM velocity (animal 116 of Sellick *et al.*, 1983, Fig. 1) after interpolation and smoothing as a function of frequency. (a) and (b) Amplitude (dB re: 1 mm/ms) and phase of the response interpolated and smoothed by one polynomial of the sixth (third) degree, using the least-squares method. (c) and (d) Amplitude (dB re: 1 mm/ms) and phase both interpolated and smoothed by one polynomial of eleventh degree, using the least-squares method. (e) and (f) Amplitude (dB re: 1 mm/ms) and phase interpolated and smoothed by cubic splines using the method of GCV. Circles: data points. Continuous lines: smoothed curves.

the impedance, which have been shown to be unacceptably large (Diependaal *et al.*, 1986b).

If we smooth the measured velocity curves by polynomials using the least-squares method, we have to choose the degrees of the smoothing polynomials beforehand. This is done as follows: we smooth the data points with polynomials up to the eleventh degree. We also calculate the root mean square residual for each degree. In general, the residual has a typical behavior as a function of the degree of the interpolant. The graph of this function consists of monotonically decreasing parts alternated with more or less constant parts. We now select the lowest degree of the smoothing polynomial, at which the graph of the residual first reaches a plateau.

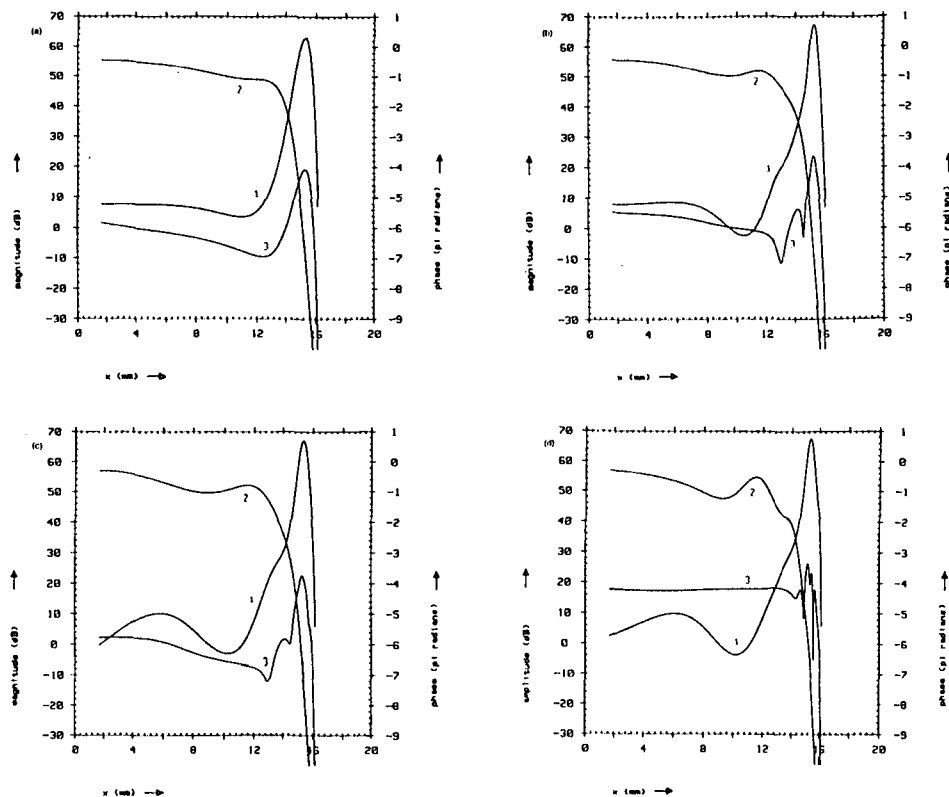
In Fig. 2, the results of our calculations are shown for the data of Johnstone and Yates (1974, Fig. 3). Curves 1 and 2 are, respectively, the amplitude and phase function of the measured BM velocity (after smoothing and cochlear map transformation). As said earlier, no correction for the middle-ear is needed here. The power flux function calculated from these data is drawn as curve 3. See the legend to the figure for further details. In Fig. 2(a), the results are plotted when the BM velocity curves have been smoothed by polynomials of the sixth degree (amplitude) and third degree (phase) using the least-squares method. For Fig. 2(b), the data were smoothed using cubic splines. We observe that, for either smoothing method, the power flux function is nearly flat in the region up to the velocity amplitude peak; there is at most an increase in the power flux of 5 dB in this region [Fig. 2(b)]. After this peak, the power flux function decays steeply.

Figure 3 presents results for experimental animal MO28 of Robles *et al.* (1986a, Figs. 2 and 4). The measured BM velocity has been modified by a middle-ear transfer filter before subjecting it to smoothing and transforming by a cochlear map. The curve label numbers 1, 2, 3 again refer to amplitude, phase of the BM velocity, and power flux function, respectively. In Fig. 3(a) a polynomial of the fourth (fifth) degree has been used as smoothing function for the amplitude (phase); the degrees of the polynomials follow from the above described procedure. Notice the strong increase of the calculated power flux function in the region just before (*i.e.*, on the basal side of) the BM velocity amplitude peak. Figure 3(b) shows the calculated power flux function when the BM velocity curves have been smoothed by cubic splines.



**Figure 2.** Power flux calculated from the data of Johnstone and Yates (1974, Fig. 3) as a function of the distance from the base. (a) Data interpolated and smoothed by one polynomial of the sixth (amplitude) and of the third (phase) degree, using the least-squares method. (b) Data interpolated and smoothed by cubic splines, using the method of GCV. Parameters:  $\rho = 1 \text{ mg/mm}^3$ ,  $b = 0.5 \text{ mm}$ ,  $\beta = 0.08 \exp(0.04x) \text{ mm}$ ,  $\epsilon_1 = 0.04 \text{ mm}^{-1}$ ,  $\omega_0 = 2\pi \cdot 0.777 \text{ kHz}$ ,  $x_0 = 4.12 \text{ mm}$ ,  $\alpha = 0.55 \text{ mm}^{-1}$ . Cochlear map parameters are derived from Robertson and Johnstone (1979). Curves: (1) amplitude of BM velocity (dB re: 1 mm/ms), (2) phase of BM velocity, and (3) power flux (arbitrary dB scale).

The power flux function is much like that plotted in Fig. 3(a), except for a few dips in the graph of the power flux in Fig. 3(b). These dips are due to the fact that the amplitude and phase curves of the BM velocity in Fig. 3(b) are less smooth than the curves of Fig. 3(a). This is further illustrated by Fig. 3(c), which shows the graphs of the BM velocity and the corresponding power flux for the case the amplitude (phase) data are smoothed by polynomials of the tenth (eighth) degree. For these values of the degrees of the interpolating polynomials the root mean square residuals reach a second plateau. In Fig. 3(d), we have applied least-squares smoothing to the data by polynomials of higher degrees, namely, eleventh degree for both amplitude and phase. The strong rise in the power flux function is now suppressed considerably.



**Figure 3.** Power flux calculated from the data of Robles *et al.* (1986a, Figs. 2 and 4, animal MO28) as a function of the distance from the base. (a) Data interpolated and smoothed by one polynomial of the fourth (amplitude) and of the fifth (phase) degree, using the least-squares method. (b) Data interpolated and smoothed by cubic splines, using the method of GCV. (c) Data interpolated and smoothed by one polynomial of the tenth (amplitude) and of the eighth (phase) degree, using the least-squares method. (d) Amplitude and phase both interpolated and smoothed by one polynomial of the eleventh degree, using the least-squares method. Parameters:  $\omega_0 = 2\pi \cdot 0.33 \text{ kHz}$ ,  $x_0 = 3.5 \text{ mm}$ ,  $\alpha = 0.554 \text{ mm}^{-1}$ ,  $C_A = 4.10^{-8} \text{ mm/mPa}$ ,  $f_A = f_p = 3 \text{ kHz}$ ,  $S_A = 9.5 \text{ dB/octave}$ ,  $S_p = 0.3\pi \text{ radians/octave}$ . Other parameters as in Fig. 2. Cochlear map parameters are derived from Eldredge *et al.*, and from private communication with Mario Ruggiero. Curves: (1) amplitude of BM velocity (dB re: 1 mm/ms), (2) phase of BM velocity, and (3) power flux (arbitrary dB scale).

We have also calculated power flux functions from BM velocity patterns measured by Sellick *et al.* (1983). The BM velocity curves of animal 116 (Sellick *et al.*, 1983, Fig. 1) have been selected as basis for the power flux calculations, since, according to Sellick *et al.* (1983), animal 116 is one of the animals of which the measured curves reflect nearly normal behavior of

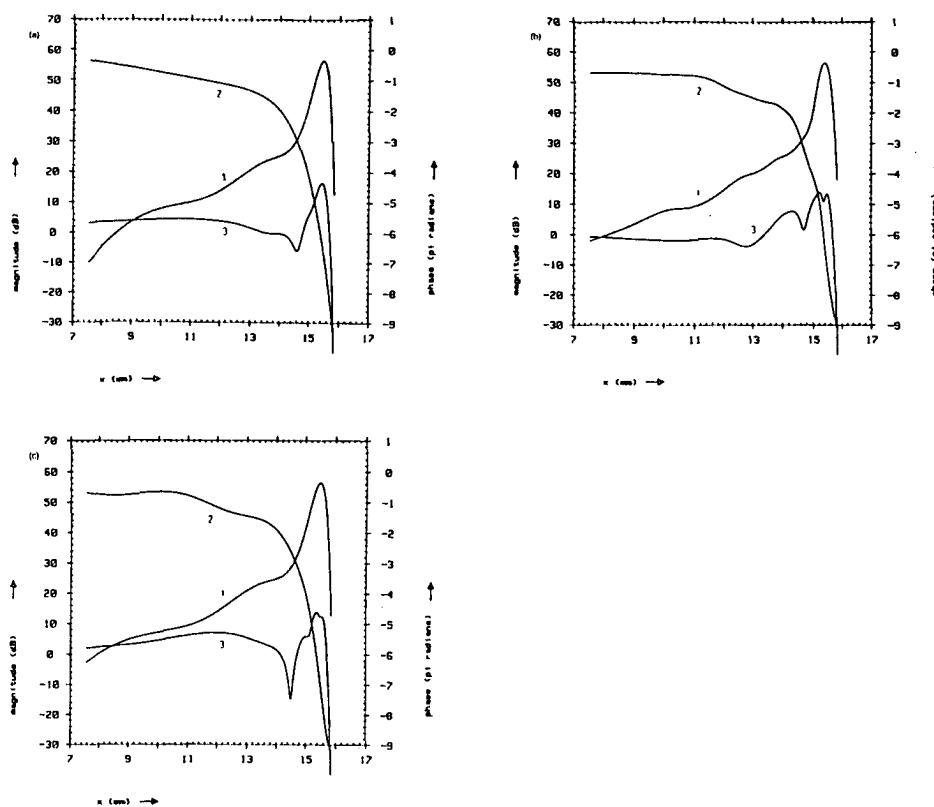


**Figure 4.** Power flux calculated from the data of Sellick *et al.* (1983, Fig. 1, animal 116) as a function of the distance from the base. (a) Data interpolated and smoothed by one polynomial of the sixth (amplitude) and of the third (phase) degree, using the least-squares method. (b) Data interpolated and smoothed by cubic splines, using the method of GCV. (c) Data interpolated and smoothed by one polynomial of the sixth (amplitude) and of the eighth (phase) degree, using the least-squares method. Parameters:  $\omega_0=2\pi \cdot 0.637 \text{ kHz}$ ,  $x_0=3.4 \text{ mm}$ . Other parameters as in Fig. 2. Cochlear map parameters are derived from Robertson and Johnstone (1979). Curves: (1) amplitude of BM velocity ( $\text{dB re } 1 \text{ mm/ms}$ ), (2) phase of BM velocity, and (3) power flux (arbitrary  $\text{dB}$  scale).

the cochlea. Figure 4 shows the results. Plotted are the amplitude and phase of the BM velocity of animal 116 (curves 1 and 2), smoothed by polynomials of the sixth degree (amplitude) and third degree (phase) using the least-squares method [Fig. 4(a)] and smoothed by cubic splines using GCV [Fig. 4(b)]. These curves are the place domain counterparts of the curves displayed in Fig. 1. Curve 3 is the graph of the calculated power flux function. See figure caption for further details. In Fig. 4(c), results are shown

when amplitude and phase of the BM velocity data are smoothed by polynomials of the sixth and eighth degree, respectively, using the least-squares method. In Fig. 4(a), the power flux function shows a strong increase in the region just before the BM velocity amplitude peak. In Fig. 4(b), some dips in the graph of the power flux can be noticed, which are like those shown in Fig. 3(b). Figure 4(c), finally, shows much the same as Fig. 3(d): the power flux increase is considerably diminished.

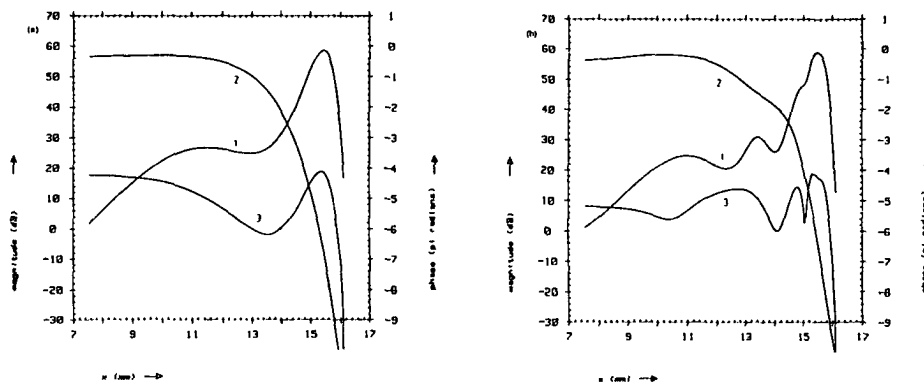


**Figure 5.** Power flux calculated from the data of Sellick *et al.* (1983, Fig. 3, animal 92) as a function of the distance from the base. (a) Data interpolated and smoothed by one polynomial of the fourth (amplitude) and of the third (phase) degree, using the least-squares method. (b) Data interpolated and smoothed by cubic splines, using the method of GCV. Parameters:  $\omega_0 = 2\pi \cdot 0.637 \text{ kHz}$ ,  $x_0 = 3.4 \text{ mm}$ . Other parameters as in Fig. 2. Cochlear map parameters are derived from Robertson and Johnstone (1979). Curves: (1) amplitude of BM velocity (dB re : 1 mm/ms). (2) phase of BM velocity. (3) power flux (arbitrary dB scale).

Power flux functions calculated from the BM velocity data of animal 92 (Sellick *et al.*, 1983, Fig. 3) are shown in Fig. 5. (In contrast to animal 116, the Mössbauer source has been placed in animal 92 in the middle of the basilar membrane.) For the results of Fig. 5(a), the data have been smoothed by polynomials of low degree using least squares; for Fig. 5(b), cubic splines has

been used to smooth the measurement points. Notice that, in Figs. 5(b), the power flux functions show no strong tendency to increase in the region just before the BM velocity amplitude peak. In Fig. 5(a), the power flux function shows a steep rise just before the BM velocity amplitude peak, but the total energy gain with respect to the beginning of the curve is only about 5dB. The behavior of the power flux, as shown in Fig. 5(b), seems to be caused by the ripples in the BM velocity function, which are more pronounced in Fig. 5(b) than in Fig. 4(b). These ripples are called inflections by Sellick *et al.* (1983); we interpret them as reflections on a microscale. These inflections are determined by the size of the Mössbauer source and by the place where the source is situated on the BM (Sellick *et al.*, 1983).

We conclude this section with the remark that the measured BM responses, which are frequency response curves, must be physically realizable. Thus their associated impulse responses must be causal. This causality has been checked for the cases presented in the article. We have taken the inverse Fourier transforms of the BM velocity functions after they have been smoothed. The resulting impulse responses are very small for negative times, as compared with the response for positive times. If we make the impulse response exactly zero for negative times, perform a Fourier transform and follow the usual procedure to calculate the power flux, the resulting power flux function is not significantly altered (the changes are, at most, of the order of a few dB).

#### IV. DISCUSSION AND CONCLUSIONS

We have developed a method to estimate the cochlear power flux from basilar membrane vibration data. The main restrictions and assumptions are:

- i. The basis for our calculations is a short-wave model; *i.e.*, the wavelength is assumed to be small compared with  $2\pi$  times the height of the scalae. This is a realistic assumption for the region around the BM velocity amplitude peak, in which we are primarily interested. The wavelength of the cochlear traveling wave near the response peak is of the order of 1 mm for frequently used mammals (*e.g.*, Rhode, 1971; Kohlöffel, 1972), whereas the cochlear channel height is in the range of 0.5–1.0 mm.
- ii. The cochlear model used is linear. There is abundant evidence that the

mechanical behavior of the BM is nonlinear. However, the reported measurements have been done near the threshold of hearing. It seems reasonable to assume that departure from linearity will be insignificant at such low amplitude levels.

- iii. In the derivation of the power flux formula, we have used the Liouville-Green (LG) approximation, which is based on slow variations in the propagation properties of the BM travelling wave. The validity of the LG approximation has been discussed by De Boer and Viergever (1982). The LG approximation does not take into account internal reflections. Thus in using our power flux method, we assume that there are only waves travelling to the right, *i.e.*, from the stapes towards the apex of the cochlea. This unidirectionality can be checked. We determined the spatial Fourier spectra (with respect to  $x$ ) of the interpolated BM velocity functions after the cochlear map transformation has been performed. For the cases considered in this article, these spectra contain only small components for negative wavenumbers (which correspond to waves travelling from the apex to the base of the cochlea). Making these spectra exactly zero for negative wavenumbers, returning to the place domain, and continuing the usual procedure to calculate the power flux changes the global shape of the resulting power flux function by not more than a few decibels.
- iv. An appropriate smoothing procedure is to smooth the measured data by cubic splines using the method of generalized cross validation, since no *a priori* knowledge about the global shape of the BM velocity curves is used by this procedure. A good alternative is to smooth the vibration data by polynomials of fixed degree using the least-squares method. The degree of the polynomials must be low in this case, because this corresponds to simple mechanical cochlear models with limited variations of the parameters. Such models are assumed to be realistic by many investigators. If the degree of the smoothing polynomial is raised in the least-squares smoothing procedure, which means that we allow greater variations in the parameters, the rise in the power flux function is considerably suppressed [see Fig. 3(d)]. The results in that case imply that the measured responses can be mimicked using a passive cochlea model. This conclusion supports the statement made by Viergever and Diependaal (1986) that sharply tuned BM data can be matched using a passive model of the cochlea without constraints on the mechanical

parameters.

In the framework of the assumptions made, the results obtained suggest the following conclusions:

- i. In the experiments of Johnstone and Yates (1974) the cochlea behaved as a passive filter. The increase in the power flux function calculated from these data is not significant (see Fig. 2).
- ii. In the experiments of Robles *et al.* (1986a,b) the cochlea behaved as an active filter; the region of activity is situated just basalwards of the BM velocity amplitude peak [Fig. 3(a)-(c)].
- iii. From the results of Sellick *et al.* (1983), it is not quite clear whether the cochlea showed mechanically active behavior. The Mössbauer source acts as an impedance load when placed on the BM, which gives rise to a pattern of inflections in the BM velocity data. This leads to power flux functions which are difficult to interpret [Figs. 4(b) and 5(b)], so conclusions about the behavior of the cochlea can hardly be drawn. However, Sellick *et al.* (1983) argue that measurements with a small source on the modiolar edge of the BM (like in animal 116) reflect best the behavior of an unloaded BM. Based on this argument, it can be concluded that the BM responses measured by Sellick *et al.* (1983) imply mechanical activity at the level of the BM, too.
- iv. In the calculations of the power flux functions from the BM velocity data, as measured by Robles *et al.* (1986a,b) and Sellick *et al.* (1983), a rise of 15-25 dB can be observed in the power flux functions. This value is about one-half of the value calculated by De Boer (1983c). At present, it is not clear whether the origin of this discrepancy is in the artificial nature of the response curves used by De Boer (1983c) or in the data processing methods used in the present work.

It is not clear why the inflection patterns in the BM velocity data, as measured by Sellick *et al.* (1983), are absent in the measurements by Robles *et al.* (1986a,b). The species difference is a likely candidate for the discrepancy: The chinchilla BM might be less loaded by the Mössbauer source than the guinea pig BM. Alternatively, there might be differences in the measurement techniques of the two groups of experimentators. It would be interesting to learn more about the influences of source size and location on the response in the chinchilla; this would enable a better comparison between

the results of the two groups.

## ACKNOWLEDGEMENT

This work has been supported by the Netherlands Organization for the Advancement of Pure Research (ZWO).

## REFERENCES

- Allen, J.B., Hall, J.L., Hubbard, A.E., Neely, S.T., and Tubis, A. (eds.) (1986). Peripheral Auditory Mechanisms, Springer, New York.
- Bialek, W.S. (1983a). Quantum effects in the dynamics of biological systems. Doctoral dissertation, Lawrence Berkeley Laboratory and University of California, Berkeley, CA.
- Bialek, W.S. (1983b). Thermal and quantum noise in the inner ear. In: Mechanics of Hearing, pp. 185-192. Editors: E. de Boer and M.A. Viergever. Martinus Nijhoff Publishers/Delft U.P., Delft.
- Bialek, W.S. and Wit, H.P. (1984). Quantum limits to oscillatory stability theory and experiments on acoustic emissions from the human ear, Phys. Lett. 104A, 173-178.
- Boer, E. de (1983a). No sharpening? A challenge for cochlear mechanics, J. Acoust. Soc. Am. 73, 567-573.
- Boer, E. de (1983b). On active and passive cochlear models - Towards a generalized analysis, J. Acoust. Soc. Am. 73, 574-576.
- Boer, E. de (1983c). Power amplification in an active model of the cochlea - Short-wave case, J. Acoust. Soc. Am. 73, 577-579.
- Boer, E. de (1983d). Wave reflection in passive and active cochlea models. In: Mechanics of Hearing, pp. 135-142. Editors: E. de Boer and M.A. Viergever. Martinus Nijhoff Publishers/Delft U.P., Delft.
- Boer, E. de and Viergever, M.A. (1982). Validity of the Liouville-Green (or WKB) mechanics, Hear. Res. 8, 131-155.
- Boer, E. de and Viergever, M.A. (eds.) (1983). Mechanics of Hearing, Martinus Nijhoff Publishers/Delft U.P., Delft.
- Craven, P. and Wahba, G. (1979). Smoothing noisy data with spline functions - Estimating the correct degree of smoothing by the method of generalized cross-validation, Numer. Math. 31, 377-403.
- Diependaal, R.J. and Viergever, M.A. (1983). Point-impedance characterization of the basilar membrane in a three-dimensional cochlea model, Hear. Res. 11, 33-40.
- Diependaal, R.J., Boer, E. de, and Viergever, M.A. (1986a). Determination of the cochlear power flux from basilar membrane vibration data. In: Peripheral Auditory Mechanisms, pp. 189-196. Editors: J.B. Allen, J.L. Hall, A.E. Hubbard, S.T. Neely, and A. Tubis. Springer, New York.
- Diependaal, R.J., Viergever, M.A., and Boer, E. de (1986b). Are active elements necessary in the basilar membrane impedance? J. Acoust. Soc. Am. 80, 124-132.
- Eldredge, D.H., Miller, J.D., and Bohne, B.A. (1981). A frequency-position map for the chinchilla cochlea, J. Acoust. Soc. Am. 69, 1091-1095.
- Guinan, J.J. Jr. and Peake, W.T. (1967). Middle ear characteristics of anesthetized cats, J. Acoust. Soc. Am. 41, 1237-1261.
- Johnstone, B.M. and Yates, G.K. (1974). Basilar membrane tuning curves in the guinea pig, J. Acoust. Soc. Am. 55, 584-587.
- Kemp, D.T. (1978). Stimulated acoustic emissions from within the human auditory system, J. Acoust. Soc. Am. 64, 1386-1391.

- Kim, D.O., Neely, S.T., Molnar, C.E., and Matthews, J.W. (1980). An active cochlear model with negative damping in the partition: Comparison with Rhode's ante- and post-mortem observations. In: Psychological, Physiological, and Behavioural Studies in Hearing, pp. 7-15. Editors: G. van den Brink and F.A. Bilsen. Delft U.P., Delft.
- Khanna, S.M. and Leonard, D.G.B. (1982). Basilar membrane tuning in the cat cochlea. *Science* 215, 305-306.
- Kohllöffel, L.U.E. (1972). A study of basilar membrane vibrations II. The vibratory amplitude and phase pattern along the basilar membrane (post-mortem). *Acustica* 27, 66-81.
- Liberman, M.C. (1982). The cochlear frequency map for the cat: Labeling auditory-nerve fibers of known characteristic frequency. *J. Acoust. Soc. Am.* 72, 1441-1449.
- Rhode, W.S. (1971). Observations of the vibration of the basilar membrane in squirrel monkeys using the Mössbauer technique. *J. Acoust. Soc. Am.* 49, 1218-1231.
- Robertson, D. and Johnstone, B.M. (1979). Aberrant tonotopic organization in the inner ear damaged by kanamycin. *J. Acoust. Soc. Am.* 66, 466-469.
- Robles, L., Ruggero, M.A., and Rich, N.C. (1986a). Mössbauer measurements of the mechanical response to single-tone and two-tone stimuli at the base of the chinchilla cochlea. In Peripheral Auditory Mechanisms, pp. 121-128. Editors: J.B. Allen, J.L. Hall, A.E. Hubbard, S.T. Neely, and A. Tubis. Springer, New York.
- Robles, L., Ruggero, M.A., and Rich, N.C. (1986b). Basilar membrane mechanics at the base of the chinchilla cochlea. I. Input-output functions, tuning curves, and response phases. *J. Acoust. Soc. Am.* 80, 1364-1374.
- Sellick, P.M., Patuzzi, R., and Johnstone, B.M. (1982). Measurements of basilar membrane motion in guinea pig using the Mössbauer technique. *J. Acoust. Soc. Am.* 72, 131-141.
- Sellick, P.M., Yates, G.K., and Patuzzi, R. (1983). The influence of Mössbauer source size and position on phase and amplitude measurements of the guinea pig basilar membrane. *Hear. Res.* 10, 101-108.
- Steele, C.R. and Taber, L.A. (1979). Comparison of WKB and finite difference calculations for a two-dimensional cochlear model. *J. Acoust. Soc. Am.* 65, 1001-1006.
- Viergever, M.A. (1980). Mechanics of the inner ear - A mathematical approach. Doctoral dissertation, Delft University of Technology (Delft U. P., Delft).
- Viergever, M.A. and Diependaal, R.J. (1986). Quantitative validation of cochlear models using the Liouville-Green approximation. *Hear. Res.* 21, 1-15.
- Zwicker, E. (1979). A model describing nonlinearities in hearing by active processes with saturation at 40 dB. *Biol. Cybernetics* 35, 243-250.



## CHAPTER FOUR

# Numerical methods for solving one-dimensional cochlear models in the time domain

**Abstract** In this article, a robust numerical solution method for one-dimensional (1D) cochlear models in the time domain is presented. The method has particularly been designed for models with a cochlear partition having nonlinear and active mechanical properties. The model equations are discretized with respect to the spatial variable by means of the principle of Galerkin to yield a system of ordinary differential equations in the time variable. To solve this system, several numerical integration methods are compared as concerns stability and computational performance. The selected algorithm is based on a variable step size fourth-order Runge-Kutta scheme; it is shown to be both more stable and much more efficient than previously published numerical solution techniques.

## LIST OF SYMBOLS

|   |   |
|---|---|
| $A, \hat{A}, A_1$                                 | system matrices [see Eqs. (17), (A4), (B17)]                            |
| $G$   | system matrix when a Green's function technique is used                 |
| $L$   | $A$ is decomposed in $LL^T$ , Eq. (25)-(27)                             |
| $Q, Q_1, Q_2$                                     | matrices containing masses in the nodal points, Eqs. (22), (B29), (B30) |
| $T$   | time at which the integration is ended                                  |
| $T_m$   | transformation ratio of middle-ear                                      |
| $a(x)$  | area of cross-section of one channel of the cochlea                     |
| $a_m$   | effective area of the middle-ear  |
| $am 1(T), am 2(T)$                                | accuracy measures in time integration procedure, Eqs. (23)-(24)         |
| $f(t)$  | input signal, Eq. (6)   |
| $g(x,t), g_1(x,t), g_2(x,t), g_{ME}(t), g_c(x,t)$ | see Eqs. (8), (B13), (B14), (A6), (B15), respectively.                  |

|   |  |
|---|--|
| $\underline{g}(t)$ , $\underline{g}_1(t)$ , $\underline{g}_2(t)$ , $\underline{g}_c(t)$ | see Eqs. (21), (B13), (B14), (B15), respectively.          |
| $\underline{h}(t)$  | additional vector in Eq. (29)                              |
| $\underline{k}(t)$ , $\hat{\underline{k}}(t)$ , $\underline{k}_1(t)$                    | see Eqs. (15), (A5), (B19), respectively.                  |
| $l$   | length of BM   |
| $m(x)$  | mass of BM per unit of area                                |
| $m_1(x)$  | mass associated with first degree of freedom               |
| $m_2(x)$  | mass associated with second degree of freedom              |
| $m_m$   | mass of middle-ear   |
| $m_s$   | mass of stapes   |
| $n$   | number of finite elements                                  |
| $p(x,t)$ , $p_1(x,t)$   | transmembrane pressure, Eqs. (2) and (B2)                  |
| $\underline{p}(t)$ , $\underline{p}_1(t)$   | see Eqs. (14) and (B18), respectively.                     |
| $p_e(t)$  | pressure at the eardrum                                    |
| $r(x,t)$  | resistance of BM   |
| $r_1(x,t)$  | resistance associated with first degree of freedom         |
| $r_2(x,t)$  | resistance associated with second degree of freedom        |
| $r_3(x,t)$  | resistance associated with coupling two degrees of freedom |
| $r_m$   | effective resistance of middle-ear and stapes              |
| $s(x,t)$  | stiffness of BM  |
| $s_1(x,t)$  | stiffness associated with first degree of freedom          |
| $s_2(x,t)$  | stiffness associated with second degree of freedom         |
| $s_3(x,t)$  | stiffness associated with coupling two degrees of freedom  |
| $s_m$   | effective stiffness of middle-ear and stapes               |
| $t$   | time variable  |

|  |   |
|--|---|
| $t_i$  | instance of time in integration process   |
| $u(x,t)$   | displacement of BM  |
| $u_1(x,t)$   | first degree of freedom   |
| $u_2(x,t)$   | second degree of freedom  |
| $u_s(t)$   | displacement of stapes  |
| $u^*(t), u^1(t), u^2(t), u^3(t)$                           | see Table 1   |
| $\underline{u}(t), \underline{u}_1(t), \underline{u}_2(t)$ | see Eqs. (20), (B24), (B25), respectively.  |
| $v_i^m(T)$   | solution of BM velocity in $i$ th nodal point,<br>when $[0,T]$ is divided into $m$ subintervals |
| $v_s(t)$   | stapes velocity   |
| $v^*(t), v^1(t), v^2(t), v^3(t)$                           | see Table 1   |
| $\underline{v}(t), \underline{v}_1(t), \underline{v}_2(t)$ | see Eqs. (18), (B20), (B21), respectively.  |
| $x$  | coordinate along the BM   |
| $\{x_0, x_1, \dots, x_i, \dots, x_{n-1}, x_n\}$            | set of nodal points, see Eq. (12)   |
| $y(t)$   | see Eq. (26)  |
| $\alpha(x), \alpha_1(x)$                                   | see Eqs. (7) and (B12), respectively.   |
| $\beta(x)$   | BM width  |
| $\omega(t,u,v)$  | see Table 1   |
| $\rho$   | fluid density   |
| $\Delta_i$   | length of $i$ th interval in spatial domain,<br>Eq. (16)  |
| $\Delta t$   | time step in the integration procedure  |

## INTRODUCTION

The *nonlinearity* of the cochlear response to sound stimuli has been firmly established for a long time. This nonlinear behaviour has been found in a huge number of psychophysical experiments and later in many neurophysiological experiments. For a review we refer to De Boer (1984) and Kim (1986). The presence of the cochlear nonlinearity at a mechanical level has been observed more recently by Rhode (1971, 1978), LePage and Johnstone (1980), Sellick, *et al.* (1982) and Robles *et al.* (1986).

Apart from being nonlinear, the cochlea is, very probably, also a mechanically *active* system. The inclusion of active features in descriptions of cochlear functioning is motivated by measurements of acoustic emissions (pioneered by Kemp, 1978). Bialek and Wit (1984) showed that such

emissions are the result of an (unstable) active filtering process rather than being filtered noise. Also, a comparison of the threshold auditory signal with the expected levels of quantum noise and thermal noise of the stereocilia provides arguments that the cochlea is an active system (Bialek, 1983a,b). Measurements of Khanna and Leonard (1982), Sellick et al. (1982) and Robles *et al.* (1984, 1986) seem to indicate that the active behaviour manifests itself already at the level of basilar membrane (BM) vibration. These experimental data show a very sharp tuning of the BM that cannot be reconciled with simulations of passive cochlear models (De Boer, 1983; Viergever and Diependaal, 1986). However, the presence of activity at the BM level has not been proven beyond all doubt (Diependaal *et al.*, 1986a,b, 1987).

Active properties may endanger the stability of the model response. Therefore, considerable attention should be given to the choice of the solution method. Furthermore, no features ought to be introduced or obscured by the mathematical treatment of the model equations. Linear active models can relatively easily be solved in the frequency domain by means of convergent numerical approximations. Numerical methods for nonlinear models are more complex and much more time consuming, though, because the solution has to be obtained in the time domain. We can alternatively use asymptotic methods, which are computationally fast and in addition will give more insight into the underlying physical mechanisms than numerical techniques do. Such methods are less accurate, however, and a measure of their accuracy can often be obtained only with the aid of a "numerically exact" solution.

The aim of the present article is to develop a robust and efficient solution method for nonlinear and active one-dimensional (1D) models. To this end we formulate the cochlear model in the time domain and solve the equations using a straightforward numerical technique. The cochlear partition is represented by coupled mass-spring-dashpot systems. In the simplest case, which corresponds to the standard 1D models in the frequency domain (for a review, see: Viergever, 1986), the partition at each point along its length has one degree of freedom (1DOF). The equations describing this model are formulated in Sec. I. One of the boundary conditions in the model is a prescribed stapes velocity. An alternative for this condition, *viz.* a simplified model of the middle-ear, is formulated in Appendix A. The numerical treatment of the middle-ear model is also outlined in Appendix A. The latter

alternative is physically more realistic than the former in the case of nonlinear models. In Sec. II, the 1DOF model equations are discretized in the spatial variable using the principle of Galerkin to obtain a system of ordinary differential equations. In order to solve this system, several numerical integration methods, *viz.* Heun's method, the fourth-order Runge-Kutta method and a modified Sielecki method, are compared in Sec. III as regards stability and efficiency. The fourth-order Runge-Kutta method appears to be the most efficient of the methods considered. Some numerical results of model calculations using this method are presented in Sec. IV. The method can easily be extended to models in which the cochlear partition at each point along its length is represented by more than one degree of freedom. Results for a two degrees of freedom model (2DOF) of Neely (1981) are presented in Sec. IV.

## I. THE 1DOF MODEL EQUATIONS

The geometry of the 1DOF cochlear model and the assumptions upon which the model is based have been discussed by Viergever (1980, Chap. 2). The partial differential equation describing the response of the BM [displacement  $u(x,t)$  averaged over the membrane width] to stapes movements is

$$p''(x,t) - \frac{2\rho\beta(x)}{a(x)} \ddot{u}(x,t) = 0, \quad 0 < x < l, t > 0, \quad (1)$$

where the overdot (prime) means differentiation with respect to time (place). For an explanation of the symbols, see the List of Symbols. The transmembrane pressure  $p(x,t)$  is defined by

$$p(x,t) = m(x)\ddot{u}(x,t) + r(x,t)\dot{u}(x,t) + s(x,t)u(x,t). \quad (2)$$

As can be observed, we allow the BM resistance  $r$  and stiffness  $s$  to depend on time  $t$ ; in particular,  $r$  and  $s$  are allowed to be functions of  $u$  and  $\dot{u}$ , which makes the model nonlinear. The BM mass  $m$  is taken to be time independent. The model description is completed by the following initial and boundary conditions:

$$u(x,0) = 0, \quad 0 \leq x \leq l, \quad (3)$$

$$\dot{u}(x,0) = 0, \quad 0 \leq x \leq l, \quad (4)$$

$$p(l,t) = 0, \quad t \geq 0. \quad (5)$$

Condition (5) expresses that the transmembrane pressure vanishes at the helicotrema ( $x=l$ ). At the base of the cochlea ( $x=0$ ), we consider two options for the boundary condition. The simplest of the two is to prescribe the movement of the stapes:

$$p'(0,t)=f(t), \quad t \geq 0. \quad (6)$$

A more realistic condition can be derived when the dynamics of the middle-ear are incorporated in the model. Matthews (1980) and Neely (1981) have analysed a model of the middle-ear with three degrees of freedom. This model can be simplified to a system with one degree of freedom, representing the motion of the stapes. The derivation of the middle-ear boundary condition and the effect of this boundary condition on the discretization of the model equations is outlined in Appendix A. With this boundary condition, the input signal to the system is the sound pressure at the eardrum instead of a prescribed stapes movement.

For linear BM dynamics (that is  $m$ ,  $r$ , and  $s$  do not depend on  $u$ ) the effect of the inclusion of a middle-ear transformation in the model is merely a scaling factor on the model response. When the BM behaves nonlinearly, there is an essential difference between the two sets of boundary conditions. Given harmonic stimulation, the stapes can only move with the input frequency when the middle-ear transformation is not included. This behaviour is physically not very realistic. When the middle-ear transformation is included, the stapes movements are not tied to the input frequency.

## II. THE DISCRETE SYSTEM FOR THE 1DOF MODEL

In order to solve the partial differential equation (1) with its boundary conditions (3)-(6) numerically, we have to discretize both in space and in time. Our strategy is to first render the partial differential equation discrete in the spatial variable so that a system of ordinary differential equations in the time variable is obtained. This system is subsequently solved by numerical integration. The advantage of this order of discretizing (first in space, next in time) is that we can integrate our system from time 0 to  $T$  and inspect the result on time  $T$ . If the result is not satisfactory (because there is still a large transient component in the response), we increase  $T$  and proceed our integration computations with the already calculated result as the new initial

value.

Upon defining  $\alpha$  and  $g$  by

$$\alpha^2(x) = 2\rho\beta(x)/\{m(x)a(x)\} \quad (7)$$

and

$$g(x,t) = r(x,t)\dot{u}(x,t) + s(x,t)u(x,t), \quad (8)$$

we can rewrite the model equations (1), (5) and (6) as

$$p''(x,t) - \alpha^2(x)p(x,t) = -\alpha^2(x)g(x,t), \quad (9)$$

$$p'(0,t) = f(t), t \geq 0; \quad (10)$$

$$p(l,t) = 0, t \geq 0. \quad (11)$$

The interval  $[0,l]$  is now divided into  $n$  finite elements by the set of nodal points

$$0 = x_0 < x_1 < \cdots < x_i < \cdots < x_{n-1} < x_n = l. \quad (12)$$

Upon introducing the customary piece-wise linear basis functions (the  $i$ th basis function has a value of 1 at  $x_i$  and of zero at all other nodal points) and applying the principle of Galerkin to Eqs. (9)–(11), we obtain the system of ordinary differential equations

$$Ap(t) = \underline{k}(t), \quad (13)$$

with

$$\underline{p}(t) = [p(x_0,t), p(x_1,t), \dots, p(x_{n-1},t)]^T, \quad (14)$$

and

$$\begin{aligned} \underline{k}(t) = & \frac{1}{2}[\alpha^2(x_0)g(x_0,t)\Delta_1 - 2f(t), \alpha^2(x_1)g(x_1,t)(\Delta_1 + \Delta_2), \\ & \alpha^2(x_2)g(x_2,t)(\Delta_2 + \Delta_3), \dots, \alpha^2(x_{n-1})g(x_{n-1},t)(\Delta_{n-1} + \Delta_n)]^T, \end{aligned} \quad (15)$$

where

$$\Delta_i = x_i - x_{i-1}, i \in \{1, 2, \dots, n\}. \quad (16)$$

Here,  $A$  is a tridiagonal matrix ( $a_{ij}$ ) given by

$$a_{ij} = \begin{cases} \frac{1}{2}\alpha^2(x_0)\Delta_1 + \frac{1}{\Delta_1}, & i=j=1 \\ \frac{1}{2}\alpha^2(x_{i-1})(\Delta_{i-1} + \Delta_i) + \frac{1}{\Delta_{i-1}} + \frac{1}{\Delta_i}, & i=j, i \in \{2, 3, \dots, n\} \\ -\frac{1}{\Delta_i}, & j=i+1, i \in \{1, 2, \dots, n-1\} \\ -\frac{1}{\Delta_{i-1}}, & j=i-1, i \in \{2, 3, \dots, n\} \end{cases} \quad (17)$$

The same equations [Eqs. (13)-(17)] will be found if one prefers to use finite differences instead of applying the method of Galerkin. The matrix  $A$  is time independent because we did not allow the BM mass to depend on  $t$ . This has the distinct advantage that  $A$  need be computed only once.

From Eqs. (2), (8), (3) and (4), we learn that the BM displacement  $u$  and BM velocity  $v$  must satisfy the system of ordinary differential equations

$$\dot{\underline{u}}(t) = \underline{v}(t), \underline{u}(0) = \underline{0}, \quad (18)$$

$$\dot{\underline{v}}(t) = Q[\underline{p}(t) - \underline{g}(t)], \underline{v}(0) = \underline{0}, \quad (19)$$

where

$$\underline{u}(t) = [u(x_0, t), u(x_1, t), \dots, u(x_{n-1}, t)]^T, \quad (20)$$

$$\underline{g}(t) = [g(x_0, t), g(x_1, t), \dots, g(x_{n-1}, t)]^T, \quad (21)$$

and

$$Q = \text{diag} \left\{ \frac{1}{m(x_0)}, \frac{1}{m(x_1)}, \dots, \frac{1}{m(x_{n-1})} \right\}. \quad (22)$$

The algorithm to solve the model equations numerically will now be clear:

- i. Divide the time interval  $[0, T]$  into a number of subintervals  $[t_0, t_1], [t_1, t_2], \dots, [t_{m-1}, t_m]$ ,  $t_0=0, t_m=T$ .  
For  $i=1$  step 1 until  $m$  perform steps (ii)-(v).
- ii. Compute at time  $t_{i-1}$  the vectors  $\underline{g}$  and  $\underline{k}$ ,
- iii. Solve  $\underline{p}$  from Eq. (13),
- iv. Compute  $Q(\underline{p} - \underline{g})$ ,
- v. Integrate Eqs. (18) and (19) from time  $t_{i-1}$  to  $t_i$ .

The method outlined in this section is more elegant and more efficient than the one presented in Diependaal and Viergever (1983). An important step in obtaining numerical solutions of the model equations is choosing an appropriate numerical integration method for the system of ordinary differential equations [step (v) of the algorithm]. This step will be treated in detail in Sec. III.

### III. NUMERICAL ANALYSIS

#### A. Numerical integration methods

We selected three integration methods whose performance we evaluated, *viz.*, Heun's method, the fourth-order Runge-Kutta method and a modified Sielecki method. The method of Sielecki is known in the field of fluid dynamics (Sielecki, 1968). In cochlear mechanics, a variant of this method has been proposed by Allen and Sondhi (1979), it has furthermore been applied by Matthews (1980) and Neely (1981).

In Table 1 the essence of the three integration methods is given. The Euler method has been taken into consideration too, but the computation time needed to arrive at a stable numerical scheme appeared to be unacceptably large. Therefore, we left it out of further analysis. Furthermore, we have not analysed implicit numerical methods; although they are ideal as regards numerical stability, their computation time is out of all proportion.

In comparing the different methods we especially pay attention to the stability and the computational efficiency of the methods. The methods have been evaluated using various model examples. In this section we give some results for one test case, namely, the model consisting of coupled Van der Pol oscillators (we use 512 oscillators in this article) as described by Van Netten and Duifhuis (1983) and Duifhuis *et al.* (1986). The choice of this model is motivated by the fact that it is both nonlinear and active, which makes it well suited for illustrating the difference in performance characteristics of the integration methods.

---

<sup>1</sup> It should be emphasized at this point that the numerical results presented for the Van der Pol model should *not* be considered as valid approximate solutions of Eq. 1 (with the appropriate boundary conditions). They represent the behaviour of a large set of Van der Pol oscillators with a coupling term  $p$  satisfying the discretized system of Eqs. (13), (18) and (19). The results for this model strongly depend on the  $x$  discretization (on the way of discretizing as well as on the number of nodal points; Duifhuis *et al.*, 1986).

**TABLE 1.** Scheme of numerical integration methods

$$\begin{cases} \dot{u}(t) = v(t) \\ \dot{v}(t) = \omega[t, u(t), v(t)] \end{cases}$$

Modified Sielecki:

$$\begin{cases} v(t + \Delta t) = v(t) + \Delta t \omega[t, u(t), v(t)] \\ u(t + \Delta t) = u(t) + \Delta t v(t + \Delta t) \end{cases}$$

Heun:

$$\begin{cases} u^* = u(t) + \Delta t v(t) \\ v^* = v(t) + \Delta t \omega[t, u(t), v(t)] \\ u(t + \Delta t) = u(t) + \frac{1}{2} \Delta t [v(t) + v^*] \\ v(t + \Delta t) = v(t) + \frac{1}{2} \Delta t \{\omega[t, u(t), v(t)] + \omega(t + \Delta t, u^*, v^*)\} \end{cases}$$

Fourth-order Runge-Kutta:

$$\begin{cases} u^{(1)} = u(t) + \frac{1}{2} \Delta t v(t) \\ v^{(1)} = v(t) + \frac{1}{2} \Delta t \omega[t, u(t), v(t)] \\ u^{(2)} = u(t) + \frac{1}{2} \Delta t v^{(1)} \\ v^{(2)} = v(t) + \frac{1}{2} \Delta t \omega(t + \frac{1}{2} \Delta t, u^{(1)}, v^{(1)}) \\ u^{(3)} = u(t) + \Delta t v^{(2)} \\ v^{(3)} = v(t) + \Delta t \omega(t + \frac{1}{2} \Delta t, u^{(2)}, v^{(2)}) \\ u(t + \Delta t) = u(t) + \frac{\Delta t}{6} [v(t) + 2v^{(1)} + 2v^{(2)} + v^{(3)}] \\ v(t + \Delta t) = v(t) + \frac{\Delta t}{6} \{\omega[t, u(t), v(t)] + 2\omega(t + \frac{1}{2} \Delta t, u^{(1)}, v^{(1)}) \\ + 2\omega(t + \frac{1}{2} \Delta t, u^{(2)}, v^{(2)}) + \omega(t + \Delta t, u^{(3)}, v^{(3)})\} \end{cases}$$

### 1. Stability

A very important condition which integration methods must satisfy is that of numerical stability. This puts limits on the size of the integration step  $\Delta t$ . For each integration method, the limit depends on the nature of the model equations under consideration. In our test case (the coupled Van der Pol oscillators model), we compute model responses from time  $t=0$  to time

$t = T$  (a characteristic value for  $T$  is 100 ms) using the chosen methods. In these computations, a constant step size has been used, i.e., the time interval  $[0, T]$  has been divided into a number of intervals  $[t_i, t_{i+1}]$  of equal length. If, for a given method, the condition of stability has not been met, the number of intervals is doubled (the step size is halved) and the calculations are carried out again. With this procedure, a conservative guess of the step size limit can be obtained. From this test case study and from others, we have found that the step size limit for the fourth-order Runge-Kutta method is approximately twice as large as that for the Heun and the modified Sielecki method.

## 2. Efficiency

The time the computer needs to integrate the system of ordinary differential equations in  $t$  will be considerable because  $T$  (the time the integration procedure is stopped) must be rather large in order to get rid of transients in the response. Furthermore, at each time  $t_i$ , an equation of the form  $A\underline{p}(t) = \underline{k}(t)$  must be solved, where  $\underline{p}(t)$  is the unknown vector. The computation of  $\underline{p}$  is rather time consuming, which calls for an efficient method in the sense that the number of times that  $A\underline{p}(t) = \underline{k}(t)$  must be solved is minimal. From Table 1 we see that at each time step the modified Sielecki method needs to solve  $A\underline{p}(t) = \underline{k}(t)$  once, the Heun method twice, and the fourth-order Runge-Kutta method four times. Thus the modified Sielecki method is two times faster than the method of Heun, which in its turn is two times faster than the fourth-order Runge-Kutta method. (In both cases, the factor of 2 is approximate; some overhead calculations have to be done which can be slightly different for the different methods.)

Thus far we have not looked at the accuracy of the methods. Therefore, we have computed responses to our model example for several values of the step size. In each case the accuracy is calculated using two distance measures, *am 1* and *am 2*:

$$am\ 1 = \left( \sum_{i=i_b}^{i_e} \frac{[v_i^m(T) - v_i^{2m}(T)]^2}{[v_i^m(T)]^2} \right)^{\frac{1}{2}}, \quad (23)$$

$$am\ 2 = \sum_{i=i_b}^{i_e} \frac{|v_i^m(T) - v_i^{2m}(T)|}{|v_i^m(T)|}. \quad (24)$$

The quantities  $i_b$  and  $i_e$  indicate the begin and end point of the region, where

the response of the test case model is entrained by the input signal. Accuracy measure *am 1* is relatively large if, on a few points along the BM, the difference  $v_i^m - v_i^{2m}$  is large. Accuracy measure *am 2* is relatively large if, on many points along the BM, the difference  $v_i^m - v_i^{2m}$  is unequal to zero. For the model example at hand, measure *am 2* is most appropriate for evaluating the accuracy of the numerical methods. We have summarized our computations in Table 2 for  $T = 101 \text{ ms}$ .

**TABLE 2.** Table of CPU times needed by the three numerical integration methods to solve the nonlinear active cochlear model of Van Netten and Duifhuis (1983) over the interval [0, 101 ms]. MS stands for 'modified Sielecki method'; RK4 for fourth order Runge-Kutta; *am 1* and *am 2* are defined by Eqs. (23) and (24); and  $i_b$  and  $i_e$  correspond to  $x = 13.0 \text{ mm}$  and  $x = 20.0 \text{ mm}$ , respectively.

| method | $\Delta t$ (ms) | CPU time    | am1                  | am2                   |
|--------|-----------------|-------------|----------------------|-----------------------|
| RK4    | 1/128           | 23 min 28 s | $<10^{-6}$           | 0.09                  |
| -      | Heun            | 1/256       | 22 min 46 s          | $<10^{-6}$            |
| -      | MS              | 1/512       | 22 min 18 s          | $3.82 \times 10^{-4}$ |
| -      | RK4             | 1/64        | 11 min 45 s          | $<10^{-5}$            |
| -      | Heun            | 1/128       | 11 min 24 s          | $8 \times 10^{-4}$    |
| -      | MS              | 1/256       | 11 min 7 s           | $4.12 \times 10^{-4}$ |
| -      | MS              | 1/128       | 5 min 33 s           | $2.44 \times 10^{-4}$ |
| -      | RK4             | 1/32        | NUMERICALLY UNSTABLE |                       |
| -      | Heun            | 1/64        | NUMERICALLY UNSTABLE |                       |
| -      | MS              | 1/64        | NUMERICALLY UNSTABLE |                       |

It shows for each method the step sizes we have used, the two accuracy measures for each case and the CPU times on a IBM 3083 JX1 computer. From the figures in Table 2 it can be seen that, if we choose the step size in such a way that the CPU times for the three methods are approximately equal, the fourth-order Runge-Kutta method is much more accurate than the Heun and modified Sielecki methods. In other words, the fourth-order Runge-Kutta is the most efficient of the methods considered.

### B. Variable step size methods

Now that the fourth-order Runge-Kutta method has been selected as the appropriate integration procedure for the system of ordinary differential equations, we should still discuss the most efficient way to implement the

method. In most cases, an equidistant mesh (in the time) as discussed above is not optimal. We therefore considered a variable step size fourth-order Runge-Kutta algorithm. The paradigm is as follows: At time  $t_i$  the appropriate step size is estimated and the system is integrated from  $t_i$  to  $t_{i+1}$  using a third-order, as well as a fourth-order, Runge-Kutta method. (This only costs a little more computing time, since the function evaluations calculated in the third-order scheme can be used in the fourth-order scheme.) If the absolute difference between the third- and fourth-order solution is larger than the tolerance supplied by the user, the step size is reduced and the procedure is repeated. When the difference is less than the tolerance, the integration over the next time interval is started.

### C. Matrix decomposition

Integration of the system of ordinary differential equations is the most important part of the algorithm. The second important part is solving  $\underline{p}$  from the matrix-vector equation  $A\underline{p}(t) = \underline{k}(t)$  [see Eq. (13)] each time step. This is accomplished by decomposing  $A$  in a lower-triangular and an upper-triangular matrix. (Decomposing has the advantage that the matrix needs not be inverted in order to solve the system of equations.) Since  $A$  is positive definite, it is best decomposed using Cholesky's method, which transforms the system of equations into

$$LL^T \underline{p}(t) = \underline{k}(t), \quad (25)$$

where  $L$  is a lower-triangular matrix. The procedure to solve  $\underline{p}$  is now: calculate  $\underline{y}$  from

$$Ly(t) = \underline{k}(t) \quad (26)$$

component by component, starting with the first equation; then calculate  $\underline{p}$  from

$$L^T \underline{p}(t) = \underline{y}(t) \quad (27)$$

component by component, starting with the last equation.

We only have to decompose the matrix  $A$  once because  $A$  does not depend on  $t$ . Solving  $\underline{p}$  from Eqs. (26) and (27) must be done at every time step since  $\underline{k}$  does depend on  $t$ . Here,  $A$  is a tridiagonal matrix, so  $L$  is a matrix with nonzero entries only on the diagonal and the subdiagonal. Hence, we can

calculate the number of elementary computer operations (one multiplication plus one addition) needed for solving  $\underline{p}$  from Eqs. (26) and (27); this number is given by

$$N_{CH} = 4n - 2, \quad (28)$$

where  $n$  is the dimension of  $\underline{p}, \underline{y}, \underline{k}$  and  $A$  and the subscript  $CH$  stands for Cholesky.

#### D. Discretizing the space domain using a Green's function technique

An alternative way of discretizing the model equations with respect to  $x$  has been presented by Furst and Goldstein (1982) and Jones *et al.* (1986). Instead of the finite element method, these authors use a Green's function technique. This leads to the same system of ordinary differential equations, but  $\underline{p}$  must now be calculated from

$$\underline{p}(t) = G\underline{g}(t) + \underline{h}(t), \quad (29)$$

where  $G$  is a full  $n \times n$  matrix and  $\underline{h}$  is an  $n$ -dimensional vector which depends on  $t$ . The number of elementary computer operations needed for calculating  $\underline{p}$  from Eq. (29) is given by

$$N_{GR} = n^2, \quad (30)$$

where the subscript  $GR$  stands for Green's function technique. By comparing (28) with (30) we see that  $N_{GR}$  is larger than  $N_{CH}$  for  $n \geq 4$ . This implies that the total CPU time for the integration procedure is proportional to a polynomial of the second degree in  $n$  when a Green's function technique is used, whereas the total CPU time is proportional to a polynomial of degree one in  $n$  when the Cholesky decomposition method is used. We have computed responses in several of our model examples using the Green's function method and compared the computation time with that of our method. We shall give one typical result: calculating the response of the Van der Pol oscillators model (see Sec. III-A) over the interval [0, 22ms] using the Green's function technique required 84 minutes on our IBM 3083 JX1 machine. An equidistant mesh in the  $x$  direction of 512 elements has been used. With our technique, the CPU time was 3½ minutes under the same circumstances, which is about 24 times faster than the Green's function technique. The ratio 24 is for the complete program; the part of the program which computes  $\underline{p}(t)$  each time step is about 128 ( $= N_{GR}/N_{CH}$  for  $n=512$ ) times

faster using our technique than using the Green's function technique. This illustrates the efficiency of our algorithm.

#### IV. NUMERICAL RESULTS

In this section, we shall give some illustrative examples of our results. First, we have computed the responses to a  $1-kHz$  tone in a linear, passive 1DOF model.

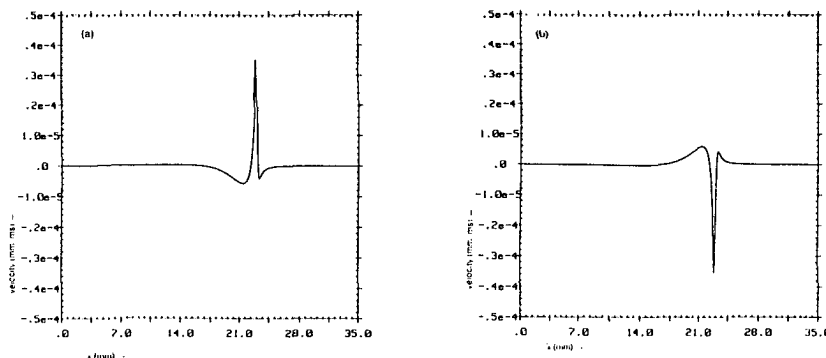


**Figure 1.** Response to a  $1-kHz$  tone in a linear, passive 1DOF model. (a) BM velocity at  $40.5\text{ ms}$  after tone onset; (b) BM velocity at  $41.0\text{ ms}$  after tone onset. Parameters:  $l=35\text{ mm}$ ,  $\alpha^2(x)=0.4\text{ mm}^{-2}$ ,  $m(x)=0.5\text{ mg/mm}^2$ ,  $r(x,t)=5\exp(-0.15x)\text{ mg}/(\text{mm}^2\text{ms})$ ,  $s(x,t)=20,000\exp(-0.3x)\text{ mg}/(\text{mm}^2\text{ms}^2)$ , with  $x$  in  $\text{mm}$ . The BM has been divided into 512 elements of equal size.

Figure 1 shows the BM velocity as a function of distance along the BM at two times. By means of a Fast Fourier Transform (FFT) technique, the frequency spectrum of the BM velocity has been computed [Fig. 2(a) and (b)]. In the frequency domain response, the transients are much better visualized (in fact, in the time domain representation, the transients cannot be seen at all). Figure 2(c) and (d) shows the response at a latter time; the transients are now much smaller. These dying transients, due to switching on the  $1-kHz$  tone, can be seen as ripples in the amplitude and phase curves of the frequency domain response. The BM velocity can also be computed directly in the frequency domain because the model is linear. The result of this calculation has been plotted in Fig. 2(e) and (f) for comparison.

The second model example we considered is the 2DOF model of Neely

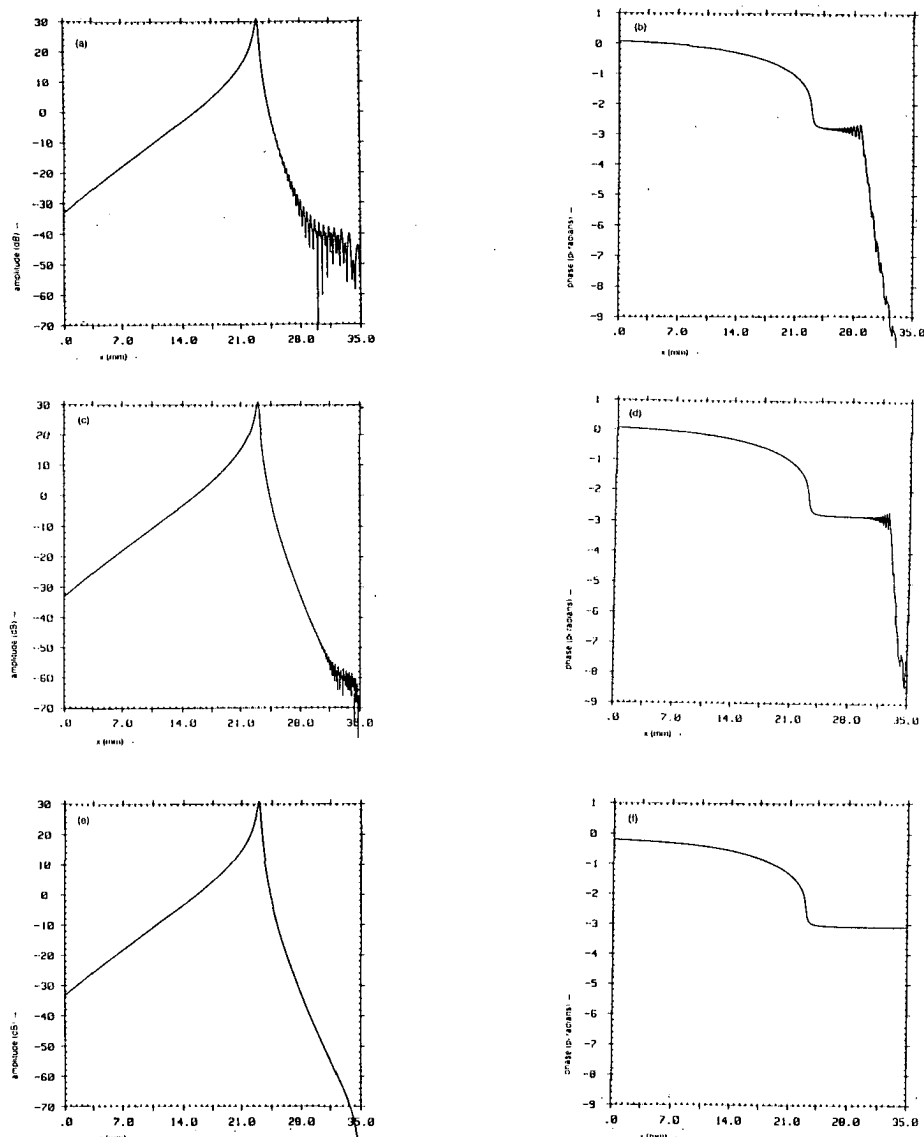


**Figure 2.** Responses of the linear, passive 1DOF model in the frequency domain. (a), (b) Amplitude and phase of first harmonic of Fourier transform of BM velocity response as in Fig. 1 (computed 41ms after tone onset). (c), (d) Amplitude and phase of first harmonic of Fourier transform of response as in Fig. 1 (computed 101ms after tone onset). (e), (f) Amplitude and phase of BM velocity calculated from a frequency domain formulation of the model equations. The decibel scale is arbitrary.

(1981). The fundamental Fourier component of the hair cell shearing displacement is shown in Fig. 3. The results are comparable with Neely's (Fig. 4.5 of his paper). The differences between Neely's results and ours are due to the fact that Neely obtained his results from calculations in a two-dimensional (2D) model.

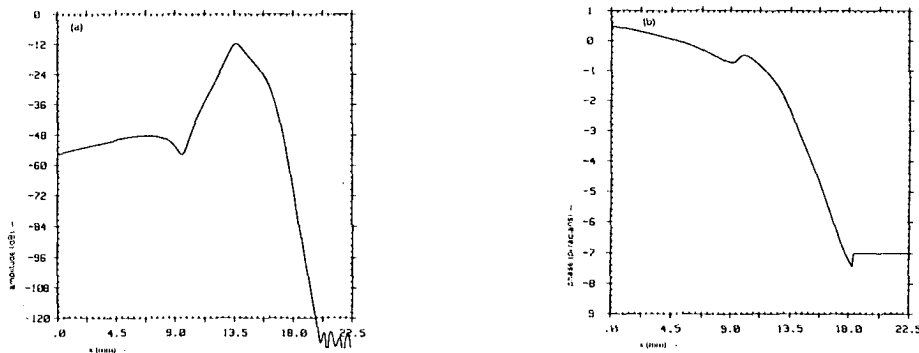


**Figure 3.** Response of Neely's (1981) 2DOF model to a harmonic stimulus (1.6 kHz). Plotted are amplitude (a) and phase (b) of fundamental Fourier component of hair cell shearing displacement. Parameter values (after Neely 1981):  $l = 22.5 \text{ mm}$ ,  $\rho = 1 \text{ mg/mm}^3$ ,  $\beta(x) = 1 \text{ mm}$ ,  $a(x) = 1 \text{ mm}^2$ ,  $a_m = 34.7 \text{ mm}^2$ ,  $m_1(x) = 0.045 \exp(0.08x) \text{ mg/mm}^2$ ,  $m_2(x) = 0.018 \exp(0.03x) \text{ mg/mm}^2$ ,  $r_1(x,t) = 0.5 \exp(0.05x) \text{ mg}/(\text{mm}^2\text{ms})$ ,  $r_2(x,t) = 0.9 \exp(-0.3x) \text{ mg}/(\text{mm}^2\text{ms})$ ,  $r_3(x,t) = 1 \exp(-0.2x) \text{ mg}/(\text{mm}^2\text{ms})$ ,  $s_1(x,t) = 4600 \exp(-0.32x) \text{ mg}/(\text{mm}^2\text{ms}^2)$ ,  $s_2(x,t) = 380 \exp(-0.526x) \text{ mg}/(\text{mm}^2\text{ms}^2)$ ,  $s_3(x,t) = 1500 \exp(-0.47x) \text{ mg}/(\text{mm}^2\text{ms}^2)$ ,  $T_m = 2$ ,  $T_m^2 m_m + m_s = 23.55 \text{ mg}$ ,  $T_m^2 r_m = 58.4 \text{ mg/ms}$ ,  $s_m = 1817 \text{ mg/ms}^2$ ,  $x$  in mm. The BM has been divided into 512 elements of equal size. Responses are shown after 25.625 ms of tone onset. The decibel scale is arbitrary.

As an example of a nonlinear and active model we have selected a model consisting of coupled Van der Pol oscillators (Van Netten and Duifhuis, 1983; Duifhuis *et al.*, 1986). The results for this model strongly depend upon the  $x$  discretization (see footnote # 1). Here, we only present the calculation for one case, *viz.*, where a part of the chain of oscillators has been entrained by an external tone. In Fig. 4 the amplitude and phase of the fundamental and the amplitudes of the second up to the fifth Fourier components are shown. The entrainment of the response can be observed in the region between 13 and 20 mm. Outside this region the response is dominated by limit cycle oscillations and by transients from the onset of the signal. In the entrained region the response consists, apart from the fundamental, of all uneven harmonics [see Fig. 4(c) and (e)]. There are at least two peaks observable in the

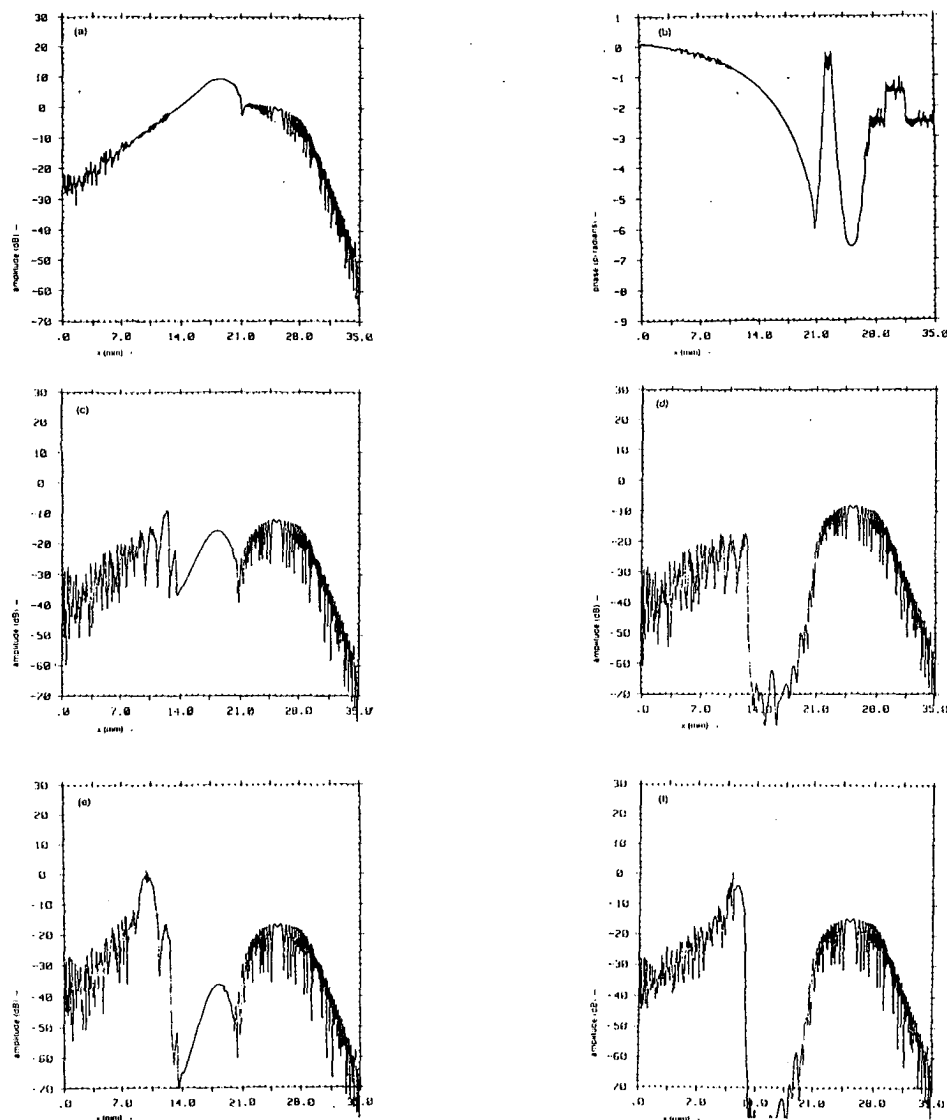


**Figure 4.** Response of a nonlinear active model (Van Netten and Duifhuis, 1983; Duifhuis et al., 1986). Parameter values (after Duifhuis et al., 1986):  $l=35 \text{ mm}$ ,  $\alpha^2=4 \text{ mm}^{-2}$ ,  $m(x)=0.5 \text{ mg/mm}^2$ ,  $r(x,t)=2.5(2)^{14}[-1+10^{12}v^2(x,t)]\exp(-0.15x) \text{ mg}/(\text{mm}^2\text{ms})$ ,  $s(x,t)=10,000 \exp(-0.3x) \text{ mg}/(\text{mm}^2\text{ms}^2)$ ,  $a(x)=1 \text{ mm}^2$ ,  $a_m=60 \text{ mm}^2$ ,  $T_m=2$ ,  $T_m^2m_m+m_s=0.792 \text{ mg}$ ,  $r_m=6.22 \text{ mg/ms}$ ,  $s_m=125.08 \text{ mg/ms}^2$ ,  $x$  in mm. Stimulus  $p_e(t)=6 \cdot 10^{-7} \sin(2\pi t) \text{ mg mm/ms}^2$ ,  $t$  in ms. The BM has been divided into 512 elements of equal size. Responses are shown after 101 ms of tone onset. (a) Amplitude (dB re 1 mm/ms) of fundamental Fourier component; (b) Phase of fundamental Fourier component; (c)-(f) Amplitude (dB re 1 mm/ms) of third, second, fifth and fourth Fourier component, respectively.

plots of the higher uneven harmonics: one at the characteristic place of the fundamental (that is, the location where the fundamental has its maximum) and one at the characteristic place for a 3-kHz input signal. The even harmonics are absent in the entrained region; the response in this region gives an indication of the total numerical error involved in the calculations [Fig. 4(d) and (f)].

## V. DISCUSSION AND CONCLUSIONS

We have developed a robust numerical method to solve 1D cochlear models in the time domain. With this method, the response of models having non-linear and active properties can be calculated for a variety of stimuli, such as pure tones, two tones, noise, and clicks. Phenomena like combination tones, two-tone suppression, and transients can thus be studied. The method is not suited for extensive parameter variation studies owing to the large computation time (in spite of its efficiency as compared with other numerical techniques). For this purpose, asymptotic methods are more appropriate. The present numerical technique can be used as a frame of reference in order to assess the accuracy of such methods.

In 1D time-domain cochlear models, there are two independent continuous variables, *viz.*,  $x$ , the coordinate along the BM, and  $t$ , the time. Numerical calculations thus require a discretization of the model equations in two directions. We have first discretized, using Galerkin's principle, in the  $x$  direction in order to obtain a system of ordinary differential equations in the time variable. Another method, which makes use of Green's functions (Furst and Goldstein, 1982; Jones *et al.*, 1986), has also been considered. Numerical calculations show that the latter method is much less efficient.

The elements, into which the interval  $[0, l]$  is divided are usually of equal size in our method. A division into elements of nonequal size would be more efficient, but criteria on which the generation of the variable step size mesh should be based are lacking. An exception is provided by linear models, for which the element dimension can be taken proportional to the local wavelength. Further studies into nonequidistant meshes for non-linear models might prove beneficial.

After the system equations have been discretized in the  $x$  direction by means of Galerkin's principle, we have to discretize the system of ordinary differential equations in  $t$ . This is the main part of the numerical analysis. We have compared three different integration methods: modified Sielecki, Heun and fourth-order Runge-Kutta. The fourth-order Runge-Kutta method turns out to be superior to the others as regards both stability and efficiency. The implementation of the fourth-order Runge-Kutta method is best accomplished by making use of a variable step size routine. That is, the step size is adjusted such that the solution stays between the limits of a given accuracy.

The method presented in this article is not limited to cochlear models with only one degree of freedom. An extension to 2DOF (two degrees of freedom) models has been outlined in Appendix B. Other extensions, such as to 2D and 3D cochlear models are also straightforward. The computing time will already be quite long, however, for the 2D model with one degree of freedom, in which case the matrix  $A$  in Eq. (13) is full instead of tridiagonal. The number of elementary computer operations needed to solve  $p$  from Eq. (13) is then  $n(n+1)$ , which is of the order of  $N_{GR}$  [Eq. (30)].

#### **ACKNOWLEDGEMENT**

This research has been supported by the Netherlands Organisation for the Advancement of Pure Research "ZWO" (RJD).

#### **APPENDIX A: INCLUSION OF A SIMPLIFIED MODEL OF THE MIDDLE-EAR**

We can include a simple description of the middle-ear dynamics in the model by following the analysis of Matthews (1980) and Neely (1981). Equation (6) should then be replaced by

$$p'(0,t) = 2\rho\ddot{u}_s(t), \quad t \geq 0 \quad (\text{A1})$$

and

$$\begin{aligned} T_m a_m p_e(t) + ap(0,t) &= [T_m^2 m_m + m_s] \ddot{u}_s(t) + \\ &+ T_m^2 r_m \dot{u}_s(t) + s_m u_s(t), \end{aligned} \quad (\text{A2})$$

where the meaning of the symbols can be found in the List of Symbols. The eardrum pressure  $p_e$  is the input signal to this system.

A discrete version of the model equations can be obtained in the same manner as in Sec. II. Instead of Eq. (10) we now use Eqs. (A1), (A2) and apply the principle of Galerkin to arrive at

$$\hat{A}\underline{p}(t) = \hat{k}(t), \quad (\text{A3})$$

where  $\hat{A}$  is a tridiagonal matrix ( $\hat{a}_{ij}$ ) which only differs from  $A$  in its first diagonal element

$$\hat{a}_{ij} = \begin{cases} \frac{1}{2}\alpha^2(x_0)\Delta_1 + \frac{1}{\Delta_1} + \frac{2\rho a}{T_m^2 m_m + m_s}, & i=j=1, \\ a_{ij}, & \text{elsewhere.} \end{cases} \quad (\text{A4})$$

Also,  $\hat{k}$  differs from  $k$  only in its first element  $\hat{k}_1$ , where  $\hat{k}_1$  is

$$\hat{k}_1(t) = \frac{1}{2}\alpha^2(x_0)g(x_0, t)\Delta_1 + \frac{4\rho[g_{ME}(t) - T_m a_m p_e(t)]}{T_m^2 m_m + m_s}, \quad (\text{A5})$$

with  $g_{ME}$  defined by

$$g_{ME}(t) = T_m^2 r_m \dot{u}_s(t) + s_m u_s(t). \quad (\text{A6})$$

The system of ordinary differential equations [Eqs. (18) and (19)] has now been extended with two equations for the motion of the stapes:

$$\dot{u}_s(t) = v_s(t), \quad u_s(0) = 0, \quad (\text{A7})$$

$$\dot{v}_s(t) = \underline{v}(t), \quad \underline{v}(0) = 0, \quad (\text{A8})$$

$$\dot{v}_s(t) = \frac{T_m a_m p_e(t) + a_p(0, t) - g_{ME}(t)}{T_m^2 m_m + m_s}, \quad v_s(0) = 0, \quad (\text{A9})$$

$$\dot{\underline{v}}(t) = Q[\underline{p}(t) - \underline{g}(t)], \quad \underline{v}(0) = 0. \quad (\text{A10})$$

The algorithm to solve Eqs. (1)-(5), (A1) and (A2) numerically is analogous to that described at the end of Sec. II.

## APPENDIX B: THE 2DOF MODEL

The model described in the main text has only one degree of freedom. In such a model, the mechanical structures of the organ of Corti/tectorial membrane complex are lumped upon the BM. Every point on the BM is then represented by a single mass-spring-dashpot system. A 2DOF model deals with independent movements of the organ of Corti/tectorial membrane complex. Models with two degrees of freedom have been proposed by Zwischki (1980a, b) and Allen (1980). A 2DOF model has been used both to achieve a transduction from BM motion to hair cell shearing which closely matches measurements of neural response (Neely, 1981) and to reduce the discrepancies between cochlear model calculations and experimental data on BM vibration (Zwischki, 1983). Such a 2DOF model can be handled in the same way as the 1DOF models. They are governed by the following equations, where the meaning of the symbols is given in the List of Symbols:

$$p_1''(x,t) - \frac{2\rho\beta(x)}{\alpha(x)}\ddot{u}_1(x,t) = 0, \quad 0 < x < l, \quad t > 0, \quad (\text{B1})$$

with  $p_1$  defined by

$$\begin{aligned} p_1(x,t) = & m_1(x)\ddot{u}_1(x,t) + [r_1(x,t) + r_3(x,t)]\dot{u}_1(x,t) + \\ & + [s_1(x,t) + s_3(x,t)]u_1(x,t) - r_3(x,t)\dot{u}_2(x,t) - s_3(x,t)u_2(x,t). \end{aligned} \quad (\text{B2})$$

The initial conditions read

$$u_1(x,0) = 0, \quad 0 \leq x \leq l, \quad (\text{B3})$$

$$\dot{u}_1(x,0) = 0, \quad 0 \leq x \leq l, \quad (\text{B4})$$

$$u_2(x,0) = 0, \quad 0 \leq x \leq l, \quad (\text{B5})$$

$$\dot{u}_2(x,0) = 0, \quad 0 \leq x \leq l. \quad (\text{B6})$$

The boundary condition at the stapes<sup>2</sup> is given by

$$p_1'(0,t) = f(t), \quad t \geq 0. \quad (\text{B7})$$

---

2. As in the 1DOF model, a simplified model of the middle-ear dynamics can be included. The description of the middle-ear dynamics and its numerical treatment is completely analogous to that given in Appendix A.

At the helicotrema, we have the condition

$$p_1(l, t) = 0, \quad t \geq 0. \quad (\text{B8})$$

This model is completed by an equation describing the balance of forces on the second degree of freedom:

$$m_2(x)\ddot{u}_2(x, t) + [r_2(x, t) + r_3(x, t)]\dot{u}_2(x, t) + \quad (\text{B9})$$

$$[s_2(x, t) + s_3(x, t)]u_2(x, t) - r_3(x, t)\dot{u}_1(x, t) - s_3(x, t)u_1(x, t) = 0,$$

with initial conditions

$$u_2(x, 0) = 0, \quad 0 \leq x \leq l, \quad (\text{B10})$$

$$\dot{u}_2(x, 0) = 0, \quad 0 \leq x \leq l. \quad (\text{B11})$$

If we now define  $\alpha_1$ ,  $g_1$ ,  $g_2$  and  $g_c$  by

$$\alpha_1^2(x) = \frac{2\rho\beta(x)}{m_1(x)a(x)}, \quad (\text{B12})$$

$$g_1(x, t) = r_1(x, t)\dot{u}_1(x, t) + s_1(x, t)u_1(x, t), \quad (\text{B13})$$

$$g_2(x, t) = r_2(x, t)\dot{u}_2(x, t) + s_2(x, t)u_2(x, t), \quad (\text{B14})$$

$$g_c(x, t) = r_3(x, t)[\dot{u}_1(x, t) - \dot{u}_2(x, t)] + s_3(x, t)[u_1(x, t) - u_2(x, t)], \quad (\text{B15})$$

we can rewrite Eq. (B1) as

$$p_1''(x, t) - \alpha_1^2(x)[p_1(x, t) - g_1(x, t) - g_c(x, t)] = 0. \quad (\text{B16})$$

The model equations (B16), (B7), and (B8) can be discretized in the same way as described in Sec. II. This yields the system of equations

$$A_1 \underline{p}_1(t) = \underline{k}_1(t), \quad (\text{B17})$$

where  $A_1$  is defined by Eq. (17) upon replacing  $\alpha$  by  $\alpha_1$ . Furthermore,  $\underline{p}_1$  is given by

$$\underline{p}_1 = [p_1(x_0, t), p_1(x_1, t), \dots, p_1(x_{n-1}, t)]^T \quad (\text{B18})$$

and  $\underline{k}_1$  is the vector

$$\underline{k}_1 = \frac{1}{2} \{ \alpha_1^2(x_0) \Delta_1 [g_1(x_0, t) + g_c(x_0, t)] - 2f(t),$$

$$\alpha_1^2(x_1) (\Delta_1 + \Delta_2) [g_1(x_1, t) + g_c(x_1, t)]$$

$$\dots, \alpha_1^2(x_{n-1}) (\Delta_{n-1} + \Delta_n) [g_1(x_{n-1}, t) + g_c(x_{n-1}, t)] \}^T. \quad (B19)$$

With this discretization in the  $x$  direction,  $u_1$  and  $u_2$  must satisfy the following system of ordinary differential equations in  $t$ :

$$\dot{\underline{u}}_1(t) = \underline{v}_1(t), \quad \underline{u}_1(0) = \underline{0}; \quad (B20)$$

$$\dot{\underline{u}}_2(t) = \underline{v}_2(t), \quad \underline{u}_2(0) = \underline{0}; \quad (B21)$$

$$\dot{\underline{v}}_1(t) = Q_1 [\underline{p}_1(t) - \underline{g}_1(t) - \underline{g}_c(t)], \quad \underline{v}_1(0) = \underline{0}; \quad (B22)$$

$$\dot{\underline{v}}_2(t) = Q_2 [\underline{g}_c(t) - \underline{g}_2(t)], \quad \underline{v}_2(0) = \underline{0}; \quad (B23)$$

where

$$\underline{u}_i(t) = [u_i(x_0, t), u_i(x_1, t), \dots, u_i(x_{n-1}, t)]^T, \quad i = 1, 2; \quad (B24)$$

$$\underline{g}_i(t) = [g_i(x_0, t), g_i(x_1, t), \dots, g_i(x_{n-1}, t)]^T, \quad i = 1, 2, c; \quad (B25)$$

$$Q_i = \text{diag} \left\{ \frac{1}{m_i(x_0)}, \frac{1}{m_i(x_1)}, \dots, \frac{1}{m_i(x_{n-1})} \right\}, \quad i = 1, 2. \quad (B26)$$

The algorithm to solve the model numerically is analogous to that described in Sec. II.

## REFERENCES

- Allen, J.B. (1980). A cochlear micromechanical model of transduction. In: *Psychophysical, Physiological and Behavioural Studies in Hearing*, pp 85-95. Editors: G. van den Brink and F.A. Bilsen. Delft University Press, Delft.
- Allen, J.B. and Sondhi, M.M. (1979). Cochlear macromechanics: Time domain solutions. *J. Acoust. Soc. Am.* 66, 123-132.
- Bialek, W. (1983a). Quantum effects in the dynamics of biological systems. Doctoral dissertation, University of California, Berkeley, CA.
- Bialek, W. (1983b). Thermal and quantum noise in the inner ear. In: *Mechanics of Hearing*, pp. 185-192. Editors: E. de Boer and M.A. Viergever. Martinus Nijhoff Publ., The Hague/Delft University Press, Delft.
- Bialek, W. and Wit, H.P. (1984). Quantum limits to oscillator stability: theory and experiments on acoustic emissions from the human ear. *Phys. Lett.* 104A, 173-178.

- Boer, E. de (1983). No sharpening? A challenge for cochlear mechanics. *J. Acoust. Soc. Am.* 73, 567-573.
- Boer, E. de (1984). Auditory Physics. Physical principles in hearing theory II. *Phys. Rep.* 105, 141-226.
- Diependaal, R.J. and Viergever, M.A. (1983). Nonlinear and active modelling of cochlear mechanics: A precarious affair. In: *Mechanics of Hearing*, pp. 153-160. Editors: E. de Boer and M.A. Viergever. Martinus Nijhoff Publ., The Hague/Delft University Press, Delft.
- Diependaal, R.J., Boer, E. de, and Viergever, M.A. (1986a). Determination of the cochlear power flux from basilar membrane vibration data. In: *Peripheral Auditory Mechanisms*, pp. 189-196. Editors: J.B. Allen, J.L. Hall, A. Hubbard, S.T. Neely, and A. Tubis. Springer Verlag, Berlin, Heidelberg, New York.
- Diependaal, R.J., Viergever, M.A., and Boer, E. de (1986b). Are active elements necessary in the basilar membrane impedance? *J. Acoust. Soc. Am.* 80, 124-132.
- Diependaal, R.J., Boer, E. de, and Viergever, M.A. (1987). Cochlear power flux as an indicator of mechanical activity. *J. Acoust. Soc. Am.* 82, 917-926.
- Duifhuis, H., Hoogstraten, H.W., Netten, S.M. van, Diependaal, R.J. and Bialek, W. (1986). Modelling the cochlear partition with coupled Van der Pol oscillators. In: *Peripheral Auditory Mechanisms*, pp. 290-297. Editors: J.B. Allen, J.L. Hall, A. Hubbard, S.T. Neely, and A. Tubis. Springer Verlag, Berlin, Heidelberg, New York.
- Furst, M. and Goldstein, J.L. (1982). A cochlear nonlinear transmission-line model compatible with combination tone psychophysics. *J. Acoust. Soc. Am.* 72, 717-726.
- Jones, K., Tubis, A., Long, G.R., Burns, E.M. and Strickland, E.A. (1986). Interactions among multiple spontaneous oto-acoustic emissions. In: *Peripheral Auditory Mechanisms*, pp. 266-273. Editors: J.B. Allen, J.L. Hall, A. Hubbard, S.T. Neely, and A. Tubis. Springer Verlag, Berlin, Heidelberg, New York.
- Kemp, D.T. (1978). Stimulated acoustic emissions from within the human auditory system. *J. Acoust. Soc. Am.* 64, 1386-1391.
- Khanna, S.M. and Leonard, D.G.B. (1982). Basilar membrane tuning in the cat cochlea. *Science* 215, 305-306.
- Kim, D.O. (1986). An overview of nonlinear and active cochlear models. In: *Peripheral Auditory Mechanisms*, pp. 239-249. Editors: J.B. Allen, J.L. Hall, A. Hubbard, S.T. Neely, and A. Tubis. Springer Verlag, Berlin, Heidelberg, New York.
- LePage, E.L. and Johnstone, B.M. (1980). Nonlinear mechanical behaviour of the basilar membrane in the basal turn of the guinea pig cochlea. *Hearing Res.* 2, 183-189.
- Matthews, J.W. (1980). Mechanical modelling of nonlinear phenomena observed in the peripheral auditory system. Doctoral dissertation, Washington University, St. Louis, MO.
- Neely, S.T. (1981). Fourth-order partition dynamics for a two-dimensional model of the cochlea. Doctoral dissertation, Washington University, St. Louis, MO.
- Netten, S.M. van, and Duifhuis, H. (1983). Modelling an active, nonlinear cochlea. In: *Mechanics of Hearing*, pp. 143-151. Editors: E. de Boer and M.A. Viergever. Martinus Nijhoff Publ., The Hague/Delft University Press, Delft.
- Rhode, W.S. (1971). Observations of the vibration of the basilar membrane in squirrel monkeys using the Mössbauer technique. *J. Acoust. Soc. Am.* 49, 1218-1231.
- Rhode, W.S. (1978). Some observations on cochlear mechanics. *J. Acoust. Soc. Am.* 64, 158-176.
- Robles, L., Ruggero, M.A. and Rich, N.C. (1984). Mössbauer measurements of basilar membrane tuning curves in the chinchilla. *J. Acoust. Soc. Am.* 76, S35.
- Robles, L., Ruggero, M.A. and Rich, N.C. (1986). Basilar membrane mechanics at the base of the chinchilla cochlea. I. Input-output functions, tuning curves, and response phases. *J. Acoust. Soc. Am.* 80, 1364-1374.
- Sellick, P.M., Patuzzi, R. and Johnstone, B.M. (1982). Measurement of basilar membrane motion in the guinea pig using the Mössbauer technique. *J. Acoust. Soc. Am.* 72, 131-141.

- Sielecki, A. (1968). An energy conserving difference scheme form storm surge equations. Monthly Weather Rev. 96, 150-156.
- Viergever, M.A. (1980). Mechanics of the Inner Ear - A mathematical approach. Doctoral dissertation, Delft University Press, Delft, The Netherlands.
- Viergever, M.A. (1986). Cochlear macromechanics - A review. In: Peripheral Auditory Mechanisms, pp. 63-72. Editors: J.B. Allen, J.L. Hall, A. Hubbard, S.T. Neely, and A. Tubis. Springer Verlag, Berlin, Heidelberg, New York.
- Viergever, M.A. and Diependaal, R.J. (1986). Quantitative validation of cochlear models using the Liouville-Green approximation. Hearing Res. 21, 1-15.
- Zwislocki, J.J. (1980a). Two possible mechanisms for the second cochlear filter. In: Psycho-physical, Physiological and Behavioural Studies in Hearing, pp 16-23. Editors: G. van den Brink and F.A. Bilsen. Delft University Press, Delft.
- Zwislocki, J.J. (1980b). Five decades of research on cochlear mechanics. J. Acoust. Soc. Am. 67, 1679-1685.
- Zwislocki, J.J. (1983). Sharp vibration maximum in the cochlea without wave reflection. Hearing Res. 9, 103-111.

**CHAPTER FIVE****Nonlinear and active two-dimensional cochlear models: time-domain solution**

**Abstract** A numerical solution method for two-dimensional (2D) cochlear models in the time domain is presented. The method has particularly been designed for models with a cochlear partition having nonlinear and active mechanical properties. The 2D cochlear model equations are reformulated as an integral equation for the acceleration of the basilar membrane (BM). This integral equation is discretized with respect to the spatial variable to yield a system of ordinary differential equations in the time variable. To solve this system the variable step size fourth-order Runge-Kutta method described in Diependaal *et al.* (J. Acoust. Soc. Am. 82, pp. 1655-1666) is used. This method is robust and computationally efficient. The incorporation of a simple middle-ear model can be handled by our method. The method can also be extended to models in which the cochlear partition at each point along its length is represented by more than one degree of freedom.

**LIST OF MAIN SYMBOLS**

|             |   |
|-------------|---|
| $A_s$       | area of stapes footplate  |
| $G(x, \xi)$ | parts of the kernel of the integral equation [see Eq. (12)]                                   |
| $G^{2D}$    | system matrix containing information about the kernel of the integral [see Eqs. (25)and (30)] |
| $L$         | length of the BM  |
| $M$         | matrix containing the BM masses in the nodal points [see Eq. (29)]                            |
| $b$         | width of the cochlear channels  |
| $g(x, t)$   | see Eq. (11)  |
| $h$         | height of the cochlear channels   |
| $k$         | see Eq. (26)  |
| $m(x)$      | mass of BM per unit of area   |

|   |   |
|---|---|
| $n$   | number of subintervals in the spatial discretization              |
| $p(x, z, t)$                                | fluid difference pressure   |
| $p_{CL}(x, t)$                              | transmembrane pressure at the BM centerline                       |
| $r(x, t)$                                   | resistance of BM per unit of area                                 |
| $s(x, t)$                                   | stiffness of BM per unit of area                                  |
| $t$   | time variable   |
| $u_{CL}(x, t)$                              | BM centerline displacement  |
| $\underline{u}_{CL}(t)$                     | vector containing BM centerline displacements in the nodal points |
| $u_s$                                       | stapes displacement   |
| $\underline{v}_{CL}(t)$                     | vector containing BM centerline velocities in the nodal points    |
| $x$   | coordinate along the BM   |
| $x_0, x_1, \dots, x_j, \dots, x_{n-1}, x_n$ | set of nodal points [see Eq. (14)]                                |
| $z$   | coordinate perpendicular to the BM                                |
| $\beta(x)$                                  | BM width  |
| $\rho$                                      | fluid density   |
| $\Delta$                                    | mesh size of spatial discretization                               |

## INTRODUCTION

In Diependaal *et al.* (1987b) a robust and efficient solution method for nonlinear and active one-dimensional (1D) models has been developed. Since 1D models are long wave models, they fall short in accurately describing the BM movements in the region of maximum displacement where the fluid waves are short (e.g., Rhode, 1971, Kohllöffel, 1972). Two-dimensional (2D) models take into account both long and short waves, hence they are considerably more adequate for a quantitative description of cochlear mechanics. This has motivated us to try and extend the numerical solution method mentioned above to 2D nonlinear and active models.

The equations are formulated for a 2D model in which the partition at each point along its length has one degree of freedom (1DOF). This model description, a partial differential equation in two spatial dimensions with suitable boundary conditions, can be reformulated as an integral equation in just one spatial dimension (Sec. I). The integral equation is discretized in order to obtain a system of ordinary differential equations in the time

variable (Sec. II). This discretization is performed by evaluating the integral in the equation according to the trapezium rule giving special attention to the logarithmic singularity of the kernel of the integral. A variable step size fourth-order Runge-Kutta method is used to solve the system of ordinary differential equations. This method has been shown to be both efficient and robust (Diependaal *et al.*, 1987b). Some numerical results of model calculations using the method are presented in Sec. III. As in the 1D case, the method can easily be extended to models in which the cochlear partition at each point along its length is represented by more than one degree of freedom. Results for the two degree of freedom (2DOF) model of Neely (1981) are also presented in Sec. III.

In Secs. I and II the input to the system is taken to be a prescribed stapes movement. For nonlinear models this boundary condition is physically unrealistic. A prescribed stapes movement as boundary condition means that the stapes can only move with the input frequency, given harmonic stimulation. So, the higher harmonics of the response generated in the nonlinear cochlea will be reflected totally at the stapes in that case. If we want the stapes movements not to be tied to the input frequency, we need a description of the mechanics of the middle ear. In the Appendix such a description (derived from Matthews, 1980) is presented and the consequences of including it in the model are discussed.

## I. THE INTEGRAL EQUATION OF THE 2D MODEL

The geometry of the 1DOF model and the assumptions upon which the model is based have been discussed by Viergever (1980, Chap. 2); the only difference is that we assume the fluid flow to be two-dimensional. In the model we write the equations in terms of a difference pressure  $p$  which is defined as

$$p(x, z, t) = p_{LC}(x, -z, t) - p_{UC}(x, z, t), \quad z > 0, \quad (1)$$

where  $p_{LC}$  and  $p_{UC}$  are (the antisymmetric parts of) the fluid pressures in the lower channel and upper channel, respectively, averaged over the channel width. For an explanation of the symbols, see the List of Symbols. Owing to the assumptions made about the fluid filling the model (Viergever, 1980), the difference pressure must satisfy Laplace's equation for potential flow

$$\frac{\partial^2 p(x,z,t)}{\partial x^2} + \frac{\partial^2 p(x,z,t)}{\partial z^2} = 0, \quad 0 < x < L, \quad 0 < z < h, \quad t \geq 0. \quad (2)$$

This elliptic partial differential equation is subject to four boundary and two initial conditions. Supposing the BM is at rest at  $t=0$ , we have as initial conditions

$$u_{CL}(x,0)=0, \quad 0 \leq x \leq L \quad (3)$$

and

$$\dot{u}_{CL}(x,0)=0, \quad 0 \leq x \leq L \quad (4)$$

where the dot means differentiation with respect to time. The movement of the stapes is a prescribed function of time

$$\frac{\partial p(x,z,t)}{\partial x} = \frac{2\rho A_s \ddot{u}_s(t)}{bh}, \quad x=0, \quad 0 \leq z \leq h, \quad t \geq 0. \quad (5)$$

Furthermore, we suppose that the pressure at the helicotrema and the fluid velocity at the upper rigid wall vanish

$$p(L,z,t)=0, \quad 0 \leq z \leq h, \quad t \geq 0 \quad (6)$$

and

$$\frac{\partial p(x,z,t)}{\partial z}=0, \quad 0 \leq x \leq L, \quad z=h, \quad t \geq 0. \quad (7)$$

Equation (6) differs from the corresponding equation in Viergever (1980), where the condition  $\partial p / \partial x = 0$  at the helicotrema was used. The present formulation makes the mathematical treatment somewhat simpler; the difference is immaterial except for very low frequencies in the range of hearing.

Finally, at the BM we have

$$\frac{\partial p(x,z,t)}{\partial z} = \frac{4\rho\beta(x)}{\pi b} \ddot{u}_{CL}(x,t), \quad 0 \leq x \leq L, \quad z=0, \quad t \geq 0. \quad (8)$$

The model description is completed by a relation between the transmembrane pressure and the displacement of the centerline of the BM

$$p_{CL}(x,t)=m(x)\ddot{u}_{CL}(x,t)+r(x,t)\dot{u}_{CL}(x,t)+s(x,t)u_{CL}(x,t), \\ 0 \leq x \leq L, \quad t \geq 0. \quad (9)$$

The BM resistance  $r$  and stiffness  $s$  may depend on time; in particular,  $r$  and

$s$  are allowed to be functions of  $u_{CL}$  and  $\dot{u}_{CL}$ , which makes the model nonlinear.

To solve the model equations, we first transform the boundary value problem consisting of Eqs. (2), (5)-(9) into an equivalent integral equation in one independent variable. This can be done in a similar way as in Viergever and Kalker (1975), Sondhi (1978), and Viergever (1980, Appendix 4a), except that we are working in the time domain rather than in the frequency domain. It is emphasized that the 2D fluid behavior is fully conserved in the transformation of the 2D boundary value problem into the 1D integral equation. We will skip the derivation here and only give the resulting integral equation, which reads

$$\begin{aligned} \frac{16\rho}{\pi^2 b} \int_0^L \beta(\xi) G(x, \xi) \ddot{u}_{CL}(\xi, t) d\xi - m(x) \ddot{u}_{CL}(x, t) = \\ = g(x, t) + \frac{8\rho A_s \ddot{u}_s(t)(L-x)}{\pi b h}, \quad 0 \leq x \leq L, t \geq 0, \end{aligned} \quad (10)$$

where  $g$  and  $G$  are defined by

$$g(x, t) = r(x, t) \dot{u}_{CL}(x, t) + s(x, t) u_{CL}(x, t), \quad (11)$$

and

$$\begin{aligned} G(x, \xi) = -2 \sum_{n=0}^{\infty} \left\{ \frac{\coth[(n+1/2)\pi h/L]}{(n+1/2)} \times \right. \\ \left. \times \cos[(n+1/2)\pi x/L] \cos[(n+1/2)\pi \xi/L] \right\}. \end{aligned} \quad (12)$$

The coefficients in Eq. (10) differ from those in the cited papers, because we use centerline quantities rather than averaging the BM displacement and transmembrane-pressure over the channel width. Since  $L \gg h$ , the sum in Eq. (12) can be approximated with a relative accuracy of  $e^{-\pi L/h}$  as follows:

$$G(x, \xi) = \frac{1}{\pi} \left\{ \ln \left[ \sinh \left( \frac{\pi |x-\xi|}{2h} \right) \right] + \ln \left[ \sinh \left( \frac{\pi(x+\xi)}{2h} \right) \right] \ln 4 - \frac{\pi L}{h} \right\}. \quad (13)$$

## II. DISCRETIZATION OF THE INTEGRAL EQUATION

In order to render the integral equation discrete we divide the interval  $[0, L]$  into  $n$  subintervals by the set of nodal points

$$0 = x_0 < x_1 < \dots < x_{n-1} < x_n = L. \quad (14)$$

For simplicity we confine ourselves to an equidistant mesh. The formulation can easily be extended to a non-equidistant mesh, however. So we have

$$x_j - x_{j-1} = \Delta, \quad j = 1, 2, \dots, n. \quad (15)$$

Of course, Eq. (10) is valid at every nodal point  $x_j, j = 0(1)n$ :

$$\begin{aligned} \frac{16\rho}{\pi^2 b} \int_0^L \beta(\xi) G(x_j, \xi) \ddot{u}_{CL}(\xi, t) d\xi - m(x_j) \ddot{u}_{CL}(x_j, t) = \\ = g(x_j, t) + \frac{8\rho A_s}{\pi b h} \ddot{u}_s(t)[L - x_j]. \end{aligned} \quad (16)$$

Since from Eq. (12) it follows that

$$G(L, \xi) = G(x, L) = 0, \quad (17)$$

the solution of Eq. (10) with initial conditions (3) and (4) at  $x = L$  is simply

$$u_{CL}(L, t) \equiv 0. \quad (18)$$

To find the BM displacement at the other nodal points the integral in Eq. (16) is evaluated numerically by means of the trapezium rule. Special attention must be given to the fact that  $G(x_j, \xi) \rightarrow -\infty$  as  $\xi \rightarrow x_j$ . We start with writing the integral in Eq. (16) as a sum of integrals over the subintervals in the following way:

$$\begin{aligned} \int_0^L \beta(\xi) G(x_j, \xi) \ddot{u}_{CL}(\xi, t) d\xi = \sum_{l=1}^{j-1} \left[ \int_{x_{l-1}}^{x_l} \beta(\xi) G(x_j, \xi) \ddot{u}_{CL}(\xi, t) d\xi \right] + \\ + \int_{x_{j-1}}^{x_j} \beta(\xi) G(x_j, \xi) \ddot{u}_{CL}(\xi, t) d\xi + \int_{x_j}^{x_{j+1}} \beta(\xi) G(x_j, \xi) \ddot{u}_{CL}(\xi, t) d\xi + \\ + \sum_{l=j+2}^n \left[ \int_{x_{l-1}}^{x_l} \beta(\xi) G(x_j, \xi) \ddot{u}_{CL}(\xi, t) d\xi \right]. \end{aligned} \quad (19)$$

The first sum of integrals in Eq. (19) is approximated by means of the trapezium rule to yield

$$\sum_{i=1}^{j-1} \left\{ \int_{x_{i-1}}^{x_j} \beta(\xi) G(x_j, \xi) \ddot{u}_{CL}(\xi, t) d\xi \right\} \approx \frac{1}{2} \Delta \sum_{i=1}^{j-1} \left\{ \beta(x_{i-1}) G(x_j, x_{i-1}) \ddot{u}_{CL}(x_{i-1}, t) + \beta(x_i) G(x_j, x_i) \ddot{u}_{CL}(x_i, t) \right\}. \quad (20)$$

The last sum of integrals in Eq. (19) is approximated likewise. The second term of Eq. (19) is approximated as follows

$$\begin{aligned} \int_{x_{j-1}}^{x_j} \beta(\xi) G(x_j, \xi) \ddot{u}_{CL}(\xi, t) d\xi &\approx \frac{1}{2} [\beta(x_{j-1}) \dot{u}_{CL}(x_{j-1}, t) + \\ &+ \beta(x_j) \dot{u}_{CL}(x_j, t)] \int_{x_{j-1}}^{x_j} G(x_j, \xi) d\xi. \end{aligned} \quad (21)$$

The integral in Eq. (21) is evaluated analytically using expression (13):

$$\begin{aligned} \int_{x_{j-1}}^{x_j} G(x_j, \xi) d\xi &= \frac{1}{\pi} \left\{ \int_{x_{j-1}}^{x_j} \ln \{\sinh[\pi |x_j - \xi| / (2h)]\} d\xi + \right. \\ &+ \left. \int_{x_{j-1}}^{x_j} \ln \{\sinh[\pi(x_j + \xi) / (2h)]\} d\xi + \int_{x_{j-1}}^{x_j} [\ln 4 - \pi L/h] d\xi \right\}. \end{aligned} \quad (22)$$

Substituting  $\xi = x_j - \sigma$  in the first integral on the right hand side of Eq. (22) and integrating by parts gives

$$\begin{aligned} \int_{x_{j-1}}^{x_j} \ln \{\sinh[\pi |x_j - \xi| / (2h)]\} d\xi &= \int_0^\Delta \ln \{\sinh[\pi \sigma / (2h)]\} d\sigma = \\ &= \Delta \ln \{\sinh[\pi \Delta / (2h)]\} - \frac{\pi}{2h} \int_0^\Delta \sigma \coth[\pi \sigma / (2h)] d\sigma \approx \\ &\approx \Delta \ln \{\sinh[\pi \Delta / (2h)]\} - \frac{\pi \Delta^2}{4h} \coth[\pi \Delta / (2h)] - \Delta/2. \end{aligned} \quad (23)$$

In the last step we applied the trapezium rule; furthermore, we made use of the limits  $\lim_{\sigma \downarrow 0} \sigma \ln \{\sinh[\pi \sigma / (2h)]\} = 0$  and  $\lim_{\sigma \downarrow 0} \sigma \coth[\pi \sigma / (2h)] = 2h/\pi$  in deriving Eq. (23). The second integral of Eq. (22) can be evaluated in the same way, so that after some arithmetics we arrive at

$$\int_{x_{j-1}}^{x_j} G(x_j, \xi) d\xi = \frac{\Delta}{\pi} \left\{ \ln[4\sinh(\pi\Delta/(2h))] + \right. \\ \left. + \frac{2x_j}{\Delta} \ln \left\{ \frac{\sinh[\pi x_j/h]}{\sinh[\pi(2x_j - \Delta)/(2h)]} \right\} + \ln\{\sinh[\pi(2x_j - \Delta)/(2h)]\} \right. \\ \left. - \frac{\pi\Delta}{4h} \coth[\pi\Delta/(2h)] - \frac{\pi x_j}{2h} \coth[\pi x_j/h] \right. \\ \left. - \frac{\pi(2x_j - \Delta)}{4h} \coth[\pi(2x_j - \Delta)/(2h)] - \frac{\pi L}{h} - \frac{1}{2} \right\}. \quad (24)$$

This gives us, via Eq. (21), an expression for the second term of Eq. (19). The third term of Eq. (19) can be treated analogously.

Now that we have evaluated the integral in the nodal points, we can write the integral equation (10) as a system of (algebraic) equations

$$[G^{2D} - M] \underline{\ddot{u}}_{CL}(t) = \underline{g}(t) + \frac{8\rho A_s \ddot{u}_s(t)}{\pi b h} \underline{k}, \quad (25)$$

where

$$\underline{k} = [L, L - x_1, L - x_2, \dots, L - x_{n-1}]^T, \quad (26)$$

$$\underline{g}(t) = [g(0, t), g(x_1, t), g(x_2, t), \dots, g(x_{n-1}, t)]^T, \quad (27)$$

$$\underline{\ddot{u}}_{CL}(t) = [\ddot{u}_{CL}(0, t), \ddot{u}_{CL}(x_1, t), \ddot{u}_{CL}(x_2, t), \dots, \ddot{u}_{CL}(x_{n-1}, t)]^T, \quad (28)$$

$$M = \text{diag}[m(0), m(x_1), m(x_2), \dots, m(x_{n-1})]^T, \quad (29)$$

and  $G^{2D}$  is the matrix  $(g_{ij}^{2D})$  given by

$$g_{ij}^{2D} = \begin{cases} \alpha\beta(0)[\gamma_1 - \gamma_4 - \gamma_6 - 1], & i=j=0 \\ \alpha\beta(0)[\gamma_2 - \gamma_4 - \gamma_5 - \gamma_6 - \frac{1}{2}], & i=1, j=0 \\ \alpha\beta(0)[\gamma_7(x_i) - \gamma_4], & i=2,3,\dots,n-1; j=0 \\ \alpha\beta(x_i)[2\{\gamma_7(x_j) - \gamma_4\} - \gamma_6 - 1], & i=0, j=1 \\ 2\alpha\beta(x_j)[\gamma_7(x_j) - \gamma_4], & i=0, j=2,3,\dots,n-1 \\ \alpha\beta(x_j)[\gamma_8(x_j) + \gamma_3(x_j) - \gamma_6 - \gamma_9(x_j) - \gamma_{10}(x_j) - \gamma_{11}(x_j) - 2\gamma_4 - 1], & i=j; j=2,3,\dots,n-1 \\ \alpha\beta(x_j)[\gamma_{12}(x_i, x_j) + \gamma_{13}(x_i) - \frac{1}{2}\{\gamma_6 + \gamma_9(x_i)\} - \gamma_{10}(x_i) - 2\gamma_4 - \frac{1}{2}], & i=j-1; j=2,3,\dots,n-1 \\ \alpha\beta(x_j)[\gamma_{12}(x_i, x_j) + \gamma_{14}(x_i) - \frac{1}{2}\{\gamma_6 + \gamma_9(x_i)\} - \gamma_{11}(x_i) - 2\gamma_4 - \frac{1}{2}], & i=j+1; j=1,2,\dots,n-2 \\ \alpha\beta(x_j)[\gamma_{12}(x_i, x_j) - 2\gamma_4], & |i-j| \geq 2, i \geq 1, j \geq 1 \end{cases} \quad (30)$$

In Eq. (30)  $\alpha$  and the  $\gamma_m$ 's are shorthand for

$$\alpha = 8\rho\Delta/(\pi^3 b), \quad (31)$$

$$\gamma_1 = \ln\{2\cosh[(\pi\Delta/h) - 1]\}, \quad (32)$$

$$\gamma_2 = \ln\{2\cosh[(2\pi\Delta/h) - 1]\}, \quad (33)$$

$$\gamma_3(x_i) = \frac{2x_i}{\Delta} \ln \left\{ \frac{\sinh[(2x_i + \Delta)\pi/(2h)]}{\sinh[(2x_i - \Delta)\pi/(2h)]} \right\}, \quad (34)$$

$$\gamma_4 = \pi L/h, \quad (35)$$

$$\gamma_5 = \frac{\pi\Delta}{2h} \coth(\pi\Delta/h), \quad (36)$$

$$\gamma_6 = \frac{\pi\Delta}{2h} \coth[\pi\Delta/(2h)], \quad (37)$$

$$\gamma_7(x_i) = \ln\{2\cosh[(\pi x_i/h) - 1]\}, \quad (38)$$

$$\gamma_8(x_i) = \ln\{4[\cosh(\pi\Delta/h) - \cosh(2\pi x_i/h)] + 2[\cosh[(2x_i + \Delta)\pi/h] + \cosh[(2x_i - \Delta)\pi/h] - \cosh(2\pi\Delta/h) - 1]\}, \quad (39)$$

$$\gamma_9(x_i) = \frac{\pi x_i}{h} \coth(\pi x_i/h), \quad (40)$$

$$\gamma_{10}(x_i) = \frac{(2x_i + \Delta)\pi}{2h} \coth \left\{ \frac{(2x_i + \Delta)\pi}{4h} \right\}, \quad (41)$$

$$\gamma_{11}(x_i) = \frac{(2x_i - \Delta)\pi}{2h} \coth \left| \frac{(2x_i - \Delta)\pi}{4h} \right|, \quad (42)$$

$$\gamma_{12}(x_i, x_j) = 2\ln[2|\cosh(\pi x_i/h) - \cosh(\pi x_j/h)|], \quad (43)$$

$$\gamma_{13}(x_i) = \frac{2x_i}{\Delta} \ln \left\{ \frac{\sinh[(2x_i + \Delta)\pi/(2h)]}{\sinh[\pi x_i/h]} \right\}, \quad (44)$$

$$\gamma_{14}(x_i) = \frac{2x_i}{\Delta} \ln \left\{ \frac{\sinh[\pi x_i/h]}{\sinh[\pi(2x_i - \Delta)/(2h)]} \right\}. \quad (45)$$

In order to find a numerical solution of the model equations we have to integrate the system of ordinary differential equations

$$\dot{u}_{CL}(t) = v_{CL}(t), \quad u_{CL}(0) = 0, \quad (46)$$

$$\dot{v}_{CL}(t) = \psi(t), \quad v_{CL}(0) = 0, \quad (47)$$

where  $\psi$  is a numerical approximation of the acceleration  $\ddot{u}_{CL}$ , obtained by solving Eq. (25). A variable step size fourth-order Runge-Kutta scheme is used for solving the differential equations, since that scheme has been shown to be both efficient and robust in comparison with other schemes (Diependaal *et al.*, 1987b).

The method can be extended to models with more than one degree of freedom at each point along the cochlear partition. This is done in an analogous way as described by Diependaal *et al.* (1987b, Appendix B).

### III. NUMERICAL RESULTS

In this section we present some model calculations on three different cochlear models. First of all, we have computed the responses to pure tones of a linear, active 2DOF model as designed by Neely (1981). We have not been able to calculate stable model responses in the time domain using the parameter sets B or D from Neely's thesis (1981), but stable time domain solutions can be obtained for Neely's parameter set C. In Fig. 1 the amplitude of the fundamental Fourier component of the BM displacement is plotted as a function of place for four different input frequencies. The input to this model is a sinusoidal stapes displacement. Our results are in agreement with Neely's (1981, Fig. 6.4).

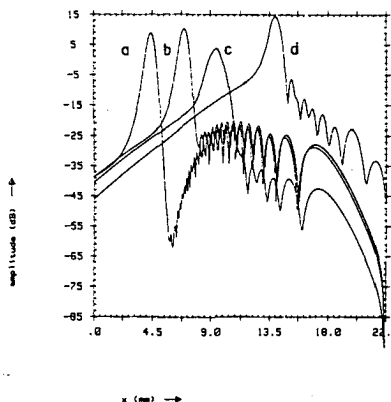


**Figure 1.** Response to pure tones in a linear, active 2DOF model. Parameter values are the same as in Neely's Doctoral dissertation (1981, parameter set C). The BM has been divided into 256 elements of equal size. Responses are shown after 20 cycles of tone onset. The dB scale is arbitrary. The amplitudes of the responses are plotted for 8, 4, 2, 0.62 kHz (resp. curves a, b, c, d).

The second model example of which we present results is the nonlinear, active model consisting of coupled Van der Pol oscillators (Van Netten and Duifhuis, 1983; Duifhuis *et al.*, 1986). The results for this model strongly depend upon the  $x$  discretization<sup>1</sup>. Results for the 1D case in the frequency domain have been presented by Van Netten and Duifhuis (1983) using asymptotic techniques and results for the 1D case in the time domain have been presented by Diependaal and Viergever (1983), Duifhuis *et al.* (1986) and Diependaal *et al.* (1987b) using numerical techniques. In this paper we show some model responses to harmonic stimulation at the eardrum in the 2D case; the middle ear is represented by a simple one-degree-of-freedom system (see the last paragraph of the Appendix). Figure 2 shows the amplitudes of the fundamental Fourier component and several uneven harmonics of the model response to a 1 kHz sinusoidal input. For Fig. 2(a)-(e) the amplitude level of the input signal has been increased by 10 dB for successive pictures. In Fig. 2(a) the oscillators around the characteristic place for a

1. The numerical results presented for the Van der Pol model should *not* be considered as valid approximate solutions of Eq. 2 (with the appropriate boundary conditions). They represent the behavior of a large set of coupled Van der Pol oscillators which satisfy the discretized system of Eqs. (25), (46), and (47). The results for this model strongly depend on the  $x$  discretization (on the way of discretizing as well as on the number of nodal points, see Duifhuis *et al.*, 1986).

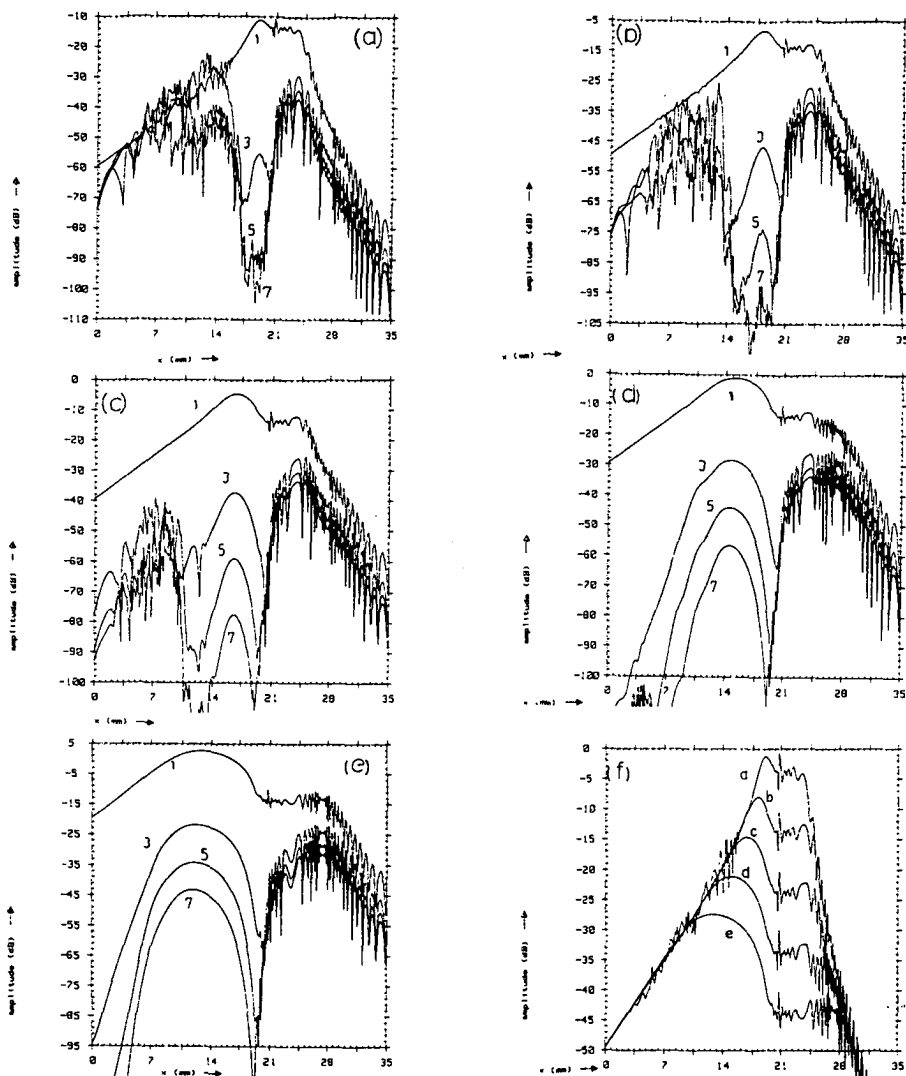


**Figure 2.** Response of a nonlinear active model, the Van der Pol oscillators model (Van Netten and Duifhuis, 1983; Duifhuis *et al.*, 1986). Parameter values (after Duifhuis *et al.*, 1986):  $L = 35 \text{ mm}$ ,  $\rho = 1 \text{ mg/mm}^3$ ,  $b = 1 \text{ mm}$ ,  $h = 1 \text{ mm}$ ,  $m(x) = 0.5 \text{ mg/mm}^2$ ,  $r(x, t) = 2.5(2)^{1/4}[-1 + 10^{12}u_{CL}^2(x, t)]\exp(-0.15x) \text{ mg/(mm}^2\text{ms)}$ ,  $s(x, t) = 10,000 \exp(-0.3x) \text{ mg/(mm}^2\text{ms}^2)$ ,  $A_s = 1 \text{ mm}^2$ ,  $A_m = 60 \text{ mm}^2$ ,  $G_m = 0.5$ ,  $G_m^{-2}M_m + M_s = 0.792 \text{ mg}$ ,  $G_m^{-2}R_m + R_s = 6.22 \text{ mg/ms}$ ,  $G_m^{-2}S_m + S_s = 125.08 \text{ mg/ms}^2$ ,  $x$  in mm. The stimulus,  $p_e(t)$ , is a sinusoid at the eardrum with frequency 1 kHz. The BM has been divided into 256 elements of equal size. Responses are shown after 40 ms of tone onset. For panels (a) through (e) the amplitude level of the input signal has been increased by 10 dB for successive pictures. Shown are the amplitudes (dB re 1 mm/ms) of first, third, fifth and seventh Fourier component, respectively curves labeled (1), (3), (5) and (7). (f) The curves labeled (1) of panels (a) to (e) are replotted for comparison. The curves have been shifted vertically so that they have the same amplitude at the stapes. The dB scale is arbitrary.

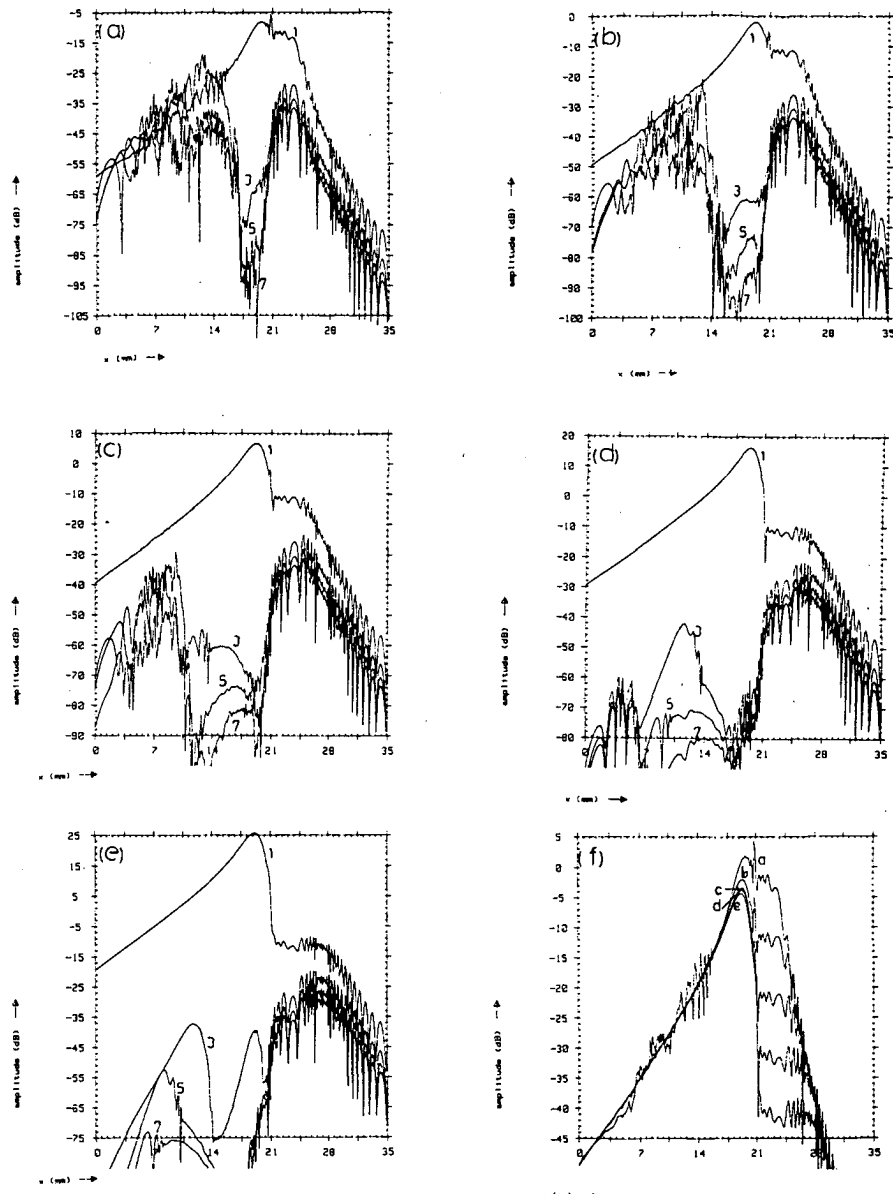


**Figure 3.** Response of the modified Van der Pol oscillators model (Duifhuis *et al.*, 1986). Stimulus, parameter values (after Duifhuis *et al.* 1986), and display as in Fig. 2, except that  $r(x,t)=2.5(2)^u[10^{-4}[\sinh[10^4\dot{u}_{CL}(x,t)]]/\dot{u}_{CL}(x,t)-2/\cosh[10^6\dot{u}_{CL}(x,t)]]\exp(-0.15x)\text{ mg}/(\text{mm}^2\text{ms})$ .

1 kHz tone are just entrained by the input tone. In Fig. 2(b)-(e) the effect of the compressive nonlinear term in the model on the response can be observed. The amplitude peak becomes broader and shifts basalwards. Furthermore, the higher harmonics of the Fourier spectrum of the signal become larger. In Fig. 2(f) the amplitudes of the fundamental Fourier components at the five input levels have been replotted for comparison. The functions have been shifted vertically so that they have the same amplitude at the stapes.

One disadvantage of the coupled Van der Pol oscillators model is the very strong compression of the nonlinearity above the limit cycle. However, the Van der Pol oscillators model can be modified such that the compressive nonlinearity is less strong. Such a modification has been proposed by Duifhuis *et al.* (1986), by defining the resistance as

$$r(x,t) = [\sinh(\nu_1 \dot{u}_{CL}) / (\nu_1 \dot{u}_{CL}) - 2/\cosh(\nu_2 \dot{u}_{CL})] r_0, \quad (48)$$

where  $\nu_1$ ,  $\nu_2$  are constants, and  $r_0$  is a exponentially decaying function of  $x$ . Results for this modified Van der Pol oscillators model are presented in Fig. 3. The input signal is again a 1 kHz pure tone at the eardrum with an amplitude which increases by 10 dB for successive pictures. As can be seen from the pictures the saturation caused by the nonlinearity is not as strong as in the case of the original Van der Pol oscillators model (Fig. 2).

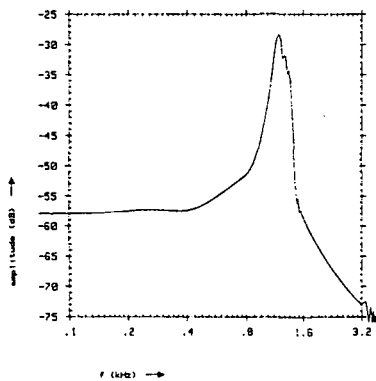


**Figure 4.** Amplitude of the Fourier transform of the impulse response of the modified Van der Pol oscillators model. Response at  $x = 18.87$  mm. Parameters as in Fig. 3.

Finally, we present the impulse response of the modified Van der Pol oscillators model. The amplitude of the Fourier transform of the response at a fixed place at the BM to a low-pass filtered (eight-pole Butterworth filter) impulse has been plotted in Fig. 4. This frequency domain result looks quite acceptable. However, in the time domain the impulse response remains oscillating with the characteristic frequency at the limit cycle level as time progresses; it does not vanish after some time (or, put it differently, the response is not asymptotically stable). This is why neither the Van der Pol oscillators model nor the modified Van der Pol model are suitable representations of the cochlea. Apparently, a realistic phenomenological model of nonlinear and active cochlear mechanics must be more complex than the (modified) Van der Pol oscillators model, e.g. by restricting the nonlinearity and the activity to the region around the characteristic place (or frequency).

#### IV. DISCUSSION AND CONCLUSIONS

We have developed a robust numerical method to solve 2D cochlear models in the time domain. With this method the response of models having nonlinear and active properties can be calculated for a variety of stimuli, such as a pure tone, two tones, noise, and clicks. Phenomena like combination tones, two-tone suppression, and transients can thus be studied. The method is not really suited for extensive parameter variation studies, owing to the large computation time<sup>2</sup>. For this purpose, asymptotic methods are more appropriate. The present numerical technique can be used as a frame of reference in order to assess the accuracy of such methods.

In 2D time-domain cochlear models there are three independent continuous variables, *viz.*  $x$ , the coordinate along the BM,  $z$ , the coordinate perpendicular to the BM and  $t$ , the time. A usual procedure for obtaining a numerical solution of the model equations is to render the model equations discrete in both spatial variables using either a finite difference or a finite element method. Subsequently the discretized equations are integrated in the time by a well chosen numerical integration method. This procedure has been followed e.g. by Neely (1981) for linear, active models and by Matthews

2. As an example: for the modified Van der Pol oscillators model with 256 points on the BM and 2560 time steps (0–40 ms cochlea time) we need 8.5 hours CPU time on a HP9050 computer or 30 minutes CPU time on a Convex C-1 computer.

(1980) for nonlinear, passive models. In this paper a different procedure has been followed. The 2D model equations are reformulated as an integral equation in just one variable (*i.e.*, the coordinate along the BM) without loosing the 2D fluid behavior. The advantage of this procedure is that we have to discretize only in one spatial variable. A similar method has been proposed by Allen and Sondhi (1979) who have used a Fourier transform technique. However, their model is linear, and it is not clear how their method can be extended to nonlinear and/or active cochlear models<sup>3</sup>.

After the integral equation has been discretized in the spatial coordinate, we have to solve a system of ordinary differential equations in the time variable. These differential equations are numerically integrated by a fourth-order Runge-Kutta method which makes use of a variable step size routine. The Runge-Kutta method has turned out to be superior to several other well known integration methods as regards both stability and efficiency (Diependaal *et al.*, 1987b).

An important property of our method is that it gives numerically stable solutions of cochlear models if these models are physically stable. For linear, passive models we have checked that the time-domain results are in good agreement with results from frequency domain descriptions; the results of these studies have not been presented in this paper for obvious reasons. Results of the linear, active model proposed by Neely (1981) agree well with Neely's results for the one parameter set which gives stable solutions in the time domain. The nonlinear, active model considered in the present paper (the Van der Pol oscillators model) is physically not asymptotically stable but stable in the sense that the solution stays bounded as time goes to infinity. Due to the variable step size routine our method produces a solution that differs from the true one by no more than an *a priori* given tolerance, also in the regions where the solution is enhanced by the activity.

The present method can handle models which are driven by an input at the stapes as well as models which have pressure at the eardrum as input. In the latter case, a description of the middle ear should be included in the model equations. In the Appendix the consequences of this extension for the analytical and numerical treatment are presented.

3. Allen and Sondhi (1979) integrate the system of ordinary differential equations by means of a 'modified Sielecki' method. In Diependaal *et al.* (1987b) it has been shown that this method is less efficient than the fourth-order Runge-Kutta method.

## ACKNOWLEDGEMENT

This research has been supported in part by the Netherlands Organization for the Advancement of Pure Research (ZWO).

## APPENDIX: INCLUSION OF A SIMPLIFIED MODEL OF THE MIDDLE EAR.

In the main text the driving force to the system is supposed to be a prescribed stapes movement. For linear cochlear models this is a suitable boundary condition, for nonlinear models it is not since the restriction to harmonic stapes movements in the case of a harmonic input is physically unrealistic. The higher harmonics of the response generated in the nonlinear cochlea will be reflected totally at the stapes in that case. Consequently, some investigators have included a middle-ear description in their cochlear models (Zwislocki, 1965; Matthews, 1980; Neely, 1981). In this Appendix such a middle-ear description is incorporated in the model and the associated integral equation is derived. Furthermore, the consequences for the discrete system of ordinary differential equations are presented.

Following Zwislocki (1962, 1963) and Matthews (1980) we associate three degrees of freedom with the middle ear. One degree of freedom ( $u_m$ ) represents movements of the malleus (mass  $M_m$ , resistance  $R_m$  and stiffness  $S_m$ ). The second degree of freedom ( $u_e$ ) reflects the inefficiency of the eardrum (mass  $M_e$ , resistance  $R_e$  and stiffness  $S_e$ ), it represents the deflection mode of the part of the eardrum that does not contribute to the movements of the malleus. The stapes and incus are assumed to move together as a single lumped mass ( $M_s$ ) with resistance  $R_s$  and stiffness  $S_s$ , their displacement is represented by the last degree of freedom ( $u_s$ ). The stapes (and incus) displacement is coupled to the malleus displacement by means of a stiff, incudo-malleolar joint with stiffness  $S_i$ . There is also a lever gain  $G_m$  between malleus and stapes displacements. The middle ear is driven by a pressure at the eardrum  $p_e(t)$  and interacts with the cochlea at the footplate of the stapes where there is an average fluid pressure over the effective area of the footplate. So, the middle ear is described by three coupled ordinary differential equations

$$A_e p_e(t) = M_e \ddot{u}_e(t) + R_e \dot{u}_e(t) + S_e u_e(t), \quad (\text{A1})$$

$$A_m p_e(t) = M_m \ddot{u}_m(t) + R_m \dot{u}_m(t) + S_m u_m(t) + G_m S_i [G_m u_m(t) - u_s(t)], \quad (\text{A2})$$

$$\frac{A_s}{h} \int_0^h p(0, z, t) dz = M_s \ddot{u}_s(t) + R_s \dot{u}_s(t) + S_s u_s(t) + S_i [u_s(t) - G_m u_m(t)], \quad (\text{A3})$$

where  $A_s$ ,  $A_m$ , and  $A_s$  are the effective areas of the stapes footplate, the malleus and the eardrum leak, respectively. These differential equations together with Eqs.(2)-(9) describe the cochlear model extended with the middle ear.

In order to solve these model equations we follow Viergever (1980, Appendix 4a). The solution of Eq. (2) that obeys conditions (5)-(8) and (A3) reads

$$p(x, z, t) = \frac{2\rho A_s (x - L)}{(2\rho A_s^2 L + M_s b h)} \left[ \frac{A_s L}{(\pi h)} \sum_{n=0}^{\infty} \left\{ \frac{A_n(t)}{(n + \frac{1}{2})} \sinh[(n + \frac{1}{2})\pi h/L] \right\} - g_s(t) \right] + \\ + \sum_{n=0}^{\infty} \left\{ A_n(t) \cosh[(n + \frac{1}{2})\pi(h - z)/L] \cos[(n + \frac{1}{2})\pi x/L] \right\}, \quad (\text{A4})$$

where  $g_s(t)$  is defined by

$$g_s(t) = R_s \dot{u}_s(t) + S_s u_s(t) + S_i [u_s(t) - G_m u_m(t)] \quad (\text{A5})$$

and  $A_n(t)$  is defined by

$$A_n(t) = \frac{-8\rho}{(n + \frac{1}{2})\pi^2 b \sinh[(n + \frac{1}{2})\pi h/L]} \int_0^L \beta(\xi) \ddot{u}_{CL}(\xi, t) \cos[(n + \frac{1}{2})\pi \xi/L] d\xi, \\ n \geq 0. \quad (\text{A6})$$

After substitution of  $z = 0$  in the expression for  $p$  and with the use of Eq. (9) and

$$p_{CL}(x, t) = \frac{4}{\pi} p(x, 0, t) \quad (\text{A7})$$

we arrive at the integral equation

$$\begin{aligned} & \frac{16\rho}{p^2 b} \int_0^L \beta(\xi) [G(x, \xi) + G_{ME}(x, \xi)] \ddot{u}_{CL}(\xi, t) d\xi - m(x) \ddot{u}_{CL}(x, t) = \\ & = g(x, t) + \frac{8\rho A_s (x-L) g_s(t)}{\pi(2\rho A_s^2 L + M_s b h)}, \quad 0 \leq x, \xi \leq L, t \geq 0. \end{aligned} \quad (\text{A8})$$

In Eq. (A8)  $G$  is defined by Eq. (12) or Eq. (13),  $g$  is given by Eq. (11) and  $G_{ME}$  has the following form:

$$G_{ME}(x, \xi) = 2\rho A_s (L-x)(L-\xi)/[\pi(2\rho A_s^2 L + M_s b h)]. \quad (\text{A9})$$

Since  $G_{ME}$  is not singular, the evaluation of that part of the integral is straightforward using the trapezium rule approximation. By following the procedure as outlined in Sec. II we write the integral equation (A8) as a system of (algebraic) equations

$$[G^{2D} + G_{ME}^{2D} - M] \ddot{u}_{CL}(t) = g(t) - \frac{8\rho A_s g_s(t) k}{\pi(2\rho A_s^2 L + M_s b h)}, \quad (\text{A10})$$

where  $G_{ME}^{2D}$  is the matrix  $(g_{ME}^{2D})_{ij}$  defined by

$$g_{ME}^{2D} = \begin{cases} \frac{16\rho^2 A_s^2 \Delta\beta(0) L (L-x_i)}{\pi^2 b h (2\rho A_s^2 L + M_s b h)}, & j=0, i=0, 1, \dots, n-1 \\ \frac{32\rho^2 A_s^2 \Delta\beta(x_j) (L-x_i) (L-x_j)}{\pi^2 b h (2\rho A_s^2 L + M_s b h)}, & i=0, 1, \dots, n-1; j=1, 2, \dots, n-1. \end{cases} \quad (\text{A11})$$

The other matrices and vectors are given by Eqs. (26)-(30).

In order to achieve a solution of the cochlear model completed with the middle-ear description, we have to integrate the system of Eqs. (46) and (47) extended with six more differential equations for the three degrees of freedom of the middle ear. We suppose that the system is at rest at  $t=0$ . The eight differential equations and their boundary conditions then read

$$\dot{u}_e(t) = v_e(t), \quad u_e(0) = 0, \quad (\text{A12})$$

$$\dot{u}_m(t) = v_m(t), \quad u_m(0) = 0, \quad (\text{A13})$$

$$\dot{u}_s(t) = v_s(t), \quad u_s(0) = 0, \quad (\text{A14})$$

$$\dot{u}_{CL}(t) = v_{CL}(t), \quad u_{CL}(0) = 0, \quad (\text{A15})$$

$$\dot{v}_e(t) = [A_e p_e(t) - g_e(t)]/M_e, v_e(0) = 0, \quad (A16)$$

$$\dot{v}_m(t) = [A_m p_e(t) - g_m(t)]/M_m, v_m(0) = 0, \quad (A17)$$

$$\dot{v}_s(t) = -\frac{2\rho A_s \Delta(q \ddot{u}_{CL}(t)) / \pi + bh g_s(t)}{2\rho A_s^2 L + M_s b h}, v_s(0) = 0, \quad (A18)$$

$$\dot{u}_{CL}(t) = \underline{\psi}(t), u_{CL}(0) = 0 \quad (A19)$$

where

$$g_e(t) = R_e \dot{u}_e(t) + S_e u_e(t), \quad (A20)$$

$$g_m(t) = R_m \dot{u}_m(t) + S_m u_m(t) + G_m S_t [G_m u_m(t) - u_s(t)], \quad (A21)$$

and

$$\underline{q} = [\beta(0)L, 2\beta(x_1)(L-x_1), 2\beta(x_2)(L-x_2), \dots, 2\beta(x_{n-1})(L-x_{n-1})]^T. \quad (A22)$$

Equation (A18) results from Eq. (A3) by substituting Eq. (A4) and evaluating the integral by means of the trapezium rule.

As in Sec. II we solve  $\dot{u}_{CL}$  from Eq. (A10) (call the solution  $\underline{\psi}$ ) at a certain instant of time and then integrate the system (A12)-(A19) to the next instant of time by using a variable step size fourth-order Runge-Kutta scheme.

The middle-ear model can be further simplified to a one-degree-of-freedom system (Neely, 1981). In that case the eardrum leak has been disregarded, so  $u_e \equiv 0$ . Furthermore, the incudo-malleolar joint has been considered as infinitely stiff, whence  $G_m u_m \equiv u_s$ . For the simplified middle-ear model the system of Eqs. (46) and (47) has to be extended with only two differential equations, given by

$$\dot{u}_s(t) = v_s(t), u_s(0) = 0, \quad (A23)$$

and

$$\dot{v}_s(t) = -\frac{2\rho A_s \Delta(q \ddot{u}_{CL}(t)) / \pi + bh g_{ME}(t) - A_m b h p_e(t) / G_m}{2\rho A_s^2 L + M_{ME} b h}, v_s(0) = 0, \quad (A24)$$

where

$$M_{ME} = (M_M + G_M^2 M_s) / G_m^2, \quad (A25)$$

and

$$g_{ME}(t) = (R_m / G_m^2 + R_s) \dot{u}_s + (S_m / G_m^2 + s_s) u_s. \quad (A26)$$

## REFERENCES

- Allen, J.B. and Sondhi, M.M. (1979). Cochlear macromechanics: Time domain solutions. *J. Acoust. Soc. Am.* 66, 123-132.
- Bialek, W. (1983a). Quantum effects in the dynamics of biological systems. Doctoral dissertation, University of California, Berkeley, CA.
- Bialek, W. (1983b). Thermal and quantum noise in the inner ear. In: *Mechanics of Hearing*, pp. 185-192. Editors: E. de Boer and M.A. Viergever. Martinus Nijhoff Publ., The Hague/Delft University Press, Delft.
- Bialek, W. and Wit, H.P. (1984). Quantum limits to oscillator stability: theory and experiments on acoustic emissions from the human ear. *Phys. Lett.* 104A, 173-178.
- Boer, E. de (1983). No sharpening? A challenge for cochlear mechanics. *J. Acoust. Soc. Am.* 73, 567-573.
- Boer, E. de (1984). Auditory physics. Physical principles in hearing theory. Part II. *Physics Reports* 105, 141-226.
- Diependaal, R.J. and Viergever, M.A. (1983). Nonlinear and active modelling of cochlear mechanics: A precarious affair. In: *Mechanics of Hearing*, pp. 153-160. Editors: E. de Boer and M.A. Viergever. Martinus Nijhoff Publ., The Hague/Delft University Press, Delft.
- Diependaal, R.J., Viergever, M.A., and Boer, E. de (1986a). Are active elements necessary in the basilar membrane impedance? *J. Acoust. Soc. Am.* 80, 124-132.
- Diependaal, R.J., Boer, E. de, and Viergever, M.A. (1986b). Determination of the cochlear power flux from basilar membrane vibration data. In: *Peripheral Auditory Mechanisms*, pp. 189-196. Editors: J.B. Allen, J.L. Hall, A. Hubbard, S.T. Neely, and A. Tubis. Springer Verlag, Berlin, Heidelberg, New York.
- Diependaal, R.J., Boer, E. de, and Viergever, M.A. (1987a). Cochlear power flux as an indicator of mechanical activity. *J. Acoust. Soc. Am.* 82, 917-926.
- Diependaal, R.J., Duifhuis, H., Hoogstraten, H.W. and Viergever, M.A. (1987b). Numerical methods for solving one-dimensional cochlear models in the time domain. *J. Acoust. Soc. Am.* 82, 1655-1666.
- Duifhuis, H., Hoogstraten, H.W., Netten, S.M. van, Diependaal, R.J. and Bialek, W. (1986). Modelling the cochlear partition with coupled Van der Pol oscillators. In: *Peripheral Auditory Mechanisms*, pp. 290-297. Editors: J.B. Allen, J.L. Hall, A. Hubbard, S.T. Neely, and A. Tubis. Springer Verlag, Berlin, Heidelberg, New York.
- Kemp, D.T. (1978). Stimulated acoustic emissions from within the human auditory system. *J. Acoust. Soc. Am.* 64, 1386-1391.
- Khanna, S.M. and Leonard, D.G.B. (1982). Basilar membrane tuning in the cat cochlea. *Science* 215, 305-306.
- Kim, D.O. (1986). An overview of nonlinear and active cochlear models. In: *Peripheral Auditory Mechanisms*, 239-249. Editors: J.B. Allen, J.L. Hall, A. Hubbard, S.T. Neely, and A. Tubis. Springer Verlag, Berlin, Heidelberg, New York.

- Kohllöffel, L.U.E. (1972). A study of basilar membrane vibrations II. The vibratory amplitude and phase pattern along the basilar membrane (post-mortem). *Acustica* 27, 66-81.
- LePage, E.L. and Johnstone, B.M. (1980). Nonlinear mechanical behaviour of the basilar membrane in the basal turn of the guinea pig cochlea. *Hearing Res.* 2, 183-189.
- Matthews, J.W. (1980). Mechanical modelling of nonlinear phenomena observed in the peripheral auditory system. Doctoral dissertation, Washington University, St. Louis, MO.
- Neely, S.T. (1981). Fourth-order partition dynamics for a two-dimensional model of the cochlea. Doctoral dissertation, Washington University, St. Louis, MO.
- Netten, S.M. van, and Duifhuis, H. (1983). Modelling an active, nonlinear cochlea. In: *Mechanics of Hearing*, pp. 143-151. Editors: E. de Boer and M.A. Viergever. Martinus Nijhoff Publ., The Hague/Delft University Press, Delft.
- Rhode, W.S. (1971). Observations of the vibration of the basilar membrane in squirrel monkeys using the Mössbauer technique. *J. Acoust. Soc. Am.* 49, 1218-1231.
- Rhode, W.S. (1978). Some observations on cochlear mechanics. *J. Acoust. Soc. Am.* 64, 158-176.
- Robles, L., Ruggero, M.A. and Rich, N.C. (1986). Basilar membrane mechanics at the base of the chinchilla cochlea. I. Input-output functions, tuning curves, and response phases. *J. Acoust. Soc. Am.* 80, 1364-1374.
- Sellick, P.M., Patuzzi, R. and Johnstone, B.M. (1982). Measurement of basilar membrane motion in the guinea pig using the Mössbauer technique. *J. Acoust. Soc. Am.* 72, 131-141.
- Sondhi, M.M. (1978) Method for computing motion in a two-dimensional cochlear model. *J. Acoust. Soc. Am.* 63, 1468-1477.
- Viergever, M.A. (1980). Mechanics of the Inner Ear - A mathematical approach. Doctoral dissertation, Delft University Press, Delft, The Netherlands.
- Viergever, M.A. and Diependaal, R.J. (1986). Quantitative validation of cochlear models using the Liouville-Green approximation. *Hearing Res.* 21, 1-15.
- Viergever, M.A. and Kalker, J.J. (1975). A two-dimensional model for the cochlea I. The exact approach. *J. Eng. Math.* 9, 353-365.
- Zwislocki, J.J. (1962). Analysis of the Middle-Ear Function. Part I: Input Impedance. *J. Acoust. Soc. Am.* 34, 1514-1523.
- Zwislocki, J.J. (1963). Analysis of the Middle-Ear Function. Part II: Guinea-Pig Ear. *J. Acoust. Soc. Am.* 35, 1034-1040.
- Zwislocki, J.J. (1965). Analysis of some auditory characteristics. In: *handbook of mathematical psychology III*, 1-97. Editors: R.D. Luce, R.R. Bush, and E. Galanter. Wiley, New York.

**CHAPTER SIX****Nonlinear and active three-dimensional cochlear models: time-domain solution**

**Abstract** A solution method is developed for three-dimensional (3D) models of the cochlea which are equipped with nonlinear and active properties. The basic feature of the derivation is that the dimensionality of the model equations is reduced. The original description, a partial differential equation for the fluid pressure containing three spatial variables and the time variable, is converted to an integral equation in only one spatial variable (and time) for the acceleration of the center line of the basilar membrane. This can be done without affecting the three-dimensional character of the fluid flow. The integral equations for the corresponding 1D and 2D models are also derived. Numerical solutions for various 3D models are presented, and compared with those for the lower dimensional models. The conclusion is that a 2D treatment of nonlinear and active models is quite satisfactory, even more so than in the linear and passive case. The computationally attractive 1D approach is a good alternative if one is not interested in details of the solution. For linear passive model examples the numerical solutions are furthermore compared with asymptotic solutions obtained by the Liouville-Green (LG) approximation. The LG approximation is the most accurate for the 1D model and the least accurate (although still quite acceptable for many applications) for the 3D model.

**LIST OF MAIN SYMBOLS**

|                 |   |
|-----------------|---|
| $A_s$           | area of stapes footplate                                    |
| $D_R(x,t)$      | internal damping of the BM fibers                           |
| $D_S(x,t)$      | bending stiffness of the BM fibers                          |
| $G_n(x,\xi)$    | parts of the kernel of the integral equation [see Eq. (36)] |
| $G^{3D}(x,\xi)$ | 3D kernel of the integral equation [see Eq. (38)]           |
| $G^{2D}(x,\xi)$ | 2D kernel of the integral equation [see Eq. (43)]           |
| $G^{1D}(x,\xi)$ | 1D kernel of the integral equation [see Eq. (47)]           |
| $H$             | system matrix [see Eq. (58)]                                |

|   |   |
|---|---|
| $L$   | length of the BM  |
| $M$   | matrix containing the BM masses in<br>the nodal points [see Eq. (58)] |
| $b$   | width of the cochlear channels  |
| $b_1(x), b_2(x)$                            | edges of the BM   |
| $g(x, t)$                                   | see Eq. (40)  |
| $\underline{g}(t)$                          | see Eq. (60)  |
| $h$   | height of the cochlear channels                                       |
| $h_{BM}(x)$                                 | thickness of the BM   |
| $\underline{k}$                             | see Eq. (59)  |
| $m(x)$                                      | mass of BM per unit of area   |
| $n$   | number of subintervals in the spatial discretization                  |
| $p(x, y, z, t)$                             | fluid difference pressure   |
| $p_1(x, t)$                                 | fluid difference pressure at the BM center line                       |
| $r(x, t)$                                   | resistance of BM per unit of area                                     |
| $s(x, t)$                                   | stiffness of BM per unit of area                                      |
| $t$   | time variable   |
| $u_{BM}(x, y, t)$                           | BM displacement   |
| $u_s(t)$                                    | stapes displacement   |
| $u_1(x, t)$                                 | BM centerline displacement  |
| $\underline{u}_1(t)$                        | vector containing BM centerline<br>displacements in the nodal points  |
| $\underline{v}_1(t)$                        | vector containing BM centerline<br>velocities in the nodal points     |
| $x$   | longitudinal coordinate along the BM                                  |
| $x_0, x_1, \dots, x_j, \dots, x_{n-1}, x_n$ | set of nodal points (see Eq. (49))                                    |
| $y$   | radial coordinate of the BM   |
| $z$   | coordinate perpendicular to the BM                                    |
| $\Delta$                                    | mesh size of spatial discretization                                   |
| $\beta(x)$                                  | BM width  |
| $\gamma_{n,k}$                              | see Eq. (31)  |
| $\rho$                                      | fluid density   |
| $\rho_p$                                    | density of the BM   |

## INTRODUCTION

Measurements of basilar membrane (BM) motion (Rhode, 1971, 1978; LePage and Johnstone, 1980; Sellick *et al.*, 1982; Robles *et al.*, 1986; LePage, 1987) and of otoacoustic emissions (Kemp, 1978; Kim *et al.*, 1980; Wilson, 1980) have firmly established that the cochlea is nonlinear at the level of BM mechanics. While the mechanisms underlying the nonlinear behavior are far from understood, it has been shown that cochlear models equipped with -largely phenomenological- nonlinear features can reproduce at least some of the effects found experimentally (Hubbard and Geisler, 1972; Hall, 1974, 1977; see also Kim, 1986). Moreover, it is known that the cochlea is a mechanically active system since Kemp (1978) first observed the phenomenon of otoacoustic emissions. Calculations on cochlear models (De Boer, 1983; Viergever and Diependaal, 1986; Diependaal *et al.*, 1987a) strongly suggest that this activity is responsible for the sharp tuning of the recently measured BM vibration data (Khanna and Leonard, 1982; Sellick *et al.*, 1982; Robles *et al.*, 1986), although this has not been proven beyond all doubt (Wickesberg and Geisler, 1986; Kolston, 1988; Kolston *et al.*, 1988).

In view of the above, it seems useful to study cochlear models with nonlinear and active BM properties. One- (1D) and two-dimensional (2D) nonlinear and active models have been considered in Diependaal *et al.* (1987b, 1988). In the present paper a three-dimensional (3D) model will be analyzed. Models equipped with nonlinear and active features put high demands on the mathematical methods used. Active properties may endanger the stability of the model response. Therefore, considerable attention should be given to the choice of the solution technique. Especially when the model equations are solved numerically, one has to ensure that the numerical solution is stable when the model response is physically stable. Contrary to linear models which may be analyzed in the frequency domain (provided the response is stable<sup>1</sup>) nonlinear models have to be solved in the time domain. This greatly complicates the analysis of the problem and significantly increases the computation times involved, in particular for 3D models. The aim of the present paper is to show that the dimensionality of the description of a 3D cochlear model can be reduced. An equivalent integral equation in one independent spatial variable, *viz.* the coordinate

1. Many linear active cochlear models violate this really trivial condition.

along the BM, is derived without doing any concessions to the three-dimensionality of the fluid flow in the model.

The plan of the paper is as follows. In Sec. I the time domain formulation of a 3D cochlear model is derived. The model selected has a representation of the BM by a system of parallel beams; that is, longitudinal mechanical coupling through the BM is ignored. From the 3D model equations a 1D integral equation for the BM center line acceleration is derived (Sec. II). In Sec. III the integral equation is simplified to describe the behavior of BM vibrations in the corresponding 2D and 1D cochlear models. Section IV describes the method chosen to solve the integral equation numerically. In Sec. V some results of numerical calculations are presented. The response of a linear passive 3D cochlear model is calculated and compared with its 2D and 1D counterparts. The numerical solutions are also compared with asymptotic solutions obtained by the LG approximation. Furthermore, the responses of a nonlinear active model, a modified Van der Pol oscillators model, on a pure tone are computed, again in 1D, 2D and 3D.

## I. THE 3D MODEL

The 1D, 2D, and 3D descriptions of cochlear mechanics to be discussed in this paper all derive from the same model geometry, shown in Fig. 1.

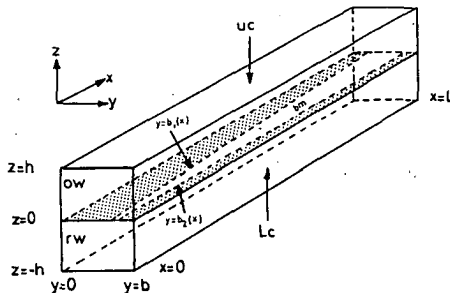


**Figure 1.** Geometry of the three-dimensional model.

The model consists of two identical rectangular channels, filled with an incompressible, inviscid fluid that behaves linearly. The channels are separated by the cochlear partition, the plane  $z=0$ . The BM has a width  $\beta$ ; it

occupies a fraction of the width  $b$  of the partition. The system is considered to be driven in push-pull; the component  $p$  of the fluid pressure<sup>2</sup> that induces a travelling wave along the BM is, consequently, antisymmetric with respect to the plane  $z=0$ . Hence we can confine ourselves to events occurring in the upper channel.

Owing to the assumptions made about the fluid filling the model, the fluid pressure must satisfy Laplace's equation for potential flow. We write the equations not in terms of fluid pressure itself, but in terms of a difference pressure  $p$  which is defined as

$$p(x,y,z,t) = p_{lc}(x,y,-z,t) - p_{uc}(x,y,z,t), \quad z > 0, \quad (1)$$

where  $p_{lc}$  and  $p_{uc}$  are the (antisymmetric parts of) the fluid pressure in the lower and upper channel, respectively. Laplace's equation now reads

$$\frac{\partial^2 p(x,y,z,t)}{\partial x^2} + \frac{\partial^2 p(x,y,z,t)}{\partial y^2} + \frac{\partial^2 p(x,y,z,t)}{\partial z^2} = 0, \quad 0 < x < L, 0 < y < b \quad (2)$$

$$0 < z < h, t \geq 0.$$

This elliptic partial differential equation is subject to six boundary conditions. The condition at the base of the cochlea is a prescribed oval window movement driving the system. Hence, we get

$$\frac{\partial p}{\partial x} = \frac{2\rho A_s \ddot{u}_s}{bh} \quad \text{at } x=0, \quad (3)$$

where a dot (') means differentiation with respect to time. Equation (3) can be replaced by a set of equations representing the middle ear. The analysis and numerical treatment of the model equations including the middle ear is completely analogous to that described in Diependaal and Viergever (1988, Appendix). At the rigid walls the normal component of the fluid velocity vanishes, which is expressed by

$$\frac{\partial p}{\partial y} = 0 \quad \text{at } y=0, \quad (4)$$

$$\frac{\partial p}{\partial y} = 0 \quad \text{at } y=b, \quad (5)$$

2. The fluid pressure consists of two parts. The antisymmetric part which we consider is uninfluenced by fluid compressibility. In addition, there is a symmetric part that does depend on compressibility but, because of the symmetry with respect to the plane  $z = 0$ , not on the characteristics of the cochlear partition. The latter pressure component is irrelevant for the motion of the BM.

$$\frac{\partial p}{\partial z} = 0 \quad \text{at } z = h. \quad (6)$$

Furthermore, it is assumed that the pressure vanishes at the helicotrema<sup>3</sup>

$$p(L, y, z, t) = 0. \quad (7)$$

Finally, at the cochlear partition we have

$$\frac{\partial p}{\partial z} \Big|_{z=0} = \begin{cases} 2\rho \ddot{u}_{BM}(x, y, t), & b_1(x) < y < b_2(x) \\ 0, & \text{elsewhere,} \end{cases} \quad (8)$$

where  $u_{BM}$  is the displacement of the BM, defined positive when directed upwards.

The boundary value problem is completed by a relation between  $p$  and  $u_{BM}$  at the level of the BM. Since the BM is not under tension in its resting state, it is a plate rather than a membrane in the terminology of mechanics. The plate is highly anisotropic in intact cochleae, as was demonstrated by Voldrich (1978). This is in conformity with anatomic data (Iurato, 1962) which show that the BM consists of a cottony ground substance reinforced with transverse fibers (*i.e.*, in the  $y$  direction). Since the stiffness of the ground substance is negligibly small in comparison with the stiffness of the fibers, we model the BM as a system of parallel visco-elastic beams (Viergever, 1978; Viergever and Diependaal, 1986):

$$\rho_p h_{BM} \ddot{u}_{BM} + D_R \frac{\partial^4 \dot{u}_{BM}}{\partial y^4} + D_S \frac{\partial^4 u_{BM}}{\partial y^4} = p(x, y, 0, t), \quad b_1(x) < y < b_2(x). \quad (9)$$

The quantities  $h_{BM}$ ,  $D_R$  and  $D_S$  are allowed to vary with  $x$ , but not with  $y$ . Furthermore,  $D_R$  and  $D_S$  may depend on  $t$ ; in particular,  $D_R$  and  $D_S$  are allowed to be functions of  $u_{BM}$  and  $\dot{u}_{BM}$ , thus rendering the BM nonlinear. The edges of each beam are to a good approximation simply supported (Steele, 1976), which means that the deflection and the bending moments at the edges must be zero:

$$u_{BM} = 0, \quad \frac{\partial^2 u_{BM}}{\partial n^2} = 0 \quad \text{at } y = b_1(x), y = b_2(x) \quad (10)$$

3. In earlier papers we used the boundary condition  $\partial p / \partial x = 0$  at the helicotrema. The condition used in this paper slightly simplifies the mathematics. The exact form of the boundary condition is not relevant since the cochlear waves do not have an appreciable magnitude near the helicotrema, except for the lowest audio-frequencies.

where  $\partial/\partial n$  denotes the normal derivative.

The boundary value problem consisting of Eqs. (9), (10) is readily solved by expanding  $u_{BM}$  in a Fourier sine series in  $y$ :

$$u_{BM}(x, y, t) = \sum_{k=1}^{\infty} u_k(x, t) \sin[k \pi(y - b_1(x))/\beta(x)], \quad b_1(x) < y < b_2(x). \quad (11)$$

This expansion obeys the boundary conditions at  $y = b_1$  and  $y = b_2$ . On physical grounds it is supposed that  $u_{BM}$  is a continuous function of bounded variation in  $b_1 < y < b_2$ . The series in Eq. (11) then converges uniformly to  $u_{BM}$  in this interval, and the coefficients  $u_k$  follow from

$$u_k(x, t) = \frac{2}{\beta} \int_{b_1(x)}^{b_2(x)} u_{BM}(x, y, t) \sin[k \pi(y - b_1(x))/\beta(x)] dy. \quad (12)$$

The trans-BM pressure  $p(x, y, 0, t)$  is expanded likewise over the width of the BM:

$$p(x, y, 0, t) = \sum_{k=1}^{\infty} p_k(x, t) \sin[k \pi(y - b_1(x))/\beta(x)], \quad b_1(x) < y < b_2(x); \quad (13)$$

$$p_k(x, t) = \frac{2}{\beta} (x) \int_{b_1(x)}^{b_2(x)} p(x, y, 0, t) \sin[k \pi(y - b_1(x))/\beta(x)] dy. \quad (14)$$

The convergence of the series (11) is very fast; the  $u_k$  are  $O(k^{-5})$  as  $k \rightarrow \infty$ , which follows from repeated integration of the right hand side of Eq. (12) using the boundary condition (10).

We therefore make a negligibly small error if we replace the series (11) with its leading term<sup>4</sup>. Furthermore, we replace the actual trans-BM pressure  $p(x, y, 0, t)$  by a half-sine-shaped distribution that produces the same displacement pattern. This is, of course, the first term of the Fourier sine expansion in Eq. (13) (Diependaal and Viergever, 1983; Viergever and Diependaal, 1986). So we have

$$u_{BM}(x, y, t) = u_1(x, t) \sin[\pi(y - b_1(x))/\beta(x)], \quad (15)$$

and

---

4. The following analysis is also possible when we do not replace the series with its leading term. However, the formulas will be much more complicated in that case.

$$p(x,y,0,t) = p_1(x,t) \sin[\pi(y - b_1(x))/\beta(x)]. \quad (16)$$

Note that  $u_1(x,t)$  is the displacement of the center line of the BM. By substituting Eqs. (15), (16) into Eq. (9) we find the following relation between  $u_1$  and  $p_1$ :

$$m(x)\ddot{u}_1(x,t) + r(x,t)\dot{u}_1(x,t) + s(x,t)u_1(x,t) = p_1(x,t) \quad (17)$$

where  $m$ ,  $r$ , and  $s$  are defined by

$$m(x) = \rho_p H(x), \quad (18)$$

$$r(x,t) = \left( \frac{\pi}{\beta(x)} \right)^4 D_R(x,t), \quad (19)$$

$$s(x,t) = \left( \frac{\pi}{\beta(x)} \right)^4 D_S(x,t). \quad (20)$$

Equations (17)–(20) complete the description of the 3D model.

## II. THE INTEGRAL EQUATION FOR THE BM ACCELERATION

The form of the boundary conditions at the walls  $y=0$  and  $y=b$  [Eqs. (4), (5)] makes it convenient to expand the pressure  $p$  in a Fourier cosine series in  $y$  (Viergever, 1980):

$$p(x,y,z,t) = \sum_{n=0}^{\infty} \phi_n(x,z,t) \cos(n\pi y/b). \quad (21)$$

On physical grounds it is supposed that  $p$  is continuous and satisfies Dirichlet's conditions in  $0 < y < b$ . The series then converges uniformly to  $p$ , and the coefficients  $\phi_n$  follow from

$$\phi_n(x,z,t) = \frac{2}{\delta_n b} \int_0^b p(x,y,z,t) \cos(n\pi y/b) dy, \quad \delta_n = \begin{cases} 2, & n=0 \\ 1, & n \geq 1. \end{cases} \quad (22)$$

The cosine series expansion is applied to the boundary value problem of Sec. I; this yields a set of equations which the  $\phi_n$  have to satisfy. The cosines form a complete system in  $0 \leq y \leq b$ , so that Laplace's equation (2) becomes

$$\frac{\partial^2 \phi_n}{\partial x^2} + \frac{\partial^2 \phi_n}{\partial z^2} - \left( \frac{n\pi}{b} \right)^2 \phi_n = 0, \quad n \geq 0, \quad (23)$$

and the boundary conditions (3), (6) and (7) change into

$$\frac{\partial \phi_n}{\partial x} \Big|_{x=0} = \begin{cases} \frac{2\rho A_s \ddot{u}_s}{bh}, & n=0 \\ 0, & n \geq 1, \end{cases} \quad (24)$$

$$\frac{\partial \phi_n}{\partial z} = 0 \quad \text{at } z=h, \quad (25)$$

$$\phi_n(L, z, t) = 0. \quad (26)$$

At the cochlear partition we have

$$\frac{\partial \phi_n}{\partial z} \Big|_{z=0} = \frac{2}{\delta_n b} \int_0^b \frac{\partial p}{\partial z} \Big|_{z=0} \cos(n \pi y/b) dy. \quad (27)$$

With the aid of Eqs. (8) and (15) this can be written as

$$\begin{aligned} \frac{\partial \phi_n}{\partial z} \Big|_{z=0} &= \frac{2}{\delta_n b} \int_{b_1(x)}^{b_2(x)} 2\rho \ddot{u}_1 \sin[\pi(y - b_1(x))/\beta(x)] \cos(n \pi y/b) dy \\ &= \frac{4\rho b \beta(x)}{\delta_n \pi} \frac{\cos[n \pi b_1(x)/b] + \cos[n \pi b_2(x)/b]}{b^2 - n^2 \beta^2(x)} \ddot{u}_1. \end{aligned} \quad (28)$$

The solution of the boundary value problem for  $\phi_n$  can be obtained in the form of the following series

$$\begin{aligned} \phi_n(x, z, t) &= \sum_{k=0}^{\infty} \left\{ A_{n,k}(t) \cosh[\gamma_{n,k}(h-z)] \cos[(k+\frac{1}{2})\pi x/L] \right\} + \\ &\quad + \alpha_n(x-L) \frac{2\rho A_s \ddot{u}_s}{bh} \end{aligned} \quad (29)$$

where

$$\alpha_n = \begin{cases} 1, & n=0 \\ 0, & n \geq 1, \end{cases} \quad (30)$$

and

$$\gamma_{n,k}^2 = [(k+\frac{1}{2})\pi/L]^2 + (n\pi/b)^2. \quad (31)$$

This solution satisfies Eqs. (23)-(26). The condition at the cochlear partition is used to determine the coefficient functions  $A_{n,k}(t)$ . We substitute Eq. (29) into Eq. (28) to yield

$$\begin{aligned}
 & -\sum_{k=0}^{\infty} \{ \gamma_{n,k} A_{n,k}(t) \sinh(\gamma_{n,k} h) \cos[(k+\frac{1}{2})\pi x/L] \} = \\
 & = \frac{4\rho b \beta(x)}{\delta_n \pi} \frac{\cos[n\pi b_1(x)/b] + \cos[n\pi b_2(x)/b]}{b^2 - n^2 \beta^2(x)} \ddot{u}_1(x,t). \tag{32}
 \end{aligned}$$

The left hand side of Eq. (32) may be considered as a Fourier cosine expansion of the right hand side. On physical grounds we assume that  $\ddot{u}_1$  is continuous and satisfies Dirichlet's conditions in  $0 < x < L$ . The series then converges uniformly to the right hand side of Eq. (32) and the  $A_{n,k}(t)$  follow from

$$\begin{aligned}
 A_{n,k}(t) = & \frac{-8\rho b}{\delta_n \gamma_{n,k} \pi L \sinh(\gamma_{n,k} h)} \int_0^L \frac{\beta(\xi) \ddot{u}_1(\xi, t) \cos[(k+\frac{1}{2})\pi \xi/L]}{b^2 - n^2 \beta^2(\xi)} \times \\
 & \times \{ \cos[n\pi b_1(\xi)/b] + \cos[n\pi b_2(\xi)/b] \} d\xi. \tag{33}
 \end{aligned}$$

Substitution of Eq. (33) into Eq. (29) gives us an expression for the  $\phi_n$  in terms of the BM acceleration  $\ddot{u}_1$ :

$$\begin{aligned}
 \phi_n(x, z, t) = & -\frac{8\rho b}{\delta_n \pi L} \sum_{k=0}^{\infty} \left\{ \frac{\cosh[\gamma_{n,k}(h-z)]}{\gamma_{n,k} \sinh(\gamma_{n,k} h)} \cos[(k+\frac{1}{2})\pi x/L] \right. \times \\
 & \times \int_0^L \frac{\beta(\xi) \ddot{u}_1(\xi, t) \cos[(k+\frac{1}{2})\pi \xi/L]}{b^2 - n^2 \beta^2(\xi)} \times \\
 & \left. \times [\cos(n\pi b_1(\xi)/b) + \cos(n\pi b_2(\xi)/b)] d\xi \right\} + \alpha_n(x-L) \frac{2\rho A_s \ddot{u}_s(t)}{bh} \tag{34}
 \end{aligned}$$

We want to eliminate the  $\phi_n$  from our formulation; this is possible with the aid of Eq. (17). Therefore Eq. (34) is evaluated at  $z=0$  to get

$$\phi_n(x, 0, t) = \frac{8\rho}{\pi b^3} \int_0^L \beta(\xi) G_n(x, \xi) \ddot{u}_1(\xi, t) d\xi + \alpha_n(x-L) \frac{2\rho A_s \ddot{u}_s(t)}{bh} \tag{35}$$

where  $G_n$  is defined by

$$\begin{aligned}
 G_n(x, \xi) = & -\frac{b^4 [\cos(n\pi b_1(\xi)/b) + \cos(n\pi b_2(\xi)/b)]}{\delta_n L [b^2 - n^2 \beta^2(\xi)]} \times \\
 & \times \sum_{k=0}^{\infty} \left\{ \frac{\coth(\gamma_{n,k} h)}{\gamma_{n,k}} \cos[(k+\frac{1}{2})\pi x/L] \cos[(k+\frac{1}{2})\pi \xi/L] \right\}. \tag{36}
 \end{aligned}$$

Equations (14) and (21) jointly yield

$$p_1(x,t) = \frac{2b^2}{\pi} \sum_{n=0}^{\infty} \left\{ \frac{\cos[n\pi b_1(x)/b] + \cos[n\pi b_2(x)/b]}{b^2 - n^2 \beta^2(x)} \phi_n(x,0,t) \right\}, \quad (37)$$

so that, using Eqs. (17) and (35)-(37), we finally arrive at the integral equation for the motion of the BM center line:

$$\begin{aligned} \frac{16\rho}{\pi^2 b} \int_0^L \beta(\xi) G^{3D}(x,\xi) \ddot{u}_1(\xi,t) d\xi - m(x) \ddot{u}_1(x,t) = \\ g(x,t) + \frac{8\rho A_s \ddot{u}_s(t)}{\pi b h} (L-x), \end{aligned} \quad (38)$$

with

$$\begin{aligned} G^{3D}(x,\xi) &= \sum_{n=0}^{\infty} \left\{ \frac{\cos(n\pi b_1(x)/b) + \cos(n\pi b_2(x)/b)}{b^2 - n^2 \beta^2(x)} G_n(x,\xi) \right\} = \\ &= -\frac{b^4}{L} \sum_{n=0}^{\infty} \left\{ \frac{[\cos(n\pi b_1(x)/b) + \cos(n\pi b_2(x)/b)]}{\delta_n [b^2 - n^2 \beta^2(x)]} \times \right. \\ &\quad \times \frac{[\cos(n\pi b_1(\xi)/b) + \cos(n\pi b_2(\xi)/b)]}{[b^2 - n^2 \beta^2(\xi)]} \times \\ &\quad \left. \times \sum_{k=0}^{\infty} \left\{ \frac{\coth(\gamma_{n,k} h)}{\gamma_{n,k}} \cos[(k+\frac{1}{2})\pi x/L] \cos[(k+\frac{1}{2})\pi \xi/L] \right\} \right\}, \end{aligned} \quad (39)$$

and

$$g(x,t) = r(x,t) \dot{u}_1(x,t) + s(x,t) u_1(x,t). \quad (40)$$

### III. THE CORRESPONDING 2D AND 1D MODELS

In Secs. I and II the 3D model equations have been presented and an integral equation for the motion of the BM has been derived. The corresponding 2D and 1D descriptions can be obtained by averaging the pressure over the channel width and the channel cross-section, respectively:

$$p^{2D}(x,z,t) = \frac{1}{b} \int_0^b p(x,y,z,t) dy, \quad (41)$$

$$p^{1D}(x,t) = \frac{1}{h} \int_0^h p^{2D}(x,z,t) dz. \quad (42)$$

From Eq. (21) it can easily be seen that  $p^{2D}$  is identical with the first term

of the Fourier cosine series,  $\phi_0$ . So, the integral equation for the 2D model can simply be obtained by retaining only the  $n=0$  term in Eq. (39) and combining this with Eq. (38):

$$\frac{16\rho}{\pi^2 b} \int_0^L \beta(\xi) G^{2D}(x, \xi) \ddot{u}_1(\xi, t) d\xi - m(x) \ddot{u}_1(x, t) = g(x, t) + \frac{8\rho A_s \ddot{u}_s(t)}{\pi b h} (L - x), \quad (43)$$

with

$$G^{2D}(x, \xi) = -\frac{2}{\pi} \sum_{k=0}^{\infty} \left\{ \coth[(k + \frac{1}{2})\pi h/L] / [k + \frac{1}{2}] \right. \\ \left. \cos[(k + \frac{1}{2})\pi x/L] \cos[(k + \frac{1}{2})\pi \xi/L] \right\}. \quad (44)$$

The series in Eq. (44) can be expressed in terms of elliptic or theta functions (Sondhi, 1978; Viergever, 1980), which can be approximated very accurately by hyperbolic functions. This approximation is advisable when one wants to solve the logarithmically singular equation numerically (Diependaal and Viergever, 1988).

To get the 1D description we return to Eq. (34). The fluid flow variations in the  $y$  direction are removed by only retaining the leading ( $n=0$ ) term, and those in the  $z$  direction by averaging this term over the channel height. The result is

$$p^{1D}(x, t) = -\frac{16\rho}{\pi b h L} \int_0^L \beta(\xi) [L - \max(x, \xi)] \ddot{u}_1(\xi, t) d\xi + \\ + \frac{2\rho A_s(t) \ddot{u}_s(t)}{b h} (x - L). \quad (45)$$

In the 1D case Eq. (37) reduces to

$$p_1(x, t) = \frac{4}{\pi} p^{1D}(x, t), \quad (46)$$

so that the integral equation (Eq. (38)) for the 1D model reads

$$\frac{16\rho}{\pi^2 b} \int_0^L \beta(\xi) G^{1D}(x, \xi) \ddot{u}_1(\xi, t) d\xi - m(x) \ddot{u}_1(x, t) = \\ g(x, t) + \frac{8\rho A_s \ddot{u}_s(t)}{\pi b h} (L - x), \quad (47)$$

where  $G^{1D}$  is defined by

$$G^{1D}(x, \xi) = \frac{4}{hL} [\max(x, \xi) - L]. \quad (48)$$

An equivalent integral formulation for the 1D model has been presented by Jones *et al.* (1986); the resulting equation has been solved numerically. However, in the 1D case a numerically more efficient method can be constructed by discretizing the 1D model equations directly (Diependaal *et al.*, 1987b).

#### IV. DISCRETIZATION OF THE INTEGRAL EQUATION

In order to render the integral equation discrete we divide the interval  $[0, L]$  into  $n$  subintervals by the set of nodal points

$$0 = x_0 < x_1 < \dots < x_i < \dots < x_{n-1} < x_n = L. \quad (49)$$

For simplicity we confine ourselves to an equidistant mesh. The formulation can easily be extended to a non-equidistant mesh, however. So we have

$$x_i - x_{i-1} = \Delta, \quad i = 1, 2, \dots, n \quad (50)$$

Of course, Eq. (38) is valid at every nodal point  $x_j$ ,  $j = 0(1)n$ :

$$\frac{16\rho}{\pi^2 b} \int_0^L \beta(\xi) G^{3D}(x_j, \xi) \ddot{u}_1(\xi, t) d\xi - m(x_j) \ddot{u}_1(x_j, t) = \\ = g(x_j, t) + \frac{8\rho A_s}{\pi b h} \ddot{u}_s(t) [L - x_j], \quad (51)$$

Since from Eq. (39) it follows that

$$G^{3D}(L, \xi) = G^{3D}(x, L) = 0, \quad (52)$$

the solution of Eq. (38) with initial conditions

$$u_1(x, 0) = \dot{u}_1(x, 0) = 0 \quad (53)$$

at  $x = L$  is simply

$$u_1(L, t) \equiv 0. \quad (54)$$

In order to solve Eq. (51) for the other nodal points  $x_0, x_1, \dots, x_{n-1}$ , the integral is evaluated numerically by means of the trapezium rule. Special attention must be given to the fact that  $G^{3D}(x_j, \xi) \rightarrow -\infty$  as  $\xi \rightarrow x_j$ . We start with writing the integral in Eq. (51) as a sum of integrals over the subintervals in the following way:

$$\begin{aligned} & \int_0^L \beta(\xi) G^{3D}(x_j, \xi) \ddot{u}_1(\xi, t) d\xi = \sum_{i=1}^{j-1} \left[ \int_{x_{i-1}}^{x_i} \beta(\xi) G^{3D}(x_j, \xi) \ddot{u}_1(\xi, t) d\xi \right] + \\ & + \int_{x_{j-1}}^{x_j} \beta(\xi) G^{3D}(x_j, \xi) \ddot{u}_1(\xi, t) d\xi + \int_{x_j}^{x_{j+1}} \beta(\xi) G^{3D}(x_j, \xi) \ddot{u}_1(\xi, t) d\xi + \\ & + \sum_{i=j+2}^n \left[ \int_{x_{i-1}}^{x_i} \beta(\xi) G^{3D}(x_j, \xi) \ddot{u}_1(\xi, t) d\xi \right]. \end{aligned} \quad (55)$$

The first sum of integrals in Eq. (55) is approximated by means of the trapezium rule to yield

$$\begin{aligned} & \sum_{i=1}^{j-1} \left[ \int_{x_{i-1}}^{x_i} \beta(\xi) G^{3D}(x_j, \xi) \ddot{u}_1(\xi, t) d\xi \right] \approx \\ & \approx \frac{1}{2} \Delta \sum_{i=1}^{j-1} \left[ \beta(x_{i-1}) G^{3D}(x_j, x_{i-1}) \ddot{u}_1(x_{i-1}, t) + \beta(x_i) G^{3D}(x_j, x_i) \ddot{u}_1(x_i, t) \right]. \end{aligned} \quad (56)$$

The last sum of integrals in Eq. (55) is approximated likewise. The second term on the right hand side of Eq. (55) is approximated as follows

$$\begin{aligned} & \int_{x_{j-1}}^{x_j} \beta(\xi) G^{3D}(x_j, \xi) \ddot{u}_1(\xi, t) d\xi \approx \frac{1}{2} [\beta(x_{j-1}) \dot{u}_1(x_{j-1}, t) + \\ & + \beta(x_j) \dot{u}_1(x_j, t)] \int_{x_{j-1}}^{x_j} G^{3D}(x_j, \xi) d\xi, \end{aligned} \quad (57)$$

The integral in Eq. (57) is evaluated analytically using expression (39). The integral over the first term of  $G^{3D}$ , which is just  $G^{2D}$ , has been evaluated elsewhere (Diependaal and Viergever, 1988); integration of the other terms is

a straightforward extension. The third term in Eq. (55) is treated analogously to the second term.

Now that we have evaluated the integral in the nodal points, we can write the integral equation (38) as a system of (algebraic) equations

$$[H - M] \underline{\ddot{u}}_1(t) = \underline{g}(t) + \frac{8\rho A_s \ddot{u}_s(t)}{\pi b h} \underline{k}, \quad (58)$$

where

$$\underline{k} = [L, L - x_1, L - x_2, \dots, L - x_{n-1}]^T, \quad (59)$$

$$\underline{g}(t) = [g(0, t), g(x_1, t), g(x_2, t), \dots, g(x_{n-1}, t)]^T, \quad (60)$$

$$\underline{\ddot{u}}_1(t) = [\ddot{u}_1(0, t), \ddot{u}_1(x_1, t), \ddot{u}_1(x_2, t), \dots, \ddot{u}_1(x_{n-1}, t)]^T, \quad (61)$$

$$M = \text{diag}[m(0), m(x_1), m(x_2), \dots, m(x_{n-1})]^T, \quad (62)$$

and  $H$  is the matrix  $(h_{jl})$  given by

$$h_{00} = g_{00}^{2D} - \alpha(0) \sum_{n=1}^{\infty} \left\{ t_n^2(0) \sum_{k=0}^{\infty} \left\{ \frac{ct_{n,k}}{(k+1/2)\pi} s(2k+1) \right\} \right\}, \quad (63)$$

$$h_{01} = g_{01}^{2D} - \alpha(\Delta) \sum_{n=1}^{\infty} \left\{ t_n(0) t_n(\Delta) \sum_{k=0}^{\infty} \left\{ ct_{n,k} \left[ \frac{s(2k+1)}{(k+1/2)\pi} + \frac{\Delta c(2k+1)}{L} \right] \right\} \right\}, \quad (64)$$

$$h_{10} = g_{10}^{2D} - \frac{1}{2}\alpha(0) \sum_{n=1}^{\infty} \left\{ t_n(0) t_n(\Delta) \sum_{k=0}^{\infty} \left\{ \frac{ct_{n,k}}{(k+1/2)\pi} s(4k+2) \right\} \right\}, \quad (65)$$

$$h_{j0} = g_{j0}^{2D} - \frac{\alpha(0)\Delta}{L} \sum_{n=1}^{\infty} \left\{ t^n(0) t_n(x_j) \sum_{k=0}^{\infty} \left\{ ct_{n,k} c[(2k+1)j] \right\} \right\}, \quad j > 1, \quad (66)$$

$$h_{0i} = g_{0i}^{2D} - \frac{2\alpha(x_i)\Delta}{L} \sum_{n=1}^{\infty} \left\{ t^n(0) t_n(x_i) \sum_{k=0}^{\infty} \left\{ ct_{n,k} c[(2k+1)i] \right\} \right\}, \quad i > 1, \quad (67)$$

$$h_{jj} = g_{jj}^{2D} - \alpha(x_j) \sum_{n=1}^{\infty} \left| t_n^2(x_j) \sum_{k=0}^{\infty} \left\{ \frac{ct_{n,k}}{(k+\frac{1}{2})\pi} [1 + c((4k+2)j)] \times \right. \right. \\ \left. \left. \times s(2k+1) \right\} \right\}, \quad j > 0, \quad (68)$$

$$h_{j,j+1} = g_{j,j+1}^{2D} - \frac{1}{2}\alpha(x_{j+1}) \sum_{n=1}^{\infty} \left| t^n(x_j) t_n(x_{j+1}) \times \right. \\ \left. \times \sum_{k=0}^{\infty} \left\{ ct_{n,k} \left[ \frac{s[(2k+1)(2j+1)] - s[(4k+2)j] + s(2k+1)}{(k+\frac{1}{2})\pi} + \right. \right. \right. \\ \left. \left. \left. + \frac{c[(2k+1)(2j+1)] + c(2k+1)}{L/\Delta} \right] \right\} \right\}, \quad j > 0, \quad (69)$$

$$h_{j,j-1} = g_{j,j-1}^{2D} - \frac{1}{2}\alpha(x_{j-1}) \sum_{n=1}^{\infty} \left| t^n(x_j) t_n(x_{j-1}) \times \right. \\ \left. \times \sum_{k=0}^{\infty} \left\{ ct_{n,k} \left[ \frac{s[(4k+2)j] - s[(2k+1)(2j-1)] + s(2k+1)}{(k+\frac{1}{2})\pi} + \right. \right. \right. \\ \left. \left. \left. + \frac{c[(2k+1)(2j-1)] + c(2k+1)}{L/\Delta} \right] \right\} \right\}, \quad j > 1, \quad (70)$$

$$h_{ji} = g_{ji}^{2D} - \frac{\alpha(x_i)\Delta}{L} \sum_{n=1}^{\infty} \left| t^n(x_j) t_n(x_i) \times \sum_{k=0}^{\infty} \left\{ ct_{n,k} \left[ c[(2k+1)(j+i)] + \right. \right. \right. \\ \left. \left. \left. + c[(2k+1)(j-i)] \right] \right\} \right\}, \quad |i-j| > 1, \quad i > 0, \quad j > 0. \quad (71)$$

In Eqs. (63)-(71)  $\alpha$ ,  $t_n$ ,  $ct_{n,k}$ ,  $s$ , and  $c$  are shorthand for

$$\alpha(x) = 8\rho\beta(x)/(\pi^2 b), \quad (72)$$

$$t_n(x) = \frac{\cos[n\pi b_1(x)/b] + \cos[n\pi b_2(x)/b]}{1 - [n\beta(x)/b]^2}, \quad (73)$$

$$ct_{n,k} = \coth(\gamma_{n,k} h)/\gamma_{n,k}, \quad (74)$$

$$s(l) = \sin(\pi l/2n), \quad (75)$$

$$c(l) = \cos(\pi l/2n). \quad (76)$$

For the matrix  $G^{2D}$  ( $=g_{ji}^{2D}$ ) we refer to Diependaal and Viergever (1988). The periodicity of  $s$  and  $c$  can be used advantageously in reading in the matrix. The coefficients  $ct_{n,k}$  can be approximated by  $1/\gamma_{n,k}$ , since for  $n \geq 1$

$$1 < \coth(\gamma_{n,k}) \leq \coth(n\pi h/b) \leq \coth(\pi h/b). \quad (77)$$

For characteristic values of  $h$  and  $b$  ( $h=b=1 \text{ mm}$ ) the upper limit is

$$\coth(\pi h/b) < 1.00375. \quad (78)$$

In order to yield a numerical solution of the model equations we now have to integrate the system of ordinary differential equations

$$\dot{u}_1(t) = v_1(t), \quad u_1(0) = 0 \quad (79)$$

$$\dot{v}_1(t) = \psi(t), \quad v_1(0) = 0. \quad (80)$$

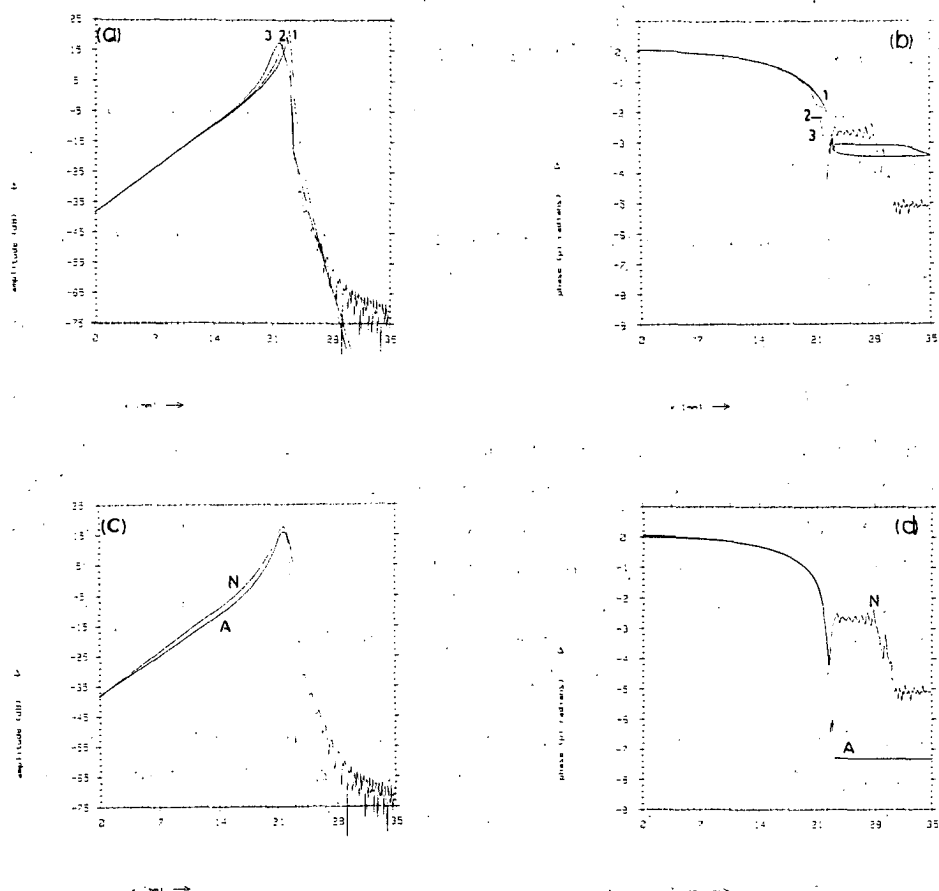
The algorithm to solve the model equations numerically will be clear: at each instant of time, the numerical approximation  $\psi(t)$  for  $\ddot{u}_1(t)$  is solved from Eq. (58), after which the system of Eqs. (79), (80) is integrated from that instant of time to the next one. A variable step size fourth-order Runge-Kutta scheme is used for solving the differential equations, since that scheme has been shown to be both efficient and robust in comparison with other schemes (Diependaal *et al.*, 1987b).

The method can be extended to models with more than one degree of freedom at each point along the cochlear partition. This is done in an analogous way as described by Diependaal *et al.* (1987b, Appendix B).

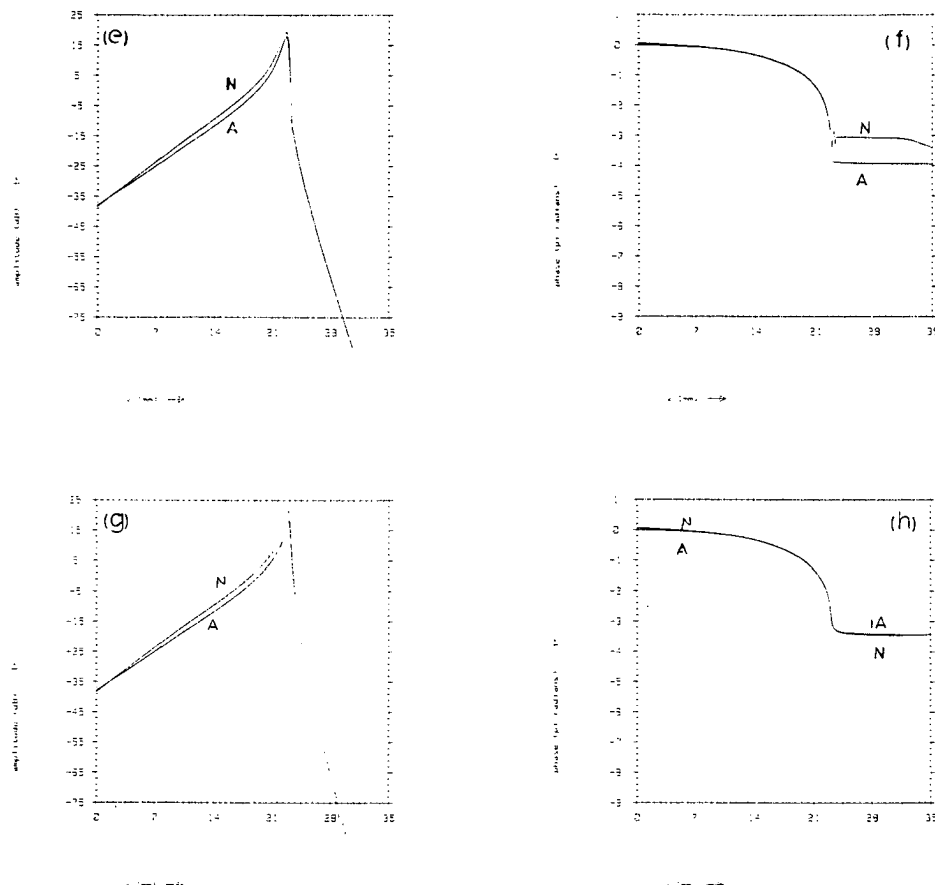
## V. NUMERICAL RESULTS

In this section, we shall give some illustrative examples of our model calculations. In order to calculate the entries of the matrix  $H$  [Eqs. (63)-(71)] we have to truncate two infinite sums, one with index  $n$  and one with index  $k$ . The sum with index  $n$  converges very rapidly, so that in practice no more than about 10 terms have to be taken into account. On the other hand, the sum with index  $k$  converges very slowly; it may only be truncated after much more (in the order of 1000) terms.

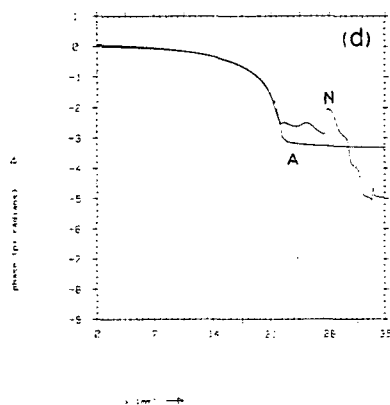
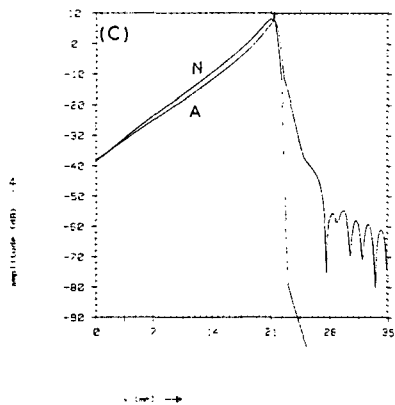
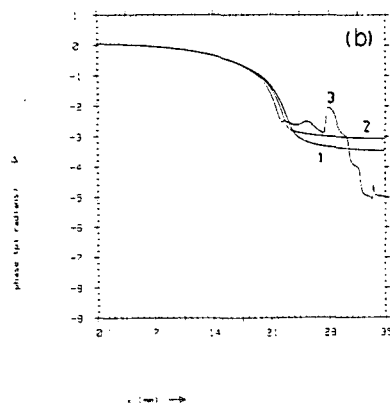
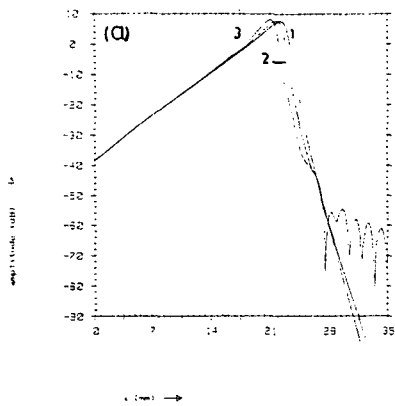
In Figs. 2a,b the graphs of the numerical solutions of the customary linear passive 1D, 2D, and 3D models are plotted for comparison (see e.g.



**Figure 2.** Amplitudes and phases of the BM velocity/pressure at the eardrum transfer ratio in linear, passive cochlear models. (a) and (b) Amplitudes and phases of numerical solutions of the transfer ratios. curve 1, 2, 3: 1D, 2D, 3D model, respectively. (c)-(h) Comparison between numerical solutions and LG approximations to the solution. (c) and (d) 3D model. (e) and (f) 2D model. (g) and (h) 1D model. Curves N: the fundamental component of the Fourier transform of the numerical solution in the time domain, curves A: LG approx-



imation to the solution. Parameters:  $A_s = 1 \text{ mm}^2$ ,  $L = 35 \text{ mm}$ ,  $b = 1 \text{ mm}$ ,  $h = 1 \text{ mm}$ ,  $\beta(x) = 0.08 \exp(0.05x) \text{ mm}$ ,  $b_1(x) = b_2(x) - \beta(x)$ ,  $b_2(x) = 0.85 + 0.003x \text{ mm}$ ,  $m(x) = 0.5 \text{ mg/mm}^2$ ,  $r(x, t) = 5 \exp(-0.15x) \text{ mg}/(\text{mm}^2 \text{ ms})$ ,  $s(x, t) = 20,000 \exp(-0.3x) \text{ mg}/(\text{mm}^2 \text{ ms}^2)$ , with  $x$  in  $\text{mm}$ . Middle-ear parameters as in Diependaal and Viergever (1988, Fig. 2). The BM has been divided into 256 elements of equal size.



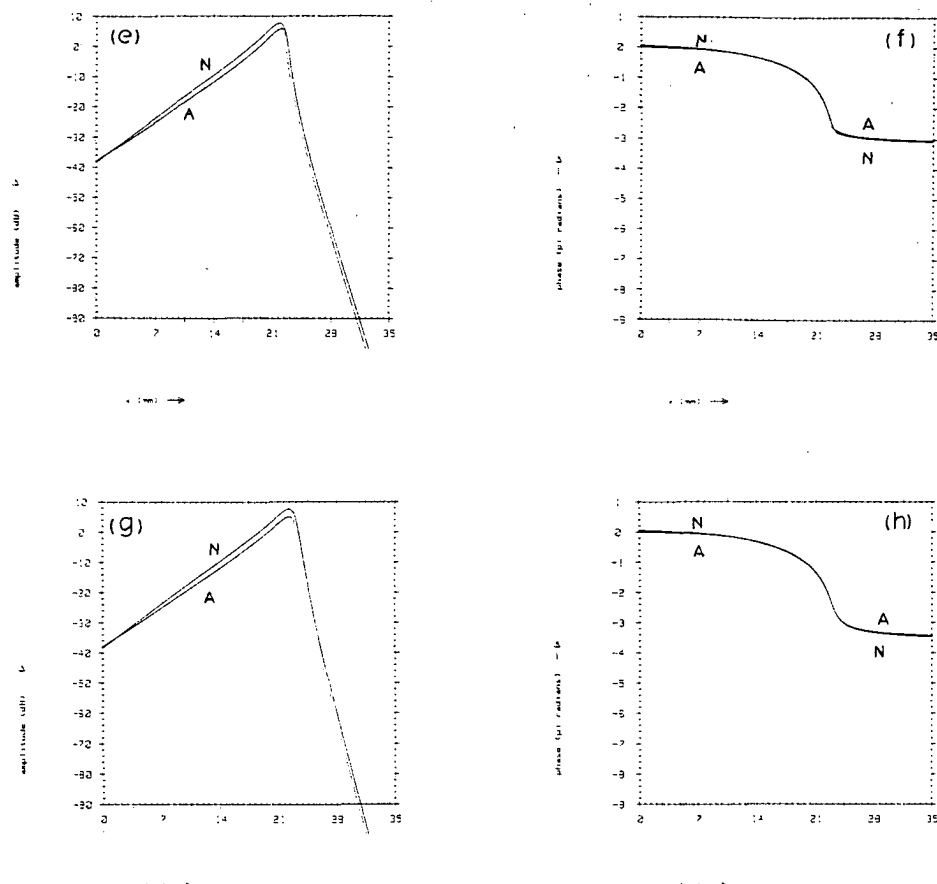


**Figure 3.** Amplitudes and phases of the BM velocity/pressure at the eardrum transfer ratio in linear, passive cochlear models. Parameter values and display as in Fig. 2, except that the resistance  $r(x,t) = 25\exp(-0.15x) \text{ mg}/(\text{mm}^2\text{ms})$ .

Diependaal *et al.*, 1987b). For the 1D model we have used the method described in Diependaal *et al.* (1987b). For the 2D and 3D models we have used the method described in Secs. II-IV (for the 2D model, see also Diependaal and Viergever, 1988). The numerical solution in the time domain has been Fourier transformed before it is displayed. Figures 2(c)-(h) show responses on a 1 kHz tone, solved by the described numerical method (curves N) and solved by an asymptotic method, the LG approximation (curves A). Using the LG approximation the solution is directly obtained in the frequency domain. In Figs. 2(c), (d) results for the 3D model are plotted, in Fig. 2(e), (f) for the 2D model, and in Fig. 2(g), (h) for the 1D model.

In Fig. 3 the graphs of the solutions of the linear, passive models are plotted in case the resistance has been increased by a factor of 5. The composition of the figure is analogous to Fig. 2. From Figs. 2 and 3 it can be seen that when the dimensionality of the model is increased, the amplitude peak shifts basally, becomes broader and decreases a little. Furthermore, the phase of the response shows a bigger roll-off when the dimension is increased. In the 3D case the numerical solution is not accurate some *mm* after the amplitude peak has been reached, because of the truncation of the sum with index *k* and because of a rather rough discretization in the *x* direction (256 points). A more accurate solution can be achieved, but only at the cost of an unacceptably large amount of computer time. Moreover, at the point where the numerical solution becomes inaccurate the solution is almost extinct (the amplitude is more than 50 dB under the peak amplitude). The results show that the LG solution is a quite good approximation of the numerical solution, although in the 3D case the LG approximation is not as good as in the 1D and 2D cases. Furthermore, in the 3D case with the higher damping the LG solution is completely wrong in the peak region; it is too sharply peaked in comparison with the numerical solution. The reason for this is the following: In the LG solution procedure a wavenumber must be computed from a transcendental equation. This equation has an infinite number of solutions, only one of which is physically meaningful. For some parameter sets the wrong wavenumber is computed (see De Boer and Viergever, 1982, for a detailed account of this insufficiency of the LG method).

We have also calculated responses on a pure tone in a nonlinear active model, a modified Van der Pol oscillators model (Duifhuis *et al.*, 1986; see also Diependaal and Viergever, 1988). In Fig. 4 we show the amplitudes of the

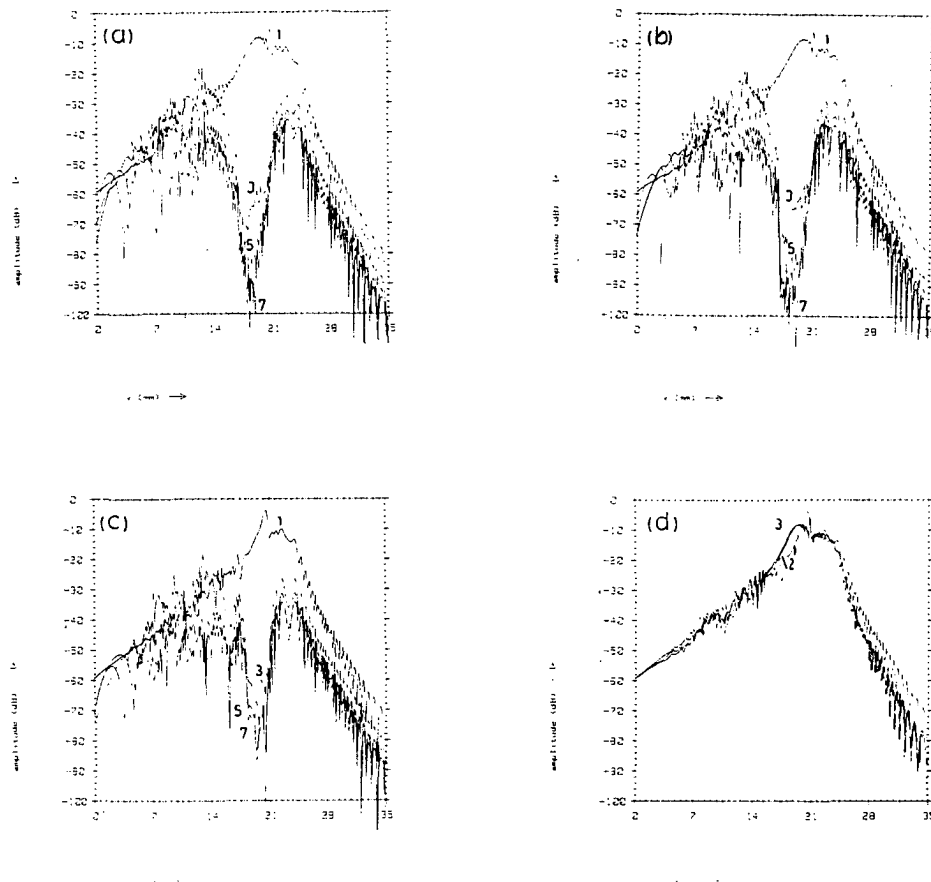


**Figure 4.** Amplitudes of the BM displacement in the modified Van der Pol oscillators model (Duifhuis et al., 1986; Diependaal and Viergever, 1988) for a low input level. (a) 3D model. (b) 2D model. (c) 1D model. The numbers of the curves indicate the frequencies of the Fourier components. (d) Curve 1, 2, 3: amplitudes of the fundamental Fourier component of the responses computed in, respectively, a 1D, 2D, 3D model. Parameter values:  $A_s = 1 \text{ mm}^2$ ,  $L = 35 \text{ mm}$ ,  $b = 1 \text{ mm}$ ,  $h = 1 \text{ mm}$ ,  $\beta(x) = 1 \text{ mm}$ ,  $b_1(x) = b_2(x) - \beta(x)$ ,  $m(x) = 0.5 \text{ mg/mm}^2$ ,  $r(x, t) = 2.5(2)^{\frac{1}{4}}[-1 + 10^{12}v^2(x, t)]\exp(-0.15x) \text{ mg}/(\text{mm}^2\text{ms})$ ,  $s(x, t) = 10,000 \exp(-0.3x) \text{ mg}/(\text{mm}^2\text{ms}^2)$ . Middle-ear parameters as in Diependaal and Viergever (1988). Stimulus: a sinusoidal pressure at the eardrum with amplitude  $3.16 \times 10^{-7} \text{ mg}/(\text{mm ms}^2)$ . The BM has been divided into 256 elements of equal size.

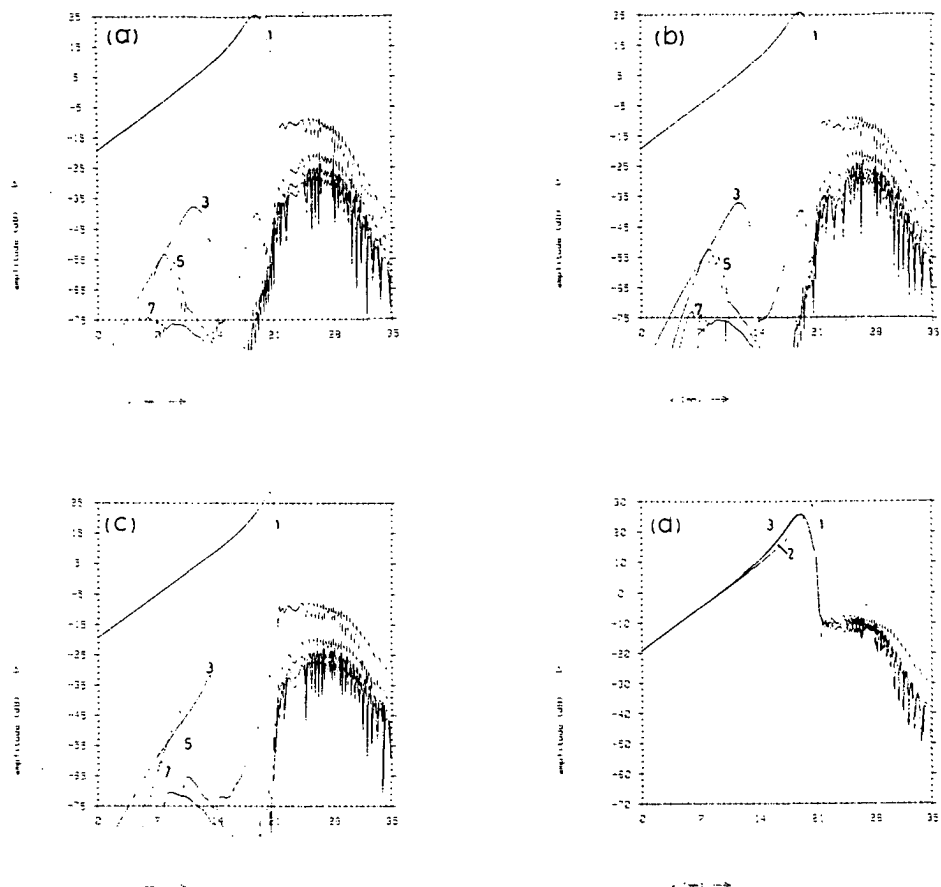


**Figure 5.** Amplitudes of the BM displacement in the modified Van der Pol oscillators model for a high input level. Parameter values and display as in Fig. 4, except that the amplitude of the eardrum pressure =  $3.16 \times 10^{-5} \text{ mg}/(\text{mm} \cdot \text{ms}^2)$ .

responses (after Fourier transformation) for a low-level 1 kHz tone stimulus at the eardrum. Presented are the amplitudes of the fundamental and the first three uneven harmonics of the response for respectively the 3D, 2D, and 1D model [Fig. 4(a)-(c)]. The fundamentals of the three model responses are replotted for comparison in Fig. 4(d). The graphs show that for this low input level there is entrainment only in the region of the 1 kHz characteristic place. In this region the higher harmonics are nearly absent. Furthermore, there is not much difference between the 2D and 3D model responses, but the 1D model response is clearly deviant. The multidimensional model responses show two amplitude peaks; a narrow one at the place of the amplitude peak of the 1D model response and a broader one slightly basalwards.

In Fig. 5 the amplitudes of the responses (after Fourier transformation) are shown for a high-level 1 kHz tone stimulus at the eardrum. The composition of the figure is analogous to Fig. 4. The high level stimulus entrains the oscillators over a wide range, and uneven higher harmonics are clearly present in the response. The third harmonic shows two peaks, at the characteristic places of a 1 kHz tone and of a 3 kHz tone. The fifth and seventh harmonics show only a clear amplitude peak at their own characteristic places. From Fig. 5(d) it can also be gathered that again there is hardly any difference between the 2D and 3D model responses, but that the 1D model response is quite different from the others. Figure 5 shows that the amplitude peak of the fundamental as well as those of the higher uneven harmonics are sharper and higher (a few dB for the fundamental, more than 10 dB for the seventh harmonic) in the 1D case than in the 2D or 3D case.

We end this section with some figures on CPU times. In order to obtain the results as shown in Figs. 2 and 3 representing the response after 1000 ms cochlear time we need about 10 hours of CPU time on a CONVEX C-1 computer for the 3D case if the system matrix is already filled, and 2½ hours more if the system matrix is not yet filled. For the 2D case also 10 hours of CPU time is needed, whereas for the 1D case only 1½ hours of CPU time is needed. We recall that every time step a system of algebraic equations has to be solved, the system matrix of which is tridiagonal in the 1D case (Diependaal *et al.*, 1987b), whereas the system matrix is full in the 2D (Diependaal and Viergever, 1988) and 3D cases. So, the number of elementary computer operations needed to solve the system of equations is of the order of  $n$  in the

1D case, and is of the order of  $n^2$  in the 2D and 3D case, where  $n$  is the number of equations. It should be noted, however, that for many qualitative purposes a model response after 100 ms of cochlear time is sufficiently accurate. This reduces the given computation times (with the exception of the filling of the matrices) by a factor of 10.

## VI. CONCLUSIONS

We have presented a robust numerical method to solve 3D cochlear models in the time domain. With this method, the response of models equipped with nonlinear and active features can be calculated for a variety of stimuli, such as pure tones, two tones, noise, and clicks. The method thus makes it possible to evaluate models with different types of nonlinearity and activity. Furthermore, the present numerical method can be used as a frame of reference in order to assess the accuracy of asymptotic methods, which generally need less computer time than numerical methods.

In 3D time-domain cochlear models, there are four independent variables, *viz.* three spatial coordinates, and the time. The model equations are not directly discretized; they are first rewritten as an integral equation in just one spatial coordinate. In this procedure the 3D character of the fluid flow is not affected. The integral equation is discretized using the trapezium rule, with special attention paid to the logarithmic singularity of the integral. The result is a system of ordinary differential equations, which is solved by a fourth-order Runge-Kutta scheme. This scheme has been shown to be both efficient and robust in comparison with other numerical integration schemes (Diependaal *et al.*, 1987b).

We have calculated responses on a pure tone in a 3D nonlinear active model, the modified Van der Pol oscillators model (Duifhuis *et al.*, 1986), using the presented method, and compared these with responses of corresponding 1D and 2D models, for two different levels of stimulus. In both cases, the 2D response is close to the 3D solution; the 1D approach is considerably less accurate. We have also calculated responses on a pure tone in a 3D linear passive model using the presented method, and compared these with responses of corresponding 1D and 2D models. The 2D responses deviate from the 3D responses, but the differences can be considerably reduced by slightly adapting the parameters (increasing the BM mass) of the 2D model.

For the 1D model, this procedure gives acceptable results only if the damping is high. The numerical solutions of the linear passive model have further been compared with asymptotic approximations using the LG method. The LG approximation is the most accurate for the 1D model and the least accurate (although still quite acceptable for many applications) for the 3D model.

The results presented in this paper indicate that nonlinear and active models can be evaluated satisfactorily in one dimension, if one is only interested in the global behavior of the model. For a more detailed evaluation of the model a 2D approach is necessary, and for most purposes also sufficient. A 3D approach will be mandatory in the case that the fluid flow in the radial ( $y$ ) direction becomes significant, as e.g. in the models of Kolston (1988) and Kolston *et al.* (1988). The only extra CPU time needed for solving the model in 3D rather than in 2D is in forming the system matrix.

## ACKNOWLEDGEMENT

This research has been supported in part by the Netherlands Organization for the Advancement of Pure Research (ZWO).

## REFERENCES

- Boer, E. de (1983). No sharpening? A challenge for cochlear mechanics. *J. Acoust. Soc. Am.* 73, 567-573.
- Boer, E. de and Viergever, M.A. (1982). Validity of the Liouville-Green (or WKB) method for cochlear mechanics. *Hearing Res.* 8, 131-155.
- Diependaal, R.J., Boer, E. de, and Viergever, M.A. (1987a). Cochlear power flux as an indicator of mechanical activity. *J. Acoust. Soc. Am.* 82, 917-926.
- Diependaal, R.J., Duifhuis, H., Hoogstraten, H.W., and Viergever, M.A. (1987b). Numerical methods for solving one-dimensional cochlear models in the time domain. *J. Acoust. Soc. Am.* 82, 1655-1666.
- Diependaal, R.J. and Viergever, M.A. (1983). Point-impedance characterization of the basilar membrane in a three-dimensional cochlea model. *Hear. Res.* 11, 33-40.
- Diependaal, R.J. and Viergever, M.A. (1988). Nonlinear and active two-dimensional cochlear models: time-domain solution. Submitted to *J. Acoust. Soc. Am.*
- Duifhuis, H., Hoogstraten, H.W., Netten, S.M. van, Diependaal, R.J. and Bialek, W. (1986). Modelling the cochlear partition with coupled Van der Pol oscillators. In: *Peripheral Auditory Mechanisms*, pp. 290-297. Editors: J.B. Allen, J.L. Hall, A. Hubbard, S.T. Neely, and A. Tubis. Springer Verlag, Berlin, Heidelberg, New York.
- Hall, J.L. (1974) Two-tone distortion products in a nonlinear model of the basilar membrane. *J. Acoust. Soc. Am.* 56, 1818-1828.
- Hall, J.L. (1977) Two-tone suppression in a nonlinear model of the basilar membrane. *J. Acoust. Soc. Am.* 61, 802-810.
- Hubbard, A.E. and Geisler, C.D. (1972). A hybrid computer model of the cochlear partition. *J. Acoust. Soc. Am.* 51, 1895-1903.

- Iurato, S. (1962). Functional implications of the nature and submicroscopic structure of the tectorial and basilar membranes. *J. Acoust. Soc. Am.* 34, 1386-1395.
- Jones, K., Tubis, A., Long, G.R., Burns, E.M., and Strickland, E.A. (1986). Interactions among multiple spontaneous otoacoustic emissions. In: *Peripheral Auditory Mechanisms*, pp. 266-273. Editors: J.B. Allen, J.L. Hall, A. Hubbard, S.T. Neely, and A. Tubis. Springer Verlag, Berlin, Heidelberg, New York.
- Kemp, D.T. (1978). Stimulated acoustic emissions from within the human auditory system. *J. Acoust. Soc. Am.* 64, 1386-1391.
- Khanna, S.M. and Leonard, D.G.B. (1982). Basilar membrane tuning in the cat cochlea. *Science* 215, 305-306.
- Kim, D.O. (1986). An overview of nonlinear and active cochlear models. In: *Peripheral Auditory Mechanisms*, pp. 239-249. Editors: J.B. Allen, J.L. Hall, A. Hubbard, S.T. Neely, and A. Tubis. Springer Verlag, Berlin, Heidelberg, New York.
- Kim, D.O., Molnar, C.E., and Matthews, J.W. (1980). Cochlear mechanics: Nonlinear behavior in two-tone responses as reflected in cochlear-nerve-fiber responses and in ear-canal sound pressure. *J. Acoust. Soc. Am.* 67, 1704-1721.
- Kolston, P.J. (1988). Sharp mechanical tuning in a cochlear model without negative damping. To appear in *J. Acoust. Soc. Am.*
- Kolston, P.J., Viergever, M.A., Boer, E. de, and Diependaal, R.J. (1988). Realistic mechanical tuning in a micromechanical cochlear model. In preparation.
- LePage, E.L. (1987). Frequency-dependent self-induced bias of the basilar membrane and its potential for controlling sensitivity and tuning in the mammalian cochlea. *J. Acoust. Soc. Am.* 82, 139-154.
- LePage, E.L. and Johnstone, B.M. (1980). Nonlinear mechanical behaviour of the basilar membrane in the basal turn of the guinea pig cochlea. *Hearing Res.* 2, 183-189.
- Rhode, W.S. (1971). Observations of the vibration of the basilar membrane in squirrel monkeys using the Mössbauer technique. *J. Acoust. Soc. Am.* 49, 1218-1231.
- Rhode, W.S. (1978). Some observations on cochlear mechanics. *J. Acoust. Soc. Am.* 64, 158-176.
- Robles, L., Ruggero, M.A. and Rich, N.C. (1986). Basilar membrane mechanics at the base of the chinchilla cochlea. I. Input-output functions, tuning curves, and response phases. *J. Acoust. Soc. Am.* 80, 1364-1374.
- Sellick, P.M., Patuzzi, R. and Johnstone, B.M. (1982). Measurement of basilar membrane motion in the guinea pig using the Mössbauer technique. *J. Acoust. Soc. Am.* 72, 131-141.
- Sondhi, M.M. (1978) Method for computing motion in a two-dimensional cochlear model. *J. Acoust. Soc. Am.* 63, 1468-1477.
- Steele, C.R. (1976). Cochlear mechanics. In: *Handbook of sensory physiology*, Vol. V/3: Auditory system; clinical and special topics, pp. 443-478. Editors: W.D. Keidel and W.D. Neff. Springer, Berlin.
- Viergever, M.A. (1978). On the physical background of the point-impedance characterization of the basilar membrane in cochlear mechanics. *Acustica* 39, 292-297.
- Viergever, M.A. (1980). Mechanics of the Inner Ear - A mathematical approach. Doctoral dissertation, Delft University Press, Delft, The Netherlands.
- Viergever, M.A. and Diependaal, R.J. (1986). Quantitative validation of cochlear models using the Liouville-Green approximation. *Hearing Res.* 21, 1-15.
- Voldrich, L. (1978). Mechanical properties of the basilar membrane. *Acta Otolaryng.* 86, 331-335.
- Wickesberg, R.E. and Geisler, C.D. (1986). Longitudinal stiffness coupling in a 1-dimensional model of the peripheral ear. In: *Peripheral Auditory Mechanisms*, pp. 113-120. Editors: J.B. Allen, J.L. Hall, A. Hubbard, S.T. Neely, and A. Tubis. Springer Verlag, Berlin, Heidelberg, New York.
- Wilson, J.P. (1980). The combination tone,  $2f_1-f_2$ , in psychophysics and ear-canal recording. In: *Psychophysical, Physiological, and Behavioural Studies in Hearing*, pp. 43-50. Editors: G. van den Brink and F.A. Bilsen. Delft U.P., Delft.

**SUMMARY****NONLINEAR AND ACTIVE COCHLEAR MODELS:  
ANALYSIS AND SOLUTION METHODS**

This thesis deals with several aspects of the mechanics of the inner ear (cochlea). The emphasis is on analyzing models of the cochlea and on finding adequate methods to solve the model equations. The ultimate aim is to understand the operation of the cochlea, by developing a model which can explain experimentally observed phenomena. In this thesis three subjects are discussed:

- A quantitative validation of the "classical" macromechanical cochlear models on the basis of measured motion of the basilar membrane (BM).
- The development of methods which test the hypothesis that the cochlea contains a mechanically active filter which manifests itself at the level of BM motion.
- The development of a robust and efficient method to solve nonlinear and active cochlear models in the time domain.

Cochlear models can be divided into two classes, *viz.* macromechanical and micromechanical models. An important property of macromechanical models is that each point along the BM has just one degree of freedom; the mechanical properties of the organ of Corti/tectorial membrane (OC/TM) complex are linked up with those of the BM. Furthermore, macromechanical models are linear and passive ("passive" meaning that no mechanical energy is added to the system other than from the stimulus). All cochlear models that do not satisfy the definition formulated above belong to the class of micromechanical models.

In the first part of the thesis (chapter 1) the BM velocity curves, calculated in macromechanical cochlear models, are compared with BM velocity curves,

obtained by measurements. Because the values of a number of model parameters are not known, a lot of simulations have to be done in order to adjust these parameters. Therefore, the model equations are solved using a fast asymptotic method, the L(iouville-G(reen) method. It is shown in chapter 1 that the amplitude and the phase of mildly tuned BM velocity curves (Johnstone and Yates, 1974; Rhode, 1971, 1978) can be simultaneously matched satisfactorily by means of macromechanical models. These mildly tuned BM velocity curves are nowadays believed to reflect pathological cochleas. In the last five years much sharper tuned BM velocity curves have been measured (Khanna and Leonard, 1982; Sellick *et al.*, 1982, 1983; Robles *et al.*, 1986); the tuning of these velocity curves is comparable to the tuning of receptor potentials in the hair cells. These sharper tuned BM velocity curves cannot be simulated by macromechanical cochlear models. They can neither be simulated by linear, passive models, extended with a second degree of freedom at each point along the BM representing the OC/TM complex.

The sharply tuned BM velocity curves have given arguments to postulate that the cochlea contains a mechanically active filter. This hypothesis is supported by the measurements of otoacoustic echos and spontaneous otoacoustic emissions over the last ten years. Furthermore, quantum-mechanical considerations and model analyses give arguments for such an active filter. Two methods which test the hypothesis that the cochlea contains a active filter that manifests itself at the level of BM motion, are presented in the thesis. The first method (described in chapter 2) is an inversion of the customary description of cochlear mechanics. Instead of computing the BM velocity for a given point-impedance of the membrane, the BM impedance function is computed from a given BM velocity pattern. The real part of the thus computed impedance gives an indication of the presence of an active filter; where the real part is negative, the cochlea adds energy to the motion of the BM. Simulation studies show that the real part of the impedance is extremely sensitive to perturbations in the BM velocity profile. The measured BM velocity curves are always afflicted with measurements errors, and therefore, using this technique, it is impossible to decide whether or not the cochlea contains active elements that manifest themself at the level of BM motion.

Compared to the real part of the impedance the power flux through a cross section of a channel of the cochlea is considerably less sensitive to perturbations in the BM velocity profile (chapter 3). The power flux is an important

indicator of mechanical activity, because a rise in this function corresponds to creation of mechanical energy. Before the power flux can be calculated from measured BM velocity curves the measured data have to be smoothed and interpolated in order to reduce numerical errors as caused by too few and noisy data. The choice of smoothing method considerably influences the calculated power flux. A cubic spline smoothing method is advocated in this thesis. In this method the regularization parameter, which determines the amount of smoothness, depends on the data. The power flux method makes a clear separation between broadly tuned BM vibration data (Johnstone and Yates, 1974) and sharply tuned data (Sellick *et al.*, 1983; Robles *et al.*, 1986). The broadly tuned data do not give rise to a significant increase in the power flux; the sharply tuned data do. In summary the conclusion from the second and third chapters of the thesis is as follows: Within the framework of the model assumptions, the recently measured sharply tuned BM velocity curves indicate that the cochlea contains a mechanically active filter; however, the amount of mechanical activity cannot be calculated, because the real part of the BM impedance cannot be determined reliably from the measured BM velocity curves.

Since the underlying mechanisms of the nonlinear and active behavior of the cochlea are hardly known, it is useful to test and compare different types of cochlear models. To this end robust and efficient solution methods are constructed, with which responses of such models to various types of input signals can be computed in the time domain. In chapters 4, 5, and 6 numerical solution methods for one-, two-, and three-dimensional (1D, 2D, 3D) models, respectively, are presented. This makes it possible to study the effect of the dimensionality of the fluid flow on the motion of the BM.

The 1D model is described by a partial differential equation in two independent variables (place and time), together with boundary and initial conditions. The partial differential equation is discretized spatially with the use of Galerkin's principle, so that a system of ordinary differential equations in the time variable is obtained. Several numerical integration methods are compared on the basis of stability and computational performance. This yields the most suitable algorithm for solving the system of differential equations. The selected algorithm is based on a variable step size fourth-order Runge-Kutta scheme. This scheme appears to be both more stable and more efficient than the other integration schemes examined.

Two- and three-dimensional cochlear models are described by partial differential equations in one time variable and two, respectively three spatial variables, together with boundary and initial conditions. In order to solve the model equations numerically, they are first reformulated as a 1D integral equation for the acceleration of the BM. This can be done without losing the multi-dimensional character of the fluid wave. The resulting integral equation needs to be discretized in one spatial variable only. After the discretization a system of ordinary differential equations has to be solved. As in the 1D case this is achieved using a fourth-order Runge-Kutta scheme. The method requires more computer time in the 2D and 3D cases than in the 1D case. At every time step a system of equations must be solved, the matrix of which is tri-diagonal in the 1D case, but full in the 2D and 3D cases. Furthermore, in the 3D case, a slowly converging series must be summed for each entry of the system matrix. However, the system matrix only has to be formed once for a given set of geometrical and mechanical model parameters, and not at every time step, because it is independent of the time variable.

The numerical methods developed in the thesis can be applied to many cochlear models, and allow for a wide range of stimuli. Consequently, the methods are very well suited to test the validity of nonlinear and active model concepts. Furthermore, the presented methods can be used to assess the accuracy of asymptotic methods, which are computationally less demanding and furthermore give more insight into the physics underlying the BM motion.

## **REFERENCES**

- Johnstone, B.M. and Yates, G.K. (1974). Basilar membrane tuning curves in the guinea pig. *J. Acoust. Soc. Am.* 55, 584-587.
- Khanna, S.M. and Leonard, D.G.B. (1982). Basilar membrane tuning in the cat cochlea. *Science* 215, 305-306.
- Rhode, W.S. (1971). Observations of the vibration of the basilar membrane in squirrel monkeys using the Mössbauer technique. *J. Acoust. Soc. Am.* 49, 1218-1231.
- Rhode, W.S. (1978). Some observations on cochlear mechanics. *J. Acoust. Soc. Am.* 64, 158-176.
- Robles, L., Ruggero, M.A., and Rich, N.C. (1986). Basilar membrane mechanics at the base of the chinchilla cochlea. I. Input-output functions, tuning curves, and response phases. *J. Acoust. Soc. Am.* 80, 1364-1374.
- Sellick, P.M., Patuzzi, R., and Johnstone, B.M. (1982). Measurements of basilar membrane motion in guinea pig using the Mössbauer technique. *J. Acoust. Soc. Am.* 72, 131-141.
- Sellick, P.M., Yates, G.K., and Patuzzi, R. (1983). The influence of Mössbauer source size and position on phase and amplitude measurements of the guinea pig basilar membrane. *Hear. Res.* 10, 101-108.

**SAMENVATTING****NIET-LINEAIRE EN ACTIEVE COCHLEA  
MODELLEN:  
ANALYSE EN OPLOSSINGSMETHODEN**

Dit proefschrift behandelt een aantal aspecten van de mechanica van het inwendig oor (slakkehuis of cochlea). De nadruk wordt gelegd op het analyseren van modellen van de cochlea en het zoeken naar adequate oplossingsmethoden voor de modelvergelijkingen. Het uiteindelijke doel hiervan is het kunnen begrijpen van de werking van het slakkehuis, door het opstellen van een model waarmee experimenteel waargenomen verschijnselen verklaard kunnen worden. In dit proefschrift komen een drietal onderwerpen aan de orde:

- Een kwantitatieve validatie van de "klassieke" macromechanische cochleamodellen, aan de hand van gemeten bewegingen van het basilaire membraan (BM).
- Het ontwikkelen van methoden waarmee de hypothese "de cochlea bevat een mechanisch actief filter dat zich op het niveau van de BM beweging manifesteert" getest kan worden.
- Het ontwikkelen van een robuuste en efficiënte methode om niet-lineaire en actieve cochleamodellen in het tijddomein op te lossen.

Cochleamodellen kunnen verdeeld worden in twee klassen, namelijk macromechanische en micromechanische modellen. Een belangrijke eigenschap van macromechanische modellen is dat elk punt van het BM slechts één vrijheidsgraad heeft, de mechanische eigenschappen van het orgaan van Corti/tectoriaal membraan (OC/TM) complex worden als het ware samengevoegd met die van het BM. Ook zijn macromechanische cochleamodellen lineair en passief; dit laatste wil zeggen dat er geen mechanische energie aan het systeem wordt toegevoegd anders dan via de stimulus. Alle

cochleamodellen die niet aan de bovenstaande beschrijving voldoen, worden tot de klasse van de micromechanische modellen gerekend.

In het eerste deel (hoofdstuk 1) van het proefschrift worden de BM snelheden, berekend in macromechanische cochleamodellen, vergeleken met die, gemeten in dierexperimenten. Omdat een aantal modelparameters binnen zekere grenzen vrij te kiezen is, worden de modelvergelijkingen opgelost met een snelle, benaderende methode, de L(iouville-)G(reen) methode. Het blijkt dat de modelresponsie zowel wat betreft amplitude als fase goed in overeenstemming te brengen is met de stompe BM-snelheidskrommen uit de experimenten van Johnstone en Yates (1974) en van Rhode (1971, 1978). Deze stompe BM-snelheidskrommen worden tegenwoordig geacht gemeten te zijn in fysiologisch niet meer intacte cochlea's. In de loop van de tachtiger jaren zijn er veel scherper afgestemde BM snelheden gemeten (Khanna en Leonard, 1982; Sellick *et al.*, 1982, 1983; Robles *et al.*, 1986); de afstemming van deze snelheidskrommen is vergelijkbaar met de afstemming van receptorpotentiaLEN in de haarschijfjes. Deze scherp afgestemde BM snelheden kunnen niet gesimuleerd worden door macromechanische cochleamodellen. Ook berekeningen in lineaire, passieve cochleamodellen die uitgebreid zijn met een tweede vrijheidsgraad per punt op het BM die het OC/TM complex representeert, leveren niet de scherper afgestemde snelheidsprofielen.

De in de laatste jaren gepubliceerde scherpe BM-snelheidskrommen geven aanleiding voor de hypothese dat de cochlea een actief mechanisch filter bevat. Dit wordt ondersteund door de eind zeventiger jaren ontdekte akoestische echo's en spontane akoestische emissies. Voorts dragen quantum-mechanische beschouwingen en modeltheoretische analyses argumenten aan voor zo'n actief filter. In dit proefschrift worden twee methoden besproken waarmee de hypothese dat de cochlea een actief filter bevat dat zich op het niveau van de BM beweging manifesteert, getest kan worden. De eerste methode (behandeld in hoofdstuk 2) is een omgekeerde behandeling van de mechanica van de cochlea. In plaats van de BM-snelheid voor een gegeven BM-impedantie te berekenen, wordt de impedantiefunctie berekend uit een gegeven BM-snelheidspatroon. Het reële deel van de aldus berekende impedantie geeft een aanwijzing voor de aanwezigheid van een actief filter; waar dit reële deel negatief is, wordt door de cochlea energie toegevoerd aan de beweging van het BM. Simulatiestudies laten zien dat het reële deel van de impedantie extreem gevoelig is voor verstoringen in het BM-

snelheidsprofiel. De gemeten BM-snelheidskrommen worden altijd gestoord door meetfouten, zodat het op deze manier niet mogelijk is om uit de experimentele gegevens te bepalen of de cochlea al dan niet actieve elementen bevat, die zich op het niveau van de BM beweging manifesteren.

Aanzienlijk minder gevoelig voor verstoringen in de BM-snelheid is de vermogensflux door een dwarsdoorsnede van een kanaal van het slakkehuis (hoofdstuk 3). De vermogensflux is een belangrijke indicator voor mechanische activiteit, daar een stijging in deze functie correspondeert met toevoer van mechanische energie. Teneinde de vermogensflux te berekenen uit gemeten BM-snelheidskrommen, moeten de meetdata eerst gladgestreken en geïnterpoleerd worden om numerieke fouten, als gevolg van te weinig meetpunten en van meetruis, te reduceren. De keuze van de "smoothing"-methode blijkt de berekende vermogensflux aanzienlijk te beïnvloeden. Gekozen is voor een "cubic spline smoothing" methode waarin de regularisatieparameter, welke de mate van gladheid bepaalt, afhangt van de data. De vermogensflux-methode brengt een duidelijke scheiding aan tussen stompe BM-snelheidskrommen (Johnstone en Yates, 1974) en scherp afgestemde BM-snelheidskrommen (Sellick *et al.*, 1983; Robles *et al.*, 1986). De stomp afgestemde krommen geven geen aanleiding tot een significante stijging in de vermogensflux, de scherp afgestemde krommen doen dit wel. Samenvattend luidt de conclusie uit het tweede en derde hoofdstuk van dit proefschrift: Uit de recent gemeten, scherp afgestemde BM-snelheidskrommen kan, binnen het kader van de modelveronderstellingen, afgeleid worden dat de cochlea een actief mechanisch filter bevat; het reële deel van de impedantie waarmee in de modellen dit mechanisch actief gedrag gesimuleerd wordt, kan echter niet betrouwbaar uit de gemeten BM-snelheidskrommen bepaald worden.

Aangezien de onderliggende mechanismen van het niet-lineaire en actieve gedrag van de cochlea niet of nauwelijks bekend zijn, is het nuttig verschillende fenomenologische cochleamodellen te kunnen testen en met elkaar te vergelijken. Daartoe worden robuuste en efficiënte oplossingsmethoden voor niet-lineaire en actieve cochleamodellen geconstrueerd, waarmee responsies van zulke modellen op diverse type ingangssignalen in het tijddomein berekend kunnen worden. In het vierde tot en met het zesde hoofdstuk van het proefschrift worden numerieke oplossingsmethoden voor respectievelijk één, twee- en drie-dimensionale (1D, 2D, 3D) modellen gepresenteerd. Dit maakt het mogelijk om het effect van de dimensionaliteit van de vloeistofgolf op de

BM bewegingen te bestuderen.

Het 1D model wordt beschreven door een partiële differentiaalvergelijking in twee onafhankelijke variabelen (plaats en tijd) met bijbehorende rand- en beginvoorwaarden. De partiële differentiaalvergelijking wordt in de plaats gediscretiseerd met behulp van het principe van Galerkin, waardoor een stelsel van gewone differentiaalvergelijkingen in de tijd wordt verkregen. Om dit stelsel op te lossen, zijn verschillende numerieke integratiemethoden getest en vergeleken wat betreft stabiliteit, nauwkeurigheid en rekensnelheid. Uit de vergelijking komt een vierde orde Runge-Kutta schema met een variabele stapgrootte als meest geschikt naar voren. Dit schema blijkt zowel stabieler als efficiënter te zijn dan de andere beschouwde integratieschema's.

Twee- en drie-dimensionale cochleamodellen worden beschreven door partiële differentiaalvergelijkingen in een tijdvariabele en twee, respectievelijk drie plaatsvariabelen met bijbehorende rand- en beginvoorwaarden. Om de modelvergelijkingen numeriek op te lossen, worden de modelvergelijkingen eerst omgevormd tot een 1D integraalvergelijking voor de versnelling van het BM; dit kan worden gedaan zonder dat het multidimensionale karakter van de beweging van de vloeistofgolf in de kanalen verloren gaat. De discretisatie van de integraalvergelijking gebeurt dan slechts in één plaatsvariabele. Het hierdoor ontstane stelsel van gewone differentiaalvergelijkingen in de tijdvariabele wordt evenals in het 1D geval geïntegreerd met een vierde orde Runge-Kutta schema. De methode voor 2D en 3D modellen kost meer rekentijd dan die voor 1D modellen. Immers, op elke tijdstap moet een stelsel vergelijkingen worden opgelost waarvan de systeemmatrix in het 1D geval tridiagonaal is, terwijl in 2D en 3D de systeemmatrix vol is. In het 3D geval moet bovendien voor elk element van die matrix een slecht convergerende reeks gesommeerd worden. Daar de systeemmatrix onafhankelijk is van de tijdvariabele, hoeft het vullen van deze matrix voor een bepaalde verzameling geometrische en mechanische modelparameters slechts één maal te gebeuren.

De in dit proefschrift ontwikkelde methoden kunnen worden toegepast op een breed scala van cochleamodellen, en voor diverse ingangssignalen. De methoden zijn derhalve zeer geschikt om niet-lineaire en actieve modelconcepten te valideren. Ook kunnen zij gebruikt worden als referentie voor het testen van benaderende oplossingsmethoden, die minder computertijd vragen

en bovendien meer inzicht geven in de fysica van de bewegingen van het BM.

## REFERENTIES

- Johnstone, B.M. and Yates, G.K. (1974). Basilar membrane tuning curves in the guinea pig. *J. Acoust. Soc. Am.* 55, 584-587.
- Khanna, S.M. and Leonard, D.G.B. (1982). Basilar membrane tuning in the cat cochlea. *Science* 215, 305-306.
- Rhode, W.S., (1971). Observations of the vibration of the basilar membrane in squirrel monkeys using the Mössbauer technique. *J. Acoust. Soc. Am.* 49, 1218-1231.
- Rhode, W.S. (1978). Some observations on cochlear mechanics. *J. Acoust. Soc. Am.* 64, 158-176.
- Robles, L., Ruggero, M.A., and Rich, N.C. (1986). Basilar membrane mechanics at the base of the chinchilla cochlea. I. Input-output functions, tuning curves, and response phases. *J. Acoust. Soc. Am.* 80, 1364-1374.
- Sellick, P.M., Patuzzi, R., and Johnstone, B.M. (1982). Measurements of basilar membrane motion in guinea pig using the Mössbauer technique. *J. Acoust. Soc. Am.* 72, 131-141.
- Sellick, P.M., Yates, G.K., and Patuzzi, R. (1983). The influence of Mössbauer source size and position on phase and amplitude measurements of the guinea pig basilar membrane. *Hear. Res.* 10, 101-108.

CURRICULUM VITAE

De schrijver van dit proefschrift werd op 1 november 1957 te 's-Gravenhage geboren. Na in juni 1976 aan de scholengemeenschap "Simon Stevin" te 's-Gravenhage het diploma atheneum-B behaald te hebben, ging hij studeren aan de Technische Hogeschool te Delft [tegenwoordig: Technische Universiteit Delft (TUD)]. In juni 1983 slaagde hij voor het examen voor wiskundig ingenieur. Van juli 1983 tot juli 1987 werkte hij als wetenschappelijk assistent op het Academisch Medisch Centrum te Amsterdam en de TUD in het kader van het onderzoekproject "Niet-lineaire en actieve cochleamodellen". Het project werd ondersteund door de Stichting voor Biofysica van de Nederlandse Organisatie voor Zuiver Wetenschappelijk Onderzoek. Sinds juli 1987 is hij verbonden aan de faculteit der Technische Wiskunde en Informatica, vakgroep Toegepaste Analyse, van de TUD.